UNIVERSITÀ DEGLI STUDI DI PADOVA
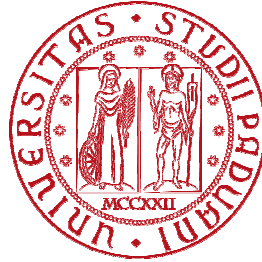
FACOLTÀ DI INGEGNERIA

DIPARTIMENTO DI INGEGNERIA DELL'INFORMAZIONE

BRAIN STEM FMRI OPTIMIZATION AT 3T

RELATORE: **PROF. ALESSANDRA BERTOLDO**

CORRELATORE: **PROF. KLAAS PAUL PRUSSMANN**

PHD MARCO PICCIRELLI

LAUREANDO: **MARCO MORO**

ANNO ACCADEMICO 2010/2011

Contents

Abstract

Unlike primary sensory fMRI activation, where discussions focus around how to best quantify the robust activation present in nearly every subject, brainstem study clearly requires novel approaches: simply finding any activation in these small regions of the moving brain is considered an accomplishment. This study provides guidelines to improve functional MRI of the brainstem at 3T. It first focused on the optimal choice of the echo time, slice tilt, and spatial resolution as well as the most suited head coil. Second a functional study was carried out using an optokinetic stimulation to elicit activation in the brainstem oculomotor system. Information such as blink events, periods of eyes closed and velocity of the eyes movements were used to build regressors to be included in the general linear model. F-tests were performed on residuals produced by regression analysis. The optimal acquisition sequence and the optimal model yielded robust neuronal activation throughout the visual cortex as well as in the lateral geniculate nuclei (LGN); but the main findings revealed in the brainstem were neuronal activation in the superior culliculus (SC) for all participants, and in the other nuclei and pathway involved in the investigated task, such as the oculomotor nuclei (OMN), the oculomotor nerve, and the abducens nucleus.

Sommario

Studi di attivazione neuronale nel tronco encefalico, condotti con metodi di risonanza magnetica funzionale richiedono nuovi approcci mirati a risolvere i problemi causati dalla vicinanza di questa struttura cerebrale alle vie aeree e ai maggiori vasi sanguigni. In questo progetto in una prima fase sono stati ottimizzati i parametri della sequenza di acquisizione, come il tempo di eco, l'inclinazione delle immagini e la risoluzione spaziale. Nella seconda fase un'analisi statistica, usando F-test, è stata eseguita per valutare le caratteristiche di diversi modelli lineari usati per fittare i dati funzionali. In fine la mappa di attivazione ottenute utilizzando i risultati dei passi precedenti hanno rivelato attivazione nella corteccia visiva, nel genicolato nucleo laterale, ma i principali risultati sono stati l'attivazione nei colliculi superiori nei nuclei oculomotori e nei nervi oculomotori.

Chapter 1: Introduction

1.1 Basic principal of MRI

Principal goal of the MRI scanner is by using a strong magnetic field to flip the atomic nuclei spins in the human body. This permits to align certain nuclei having odd number of protons or of neurons or both have I≠0 (angular moment) and a nuclear magnetic moment, e.g. hydrogen within water molecules or in the fat molecules, in the same direction of magnetic field generated.

1.1.1 MRI scanner

One of the most important MRI scanner component is the main static magnetic field, called B0. MRI scanner generates a magnetic field using two important finding that led to the development of electromagnetism. The first was by the Danish physicist Hans Oersted in 1820, when he discovered that a current-carrying wire generates a magnetic field perpendicular to the direction of the current. He demonstrated that a current-carrying wire influenced the direction of a compass needle placed below the wire,

redirecting it perpendicularly to the wire. This relationship was quantified one year later by the French physicists Jean-Baptiste Biot and Félix Savart: In their experiment they showed that is possible control the magnetic field intensity by adjusting the current in a wire, so they demonstrated that the magnetic field strength is proportional to current strength.

The modern MRI scanners are composed by the loops of wire made of metal alloys such as niobium-titanium, which are cooled to temperature near absolute zero to increase the conductivity of the material. Furthermore a huge electrical current must be injected in the loop and optimized to achieve a homogeneous magnetic field of the desired strength. The field homogeneity and the field strength are two important proprieties in MRI. Having a strong and uniform magnetic field ensures to create body image that do not depend on external factor (Scott, Allen et al. 2009).

Another important component of the MRI scanner necessary to create the MR signal are the radiofrequency coils. These coils allow generating and receiving electromagnetic field at the resonant frequencies of the atomic nuclei. This frequency depends by the strength of the static magnetic field and is calculated by the relation:

$$Larmor\ frequency \qquad \omega = \gamma B_0 \,,$$

where γ is the gyromagnetic ratio (unique for each nuclide that has a nuclear magnetic moment) and B_0 the external magnetic field. The atomic nuclei absorbs the energy of the radiofrequency pulse at the Larmor frequency. This process perturbing the equilibrium created by the static magnetic field is known as excitation. Unlike the static magnetic field the radiofrequency field, called B_1, is turned on and off during the measurement. When B_1 ends, the atomic nuclei return to the equilibrium state, and release of energy they absorbed during excitation. The released energy can be detected by the radiofrequency coil. These steps lead to create the raw MR signal.

The radiofrequency coils in MRI are tuned for a narrow frequency band to excite the hydrogen atom in several molecules. ^{1}H nuclei in water (H_2O) and fat ($\sim CH_2$) are in different molecules and experience a slightly different local magnetic field which results in slightly different resonant frequencies. These local magnetic field variations contribute to the eventual contrast between various tissues in an MRI image.

Usually to get a suitable measure of the signal, the radiofrequency coils should be located close of the body area to be measured. In case of fMRI, the radiofrequency coils are placed immediately around the head. There are three main types of RF coils: surface coils, volume coils and phased array.

Surface coils are composed by a single loop inductor-capacitor (LC) circuit. The rapid change of electricity between these two component generates an oscillating currents that can be turned to the specific band of frequency. This device must be placed on or around the surface of patient; because of this surface coils usually provide high imaging sensitivity and it has a good signal to noise ratio (SNR) for superficial tissues. In fMRI are often used to investigate specific brain region, e.g. visual cortex.

Volume coils have a cylindrical shape; in this case the LC circuit is replaced around the whole surface to achieve a uniform distribution of energy within the enclosed volumes. This device is used for surrounding either the whole body or a specific region, such as the head. It is has better magnetic field homogeneity the surface coils but less sensitivity.

The thirds kinds of coils was built to unite the best features of the devices describe above. It uses a volume coil for exciting a body area and a set of overlapping surface coils for receiving the MR signal. In this way it is possible to maintain the homogeneity in the volume coverage having a high sensitivity and a high SNR.

In the previous steps it was been explain how to generate and measure the MR signal, but to create the MR images the spatial information must be known. The gradient coils provide this component necessary for imaging. Like the RF coils the gradient coils are turned on and off during the images recording. When and for how long they are on depend from the acquisition sequence as it will be explained below. The gradient coils are located in the internal sides of the scanner and create linearly varied magnetic fields along the cardinal direction relative to the static magnetic field. The gradient create in the static magnetic field is called z and the others perpendicular with B_0 direction are called x and y. These gradients allow the spatially encoding of the MR signal.

1.1.2 MR contrast and pulse sequences

The MR contrast permits to determine brain anatomy and to create functional images for fMRI study. The gray value in a pixel in the MR image depends on the number, type, relaxation times and resonance frequencies of hydrogen nuclei within that voxel.

When a body is placed in a MR scanner the hydrogen nuclei are realigned in the direction of the static magnetic field either parallel to B_0 (lower energy level) or antiparallel to B_0 (higher energy level). In this state a great number of spin is parallel to the scanner's magnetic field, thus result a difference of magnetization, or a net magnetization (expressed with the vector M_0). As reported above, to generate a MR signal a RF pulse (B_1) must to be applied. B_1 is a small magnetic field perpendicular to B_0 that perturbs the state of equilibrium. It transfers energy to same hydrogen atoms which change their level and causes the tipped of M_0. The amount of electromagnetic energy that is transferred can be quantified with a vector M_{xy} whose angle with M_0 depends on how long the RF pulse is turned on.

After the process of excitation the system returns in equilibrium state, this step is called relaxation. There are two component of relaxation: i) Longitudinal, the recovery to the magnetization parallel to B_0 and characterized by the time constant T_1; ii) Transverse, the decay of the transverse magnetization due to accumulate phase differences cause by spin-spin interaction and characterized by the time constant T_2.

The several tissues within the body have different physical and physiological characteristic such as proton density ρ and relaxation time constant T_1 and T_2. MR signal amplitude, and therefore the image contrast depends on this parameter. It may be possible describe the MR signal as the equation:

$$M_{xy}(t) = M_0(1 - e^{-TR/T_1})e^{-TE/T_2}$$

where M_0 is proportional to spin density ρ. TR is define as the time interval between successive excitation pulses; and TE the time interval between an excitation pulse and data acquisition.

The contrast between two kinds of tissue A and B is defined as the difference in MR signal between these tissues and equals:
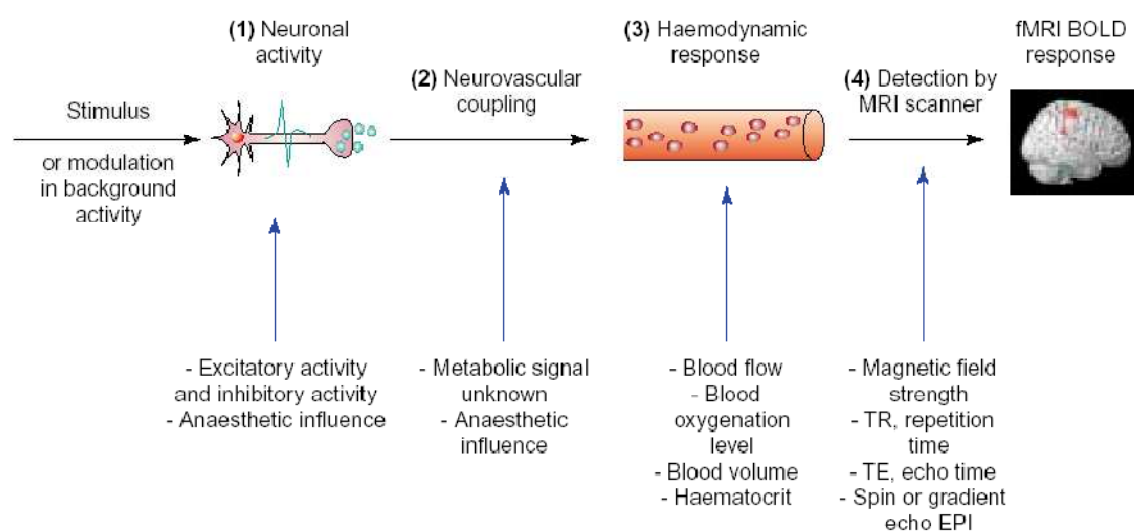
$$C_{AB} = M_{0A}\left(1 - e^{-TR/T_{1A}}\right)e^{-TE/T_{2A}} - M_{0B}\left(1 - e^{-TR/T_{1B}}\right)e^{-TE/T_{2B}}$$

When the pulse sequence have a very long TR value a very short TE value signal intensity will mainly depend on ρ; the resulting images are therefore proton-density weighted. In these images the highest signal come from the tissues with major concentration of hydrogen atom, such as cerebrospinal fluid (CNR); with less signal in the gray matter and even less signal in the white matter. Instead, if the pulse sequence have a very short TE to minimize the T_2 contrast and a TR value that ensures a good T_1 contrast, the images are called $T_1 - weigthed$. The most commonly use of images sensitive to T_1 contrast is for anatomical information. Tissues with a shorter T_1 value have a greater MR signal and appears brightest (e.g., white matter), on the other hand tissues with a longer T_1 value have a low MR signal and appear darkest (e.g., CSF). Finally, to measure $T_2 - weighted$ images is necessary a pulse sequence with a very long TR and a TE that maximizes the T_2 contrast. The resulting image is brightest in the tissues with long T_2 value (e.g., CSF) and darkest in the tissues with short T_2 values (e.g. white matter). This sequence measures the decay of the transverse component of magnetization due to the spin-spin interaction. Other pulse sequences instead measures the transverse magnetization decay due on two causes: spin-spin interaction and change in precession frequencies due to inhomogeneities in the magnetic field. The images created are called $T_2^* - weigthed$ images. The relationship between T_2^* and T_2 is given by $1/T_2^* = (1/T_2) + (1/T_2')$ where T_2' reflect the dephasing effect caused by field inhomogeneity. Because of these images are sensitive to the amount of deoxygenated hemoglobin present in the tissues, they are the contrast basis for fMRI.

1.1.3 About BOLD functional fMRI

Functional magnetic imaging (fMRI) creates images of physiological activity that is correlated with neuronal activity. In local brain regions with activity changes the cells

requires external sources of energy to support metabolic processes. The vascular system supplies cells with two fuel sources, glucose and oxygen, the latter bound to hemoglobin molecules. This hemodynamic response occurs after a delay of approximately 1-6 seconds, and leads to local changes in the relative concentration of oxygenated and deoxygenated hemoglobin. Commonly fMRI studies use the blood oxygenation level-dependence (BOLD) susceptibility effects occurring in areas of neuronal activity. It is important to recognize that BOLD contrast is a consequence of effects (Figure 1). It results from changes in the magnetic proprieties of water molecules, which in turn reflect the influence of paramagnetic deoxyhemoglobin, which is a physiological correlate of oxygen consumption, which itself is a correlate of a change in neuronal activity evoked by sensory, motor, or cognitive processes.


Figure 1. This image shows the several phases in the path from stimulus to BOLD effect. Source: Arthurs & Boniface, 2002.

The BOLD occurs because of the different magnetic properties of the hemoglobin molecules, with differ depending upon whether or not it is bound to oxygen. Oxygenated hemoglobin (Hb) is diamagnetic; that is, it has no unpaired electrons and zero magnetic moment. Deoxygenated hemoglobin (dHb) is paramagnetic; it has both unpaired electrons and a significant magnetic moment. Completely deoxygenated blood has a magnetic susceptibility about of 20% greater than fully oxygenated blood (Scott, Allen et al. 2009). It was found that changes in blood oxygenation could be visualized

using T_2^*-weighted images (Ogawa, Lee et al. 1990). Indeed, the magnetic susceptibility inhomogeneities of an object into a magnetic field increases occurring the spin dephasing. The resulting decay of transverse magnetization depends on the time constant T_2^*. Because bold deoxygenation affects magnetic susceptibility, MR pulse sequences sensitive to T_2^* should show more MR signal where blood is highly oxygenated and less MR signal where blood is highly deoxygenated.
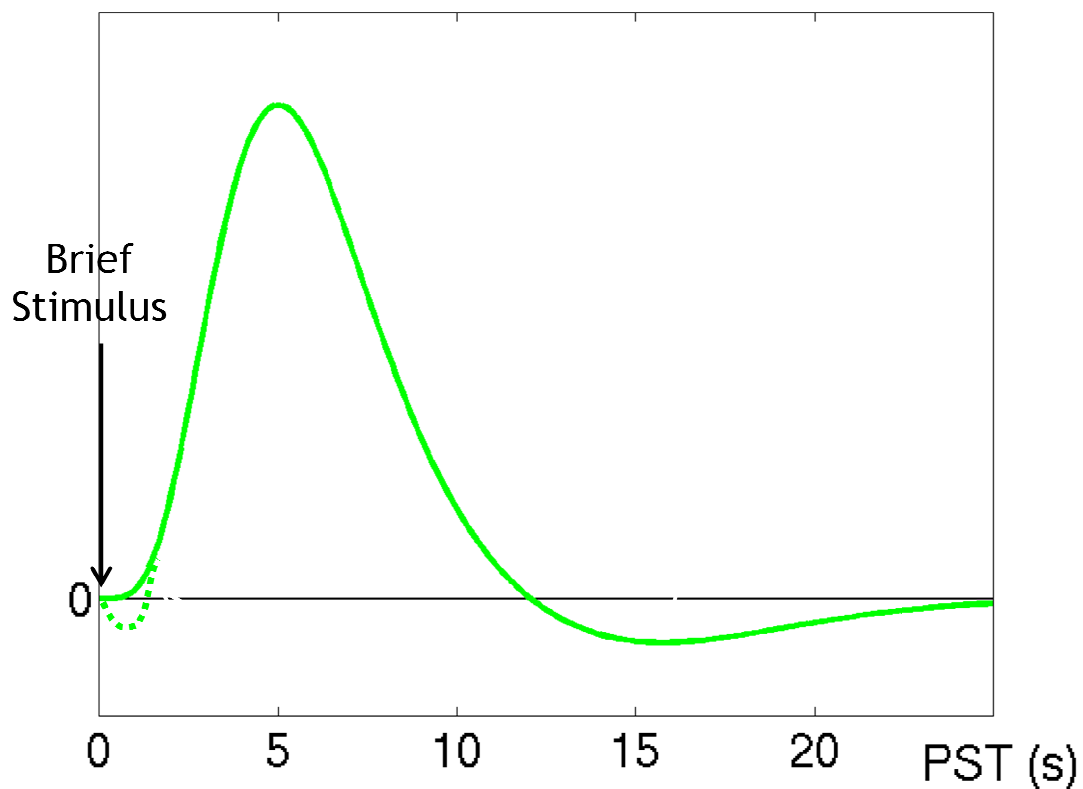
unction to a short

The change in the MR signal triggered by neuronal activity is known as the hemodynamic response (Figure 2). In beginning the metabolic demands of the increased neuronal activity increases over baseline levels result in an increased inflow of oxygenated blood. After the peak, the BOLD signal decreases in amplitude to a below baseline level and remains below for an extended interval. The aim in MR functional studies is to recognize the hemodynamic response (HRF) in a voxel time series, for this purpose it must considered that the BOLD signal in a voxel reflects the total amount of

deoxygenated hemoglobin that is present, as well as noise resulting from several sources.

1.2 Brainstem

The brainstem is located in the posterior cranial fosse, structurally continuous with the spinal cord. The brainstem is composed of three parts: in ascending order the medulla, the pons and the mesencephalon (Thomas 2009). This structure is an important part of the brain as it allows the nerve connections of the motor and sensory systems from the brain to the rest of the body, encompassing also face and neck. In Figure 3 a drawing of the postero-lateral view of the brainstem evidencing the nerve paths is shows.
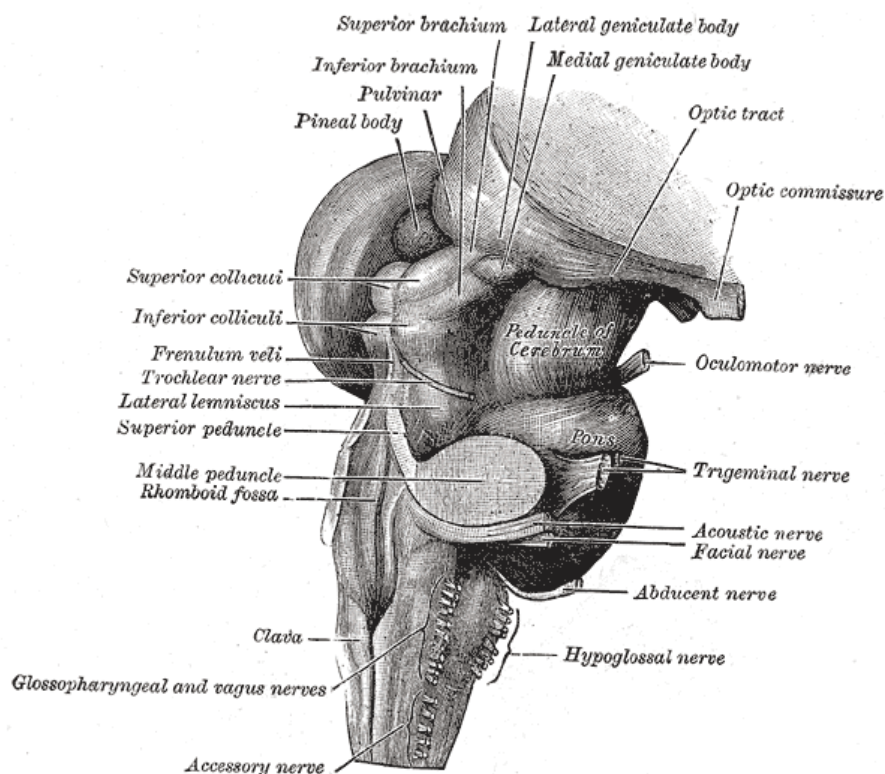
Figure 3. Drawing of the brainstem structure and principale nerve. Source:
http://education.yahoo.com/reference/gray/subjects/subject/187 Date/time: 06 April 2011, 11.39

The medulla, lower half of the brainstem, contains the cardiac, respiratory, vomiting, vasomotor centers and deals with autonomic, involuntary functions, such as heat rate,

breathing and blood pressures. In the middle there is the pons, which is composed mainly of white matter, and contains nuclei that relay signals from the forebrain to the cerebellum, along with nuclei that deal primarily with sleep, respiration, swallowing, bladder control, hearing, equilibrium, taste, eye movement, facial expression, facial sensation and posture. The mesencephalon is located below the cerebral cortex, and above the hindbrain placing it near the center of the brain; it contains nuclei and paths associated with vision, hearing, motor control, sleep/wake, arousal, and temperature regulation.

As it is shown in Figure 4, the brainstem arteries arising from the main trunks are divided into anteromedial, anterolateral, lateral and posterior groups according to their point of penetration into the surface of the brainstem (Thomas 2009). To knowledge of vascular system that supplied the tissues in the brainstem is important to understand the BOLD effect in these areas and the physiological noise occurs during functional studies.
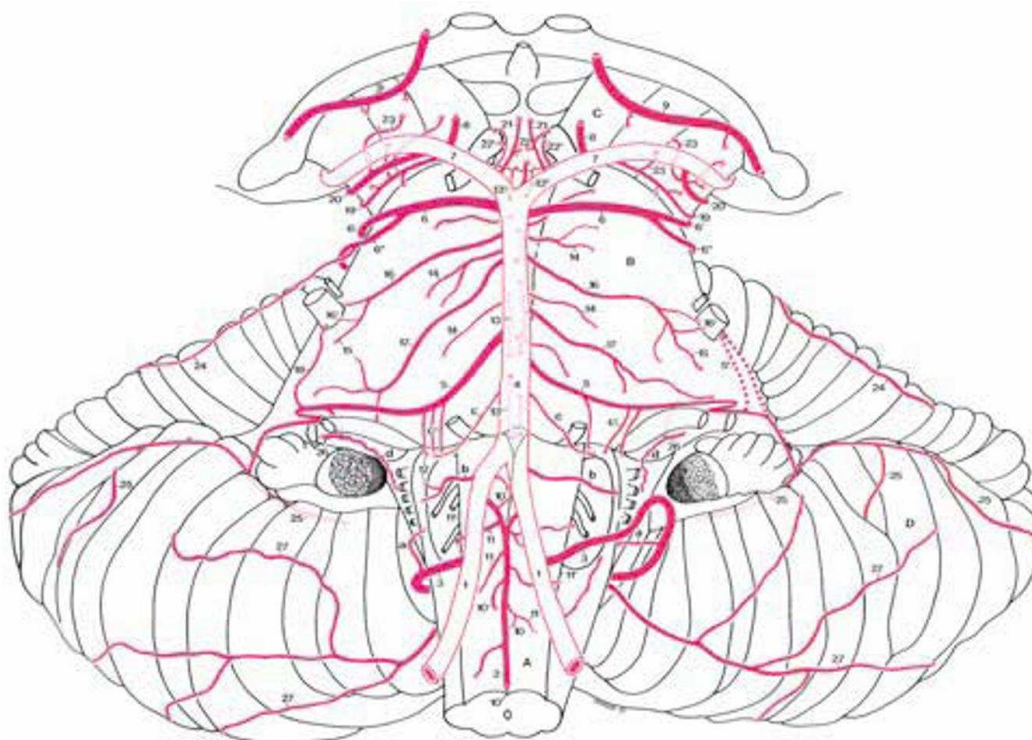

Figure 4. The arterie of the brainstem an cerebellum. Drawing adapted from Duvernoy's atlas of human brainstem (Thomas 2009).

1.2.1 Brainstem function

As described above, the brainstem is involved in many of the basic function of the central nervous system (CNS). The three important systems are: sensory, motor, and autonomic. Herein are described the functional pathways concerned in this study. In the sensory system are encompassed multiple visual subsystem (Thomas 2009):

- *Retinogeniculocortical system*. The optic tracts conduct visual impulses from the retina to the lateral geniculate bodies (or lateral geniculate nuclei), which relate them to the primary visual cortex (V1).
- *Retinocolliculocortical system*. The superior colliculus receives visual input from the retina. They give rise to descending motor fibers that pass to the spinal cord and to the nuclei of the cranial nerves (oculomotor nuclei).
- *The accessory optic system* is composed of dorsal and lateral terminal nuclei, which play a role in the control of eye and head movements.

The other system involved in this study is the oculomotor system, as a sub pathways of the motor system. The oldest oculomotor systems (vestibule-oculomotor and optokinetic reflexes) serve to maintain the stability of vision during movements of the head. The more recent oculomotor systems (saccades and smooth-pursuit eye movements) serve to fix and follow a special target.
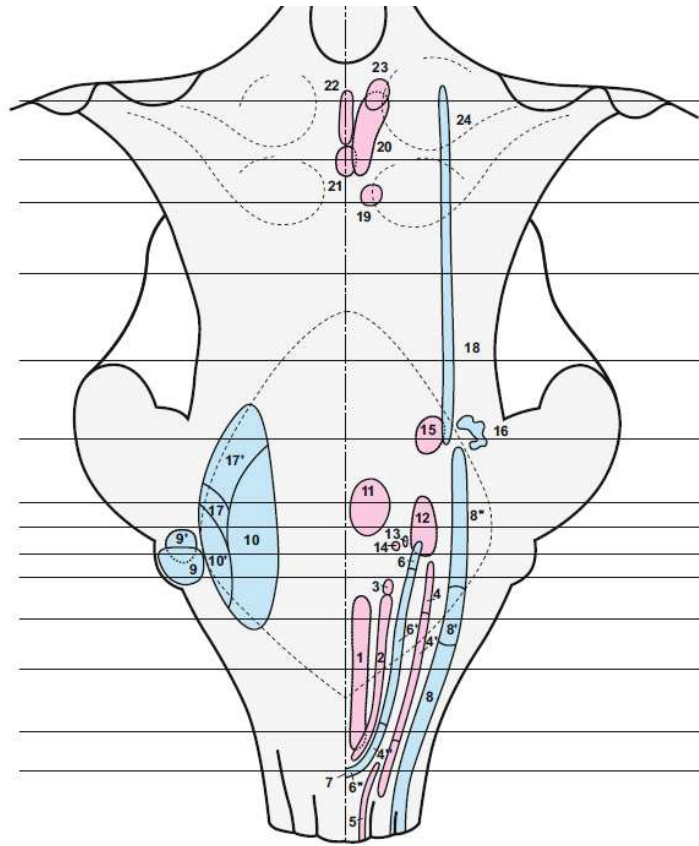
Figure 5. The general arrangement of the motor (pink) and sensory (blue) cranial nerve nuclei. Drawing adapted from Duvernoy's atlas of human brainstem (Thomas 2009). The structures of interest: 11 Abducens nucleus, motor to lateral rectus muscle belonging to the group of extra-ocular muscles; 19 Trochlear nucleus (CN IV), motor to the superior oblique muscle belonging to the group of extra-ocular muscles; 20–23 Oculomotor nuclei (CN III), supplying all the extraocular muscles except the superior oblique and lateral rectus; 20 Principal oculomotor nucleus; 21 Caudal central oculomotor nucleus; 22 Nucleus of Perlia; 23 Accessory oculomotor nucleus (of Edinger-Westphal), parasympathetic center for motor innervations of intra-ocular muscles.

1.2.2 OKN Stimulus

The optokietic nystagmus is a physiological reflex composed of two phase: the slow phase when the eyes follows a moving object and the quick phase when they jerk back in the opposite direction. During the compensation movement induced by optokinetic stimulus, fast or rapid movements, include saccades and quick phases of nystagmus, bring the eyes rapidly from one fixation point to another or reset (Raphan and Cohen 1978). For saccades, the pathways that connect visual area in the cerebral cortex to motor regions in the cerebellum include direct projections form cortical eye field to eye-movement-related structure in the brainstem such as the superior colliculus

(SC) and premotor including nuclei in the reticular formation (PMN), and also pathway through the basal ganglia, including the caudate nucleus (CN), the substantia nigra pars reticulate (SNr), and other nuclei of the motor system (Krauzlis 2004). Using the optokinetic stimulus it was interested to measure neuronal activation in the brainstem and in specific, in the superior colliculus because the SC and the cerebellum provide additional level of control to the ocular motor command, during the saccades. In particular the principal pathways of the horizontal optokinetic reflex (OKR) begin in the retina and successively link the nucleus of the optic tract (in the pretectal area), the nucleus reticularis tegmenti pontis, and the vestibular nucleus. As with the vestibule-ocular system, the fibers of the vestibular nucleus reach the abduncens nucleus, with controls the oculomotor nucleus (Thomas 2009).

1.2.3 Brainstem functional image

To investigate in the nucleus and pathways of the brainstem using fMRI studies is technically challenging, because of its small size, proximity to tissues and cavity producing magnetic susceptibility effects leading to image distortion, and its situation next to large blood vessels within and around brainstem, as can be seen in Figure 6. This T1-weithed image, acquired during this functional studies, shows as a blood vessel covers the anterior side of the brainstem.
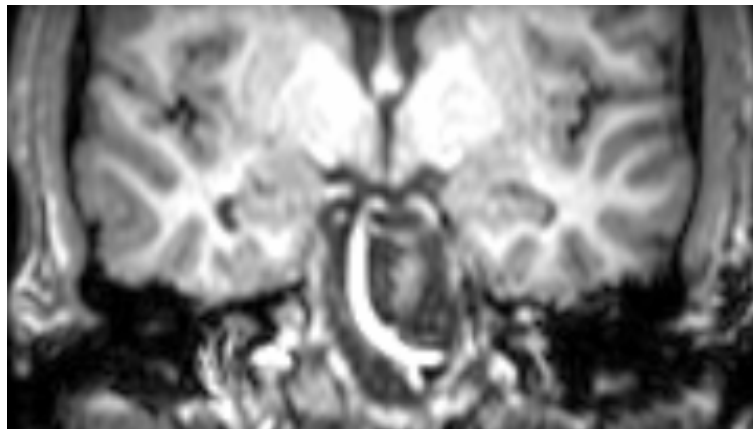

Figure 6. T1-weithed image acquired with 3D high resolution technique. This image show as a blood vessol cover the anterior side of the brainstem.

The movement due to the blood pulsation and breathing introduces substantial temporal noise artifacts into the time series of the functional data (Wall, Walker et al. 2009). Functional studies of small brain structures requires advanced scanning technology. The advent of high field strength (i.e. 3T or more) MRI systems for human research purposes has enabled the use high spatial resolution and an increased of the signal to noise ratio. Regarding the physiological artifacts many techniques were developed. Triggered fMRI acquisition phase locked to a particular time point of the subject's cardiac cycle is an approach used to minimize the pulsatile artifact in the functional studies (Backes and van Dijk 2002). In alternative, the correction/compensation of the physiological noise can be carry on during the postacquisition analysis. Analysis technique such as Independent Component Analysis (ICA) may be generally useful in terms of identifying noise sources and eliminating them from the fMRI signal. Another approach used to compensate these artifacts is RETROICOR (Glover, Li et al. 2000); it is a retrospective image-based correction technique that extract cardiac and respiratory related noise effects from the MR signal by assigning cardiac and respiratory phases to each image in a time series.

In the functional study carried out in this project an adapted version of RETROICOR method was used. Herein the noise sources (heart beat and respiratory) were measured at the time of data acquisition, and used that data to define regressors of no interest (nuisance regressors) to allow the noise to be modeled in a multiple regressors analysis (GLM). The numbers of phase terms considered in the linear model that describe the data was chosen in accordance to (Harvey, Pattinson et al. 2008). In this paper the considered method was implemented on resting brainstem EPI images to improve detection of brainstem activation, assessing a statistically optimal set of regressors.

1.3 Functional data optimization

MR signal amplitude and the image contrast depend on the physiological characteristic of the tissues, but on the other hand also on the acquisition parameters such as select the excitation mode and from time intervals between several pulses. Optimizing the acquisition parameter leads to increase the image contrast. In this project was shown that the choice of the appropriate devices such as head coils, and the

choice of the acquisition sequence parameters such as echo time, slices tilt, and spatial resolution, may influence considerably the amplitude and quality of signal.

1.3.1 Acquisition sequences

For functional magnetic resonance imaging of the brain is widely used the gradient –echo echo-planar imaging (GE EPI) technique. GE EPI is sensitive to the macroscopic field alterations caused by BOLD susceptibility effects in areas of neuronal activity (Ogawa, Lee et al. 1990). T_2^*-weighted images are often acquired using this technique, which uses gradients to generate the MR signal changes that are measured at data acquisition. A gradient in z direction is used to excite the spins encompassed in a specific slice (phase of slice selection). The first step is immediately followed by a phase encoding periods; using a gradient varying intensity in the y direction the spins shows different phases accord to their y coordinate. Thus the y coordinate is coded into the phase. During the same stem also a gradient varying in the x direction is applied. After the switching off this gradient the spin in the same x coordinate shows the same Larmor frequency. This step allows to encode the x coordinate. Thereby it is achieved spatial information of each voxel in the FOV. A drawing of the time diagram is show in Figure 6. To reduce the time of acquisition is widely used the echo planar imaging (EPI). EPI is a ultra-fast imaging technique which allows acquisition of images with only one excitation.
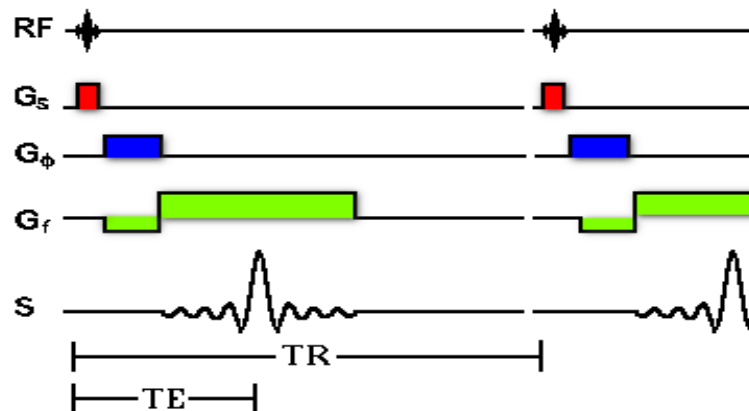

Figure 7. Drawing of the time diagram of the gradient echo.

The GA EPI advantages includes its high signal to noise ratio (SNR) and high temporal resolution. However, the GE EPI has important disadvantages; it is also sensitive to macroscopic field inhomogeneities caused by the differences of magnetic

susceptibility of air and tissue which may result in local image distortions and signal losses. The missing signal has often compromised fMRI studies of the inferior frontal, the medial temporal and the inferior temporal lobes (Weiskopf, Hutton et al. 2007); presumably this artifact may influence functional study involving the brainstem. The GRASE T2*-weighted is a technique which was investigated as a method to increase the signal, because it has already been demonstrated (Jovicich and Norris 1999), that this techniques allows to achieve high functional sensitivity in single shot images together with lower sensitivity to susceptibility effects (image distortions and signal loss). Its disadvantages is the artifact that appear in the phase-encode direction due to the modulation of both the phase and the amplitude of the signal during acquisition. GRASE is a multi-echo sequence that uses a 90° excitation pulse and creates an echo train by combining gradient and radiofrequency (RF) refocusing. Other techinique were proposed to improve the fMRI studies in regions with close proximity to air and bone tissues, and in regions close to large blood vessels, such as signal enhancement by extravascular water protons (SEEP). The contribute to the MR signal change in SEEP is the result of the activity-dependent changes in tissues water content due to swelling of neurons and glial cells. This method was found to be particularly useful when measuring neuronal activity in the brainstem and spinal cord (Figley, Leitch et al.). In the present study were investigate the features of GE EPI and GRASE to chose the most appropriate technique for the functional study. In addition their parameters were analyzed to achieve the optimized sequence.

1.3.2 Scan parameter optimization

Brainstem fMRI studies are often limited by several artifacts involving this particular brain region. Technique as GE EPI besides suffers from substantial signal loss and consequently of reduced BOLD (BS) sensitivity in the inferior brain region caused by inhomogeneities in the statistic magnetic field. This field inhomogeneities occur between brain tissues and near the air-filled cavities. To reduce the susceptibility related signal losses several method have been devised. Resistive coils have been used to homogenize the magnetic field in the investigated area (Cho and Ro 1992). Signal losses

may be also reduced by using tailored radiofrequency (RF) pulses for excitation, opposing the dephasing effect of the susceptibility related field gradients (GRASE).

In EPI single shot the set of the parameters is very important to avoid signal dropout in the involved regions and to increase the BS. In the case of long echo times and low spatial resolution occurs that the signal loss increase (Turner and Ordidge 2000). Besides, the slice orientation may have a considerable impact on the extent of signal dropout; this effect is due to a redistribution of susceptibility gradients in slice and in phase direction (Deichmann, Gottfried et al. 2003). Several investigations of the dependence of the signal loss on the parameters sequence were carried out either for the orbitofrontal cortex (OFC) and inferior temporal lobe (Weiskopf, Hutton et al. 2007), or for the whole brain (Weiskopf, Hutton et al. 2006).

In the first steps of this project it has been sought to optimize the BS for the brainstem region by testing the features of a sequence less influenced by field inhomogeneity (GRASE), testing different head coils, and specifically adjusting the echo time (TE), the slice tilt, and spatial resolution. Tilting the imaging slice cause a redistribution of in-plain and through-plane susceptibility gradients. For an adapted choice of the tilt angle, critical values of the in-plane gradients, which may cause complete signal loss, can be avoided. Also a adapted choice of the echo time value can avoid artifacts and signal loss in the areas near the brainstem involved in effects of magnetic inhomogeneity.

1.3.3 Analysis data methods

The idea is to represent the data with a linear models These models contain predicted time courses for the entire session, rather than for individual epochs, and they typically contain several distinct predictions (i.e. regressors) that correspond to different hypothesized processes (e.g. visual processeing). The relative contribution of each of these regressors to the measured data, with each voxel, is then statistically evaluated. The linear model with multiple regressors is based on the idea that the value of the observed data (y) can be attributed to two sources: a model comprising a linear combination of several reagressors (x_i), each with a variable weighting (β_i); and residual

noise in the data, or error in the measurements (ε). The formula for a regression analysis appears:

$$y = \beta_0 + \beta_1 x_1 + \beta_2 x_2 + \ldots + \beta_n x_n + \varepsilon$$

Given the data and a specific set of regressors, the model is estimated identifying a combination of parameters weights that minimize the error term. This approach, when applied to data set with many dependent variables, is known as the general linear model (GLM); it can be represent by a set of matrices shows in figure 8.
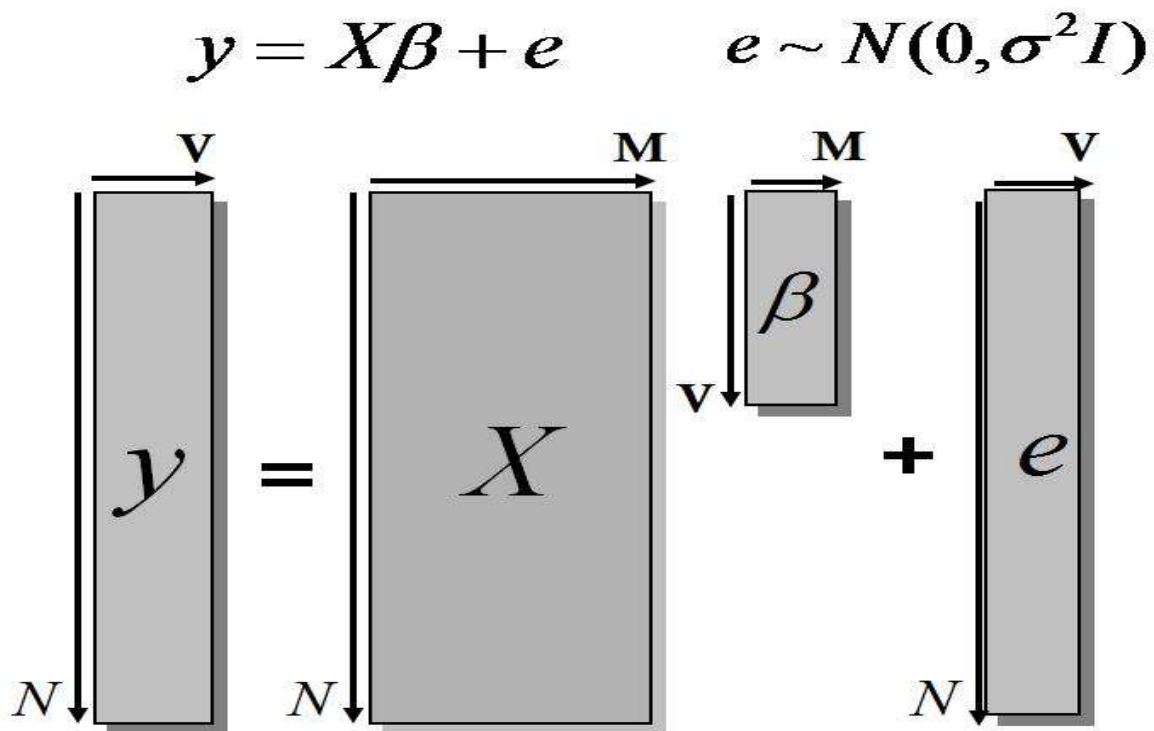
$$y = X\beta + e \qquad e \sim N(0, \sigma^2 I)$$

Figure 8. Basic principles of the general linear model in fMRI. The general linear model attempts to finds the set of experimental parameters (β, V = voxel, M = parameter weights) for a design matrix (G, N = time points, M = regressors) that best accounts for the original data (Y, N = time points, V = voxels), by minimizing the error (e).

The fMRI data are represented as two-dimensional data matrix y, consisting N time point by V voxels. The design matrix X, which specifies the linear model to be evaluated, consists of M regressors, each N time points in length. The parameter matrix contains M parameter weights and V voxels. Finally, the error matrix expresses the residual error for

each voxel, and thus is an N-by-V matrix. After the design matrix has been established, the linear model must be solved, estimating the parameter matrix that lead to the smallest values in the error matrix. The LGN assumes that the raw data can be modeled as the sum of separate factors, each of which may vary independenly across voxels, along with additive Gaussian noise that is also independently distributed across voxels.

The regressors in the design matrix represent the hypothesized contributors to the fMRI time course. There are two kinds of resressors: regressors of interest and nuisance regressors. The regressors of interest (or experimental regressors) are specific hypothesis associated with the experimental. Instead, the nuisance regressors are associates with known non-experimental sources of variability. In this study, during the statistical analysis of the functional data the velocity of the eyes movement (during the task) was considered as a regressors of interest, while the blink, the periods of eyes closed and the physiological noise were considered as nuisance regressors. The importance of the regressors related with the stimulus (velocity of eyes movement, blink and periods of eyes closed) on signal variability was assessed to achieve an optimized procedure to set the GLM for this functional study. F-test were performed on residuals produced by regression analysis. This analysis considers two models 1 and 2, where model 1 is contents within model 2. Consider, model 1 has p1 regressors, and model 2 has p2 regressors, where p2>p1. The model with more regressors will always be able to fit the data at least as well as the model with fewer parameters. Using the F-test is possible to determine whether a model gives a significantly better (i.e. lower error) fit to the data than the other model. If there are n data points to estimate parameters of both models from, then one can calculate the F statistic (coefficient of determination), given by:

$$F = \frac{\left(\dfrac{RSS_1 - RSS_2}{p2 - p1}\right)}{\left(\dfrac{RSS_2}{n - p2}\right)}$$

where RSS_i is the residual sum of squares of model i. Under the null hypothesis (model 2 does not provide a significantly better fit), this quantity should follow a statistic

distribution called the F distribution, and so its significance can be evaluated as a function of the available degrees of freedom.

Chapter 2: Material and methods

The project consisted of two different experiments: parameters sequence optimization and functional study. Then, the first experiment can be split in three steps, which includes TE optimization, slice tilt optimization and evaluation the most appropriated spatial resolution and head-coil. The first and second parts demonstrated the predicted dependence of the functional signal dropout in several brain regions induced by the TE value and the slice tilt. The third part was designed to assess the effect of the spatial resolution or the head-coil on the activation maps. The second part investigated whether the findings in the first part, allow BOLD signal recovering in the brain stem in an fMRI visual experiment. In this functional study several methods were developed to improve the functional contrast in the activation maps during visual stimuli.

2.1 MRI data acquisition

Separate measures were conducted for the two parts of the project. They were carried out using different devices. Scanner sequence optimization required just the use of the scanner. On the other hand the functional experiment required stimulus presentation devices inside the scanner room, besides eye tracker to measure the pupil position, electrocardiogram and respiration belt. Important is that these additional component are MRI compatible for the users safety and for their proper function. For this reason, experimenters must be trained MR safety and use before participating in these studies.

2.1.1 Scanner, hardware and software.

The whole study was carried out in the Laboratory for Social and Neuronal System Research (SNS Lab). MRI images were obtained with a Philips Achieva 3T whole-body scanner. The scanner is equipped with Philips 8-channel head coil and 16-channel head and neck coils as well as wrap-around surface coils. Other peripheral equipment used in the study includes LCD back-projection system, an remote eye-tracking system and devices for the recording of peripheral physiology, such as heart-beat and respiration. The softwares used in this study includes *SPM8* (Wellcome Trust Centre for Neuroimaging, London, UK) to perform the data analyses, *etc2asm* (script by Eye-Link) to convert file logged by Eye-Link in file MatLab compatible, *MRIcro* (Neuropsychology Lab, Atlanta, USA) to view the MRI images and *MatLab R2010b* (The MathWorks Natick, MA, USA) to create custom-made script for data analysis.

2.1.2 Volunteer recruiting and preparation

The volunteers were recruited via email advertisements sent to students of University of Zurich or ETH. They provided informed consent prior to participating signing a document explaining the standard procedures of an MRI study. Furthermore it was requested them to fill a security questionnaire to exclude individuals with history of claustrophobia or anxiety, neuronal disturbs (e.g. previous injury to the brain), tattoos, or any MRI safety risk (e.g. implants, artificial limps, pacemaker).

In each experimental session the subjects were paced supine in the scanner and wore ear plugs and headphones to limit the noise disturbance. An emergency bell

enabled to contact with the control room at any time. Foam pads were added between their head and the head-coil to restrict head movements. During each scan run, subjects were requested to remain as still as possible. In the functional experiment ECG and respiration detector were placed on the subject's body. The four ECG electrodes were places in the chest following the basic rules and the pneumatic sensor was positioned around the abdomen. Both devices were connected to the scanner. Furthermore, the stimulus was projected at the rear of the scanner on a translucide screen positioned at the head side on the end of the scanner bore. The subject viewed the screen via a mirror fixed on the top of the head-coil.

Before the dynamic images acquisition, localizer images were acquired for each subject in three orthogonal planes. This initial acquisition gives the anatomical reference for manual orientation of the FOV. Further, at the start of each experimental run the eye-tracker was calibrated. The calibrations consist in letting the subject stare points with a defined positions on the stimulus screen.

2.1.3 OKN generation and experimental design

During the fMRI experiment the stimulus was presented in a block design. This valuable technique is often used in fMRI field due to the robustness of the results, increased statistical power and relatively large BOLD signal change related to baseline *(Amaro and Barker 2006)*. Block design is a category of paradigm based on maintaining for a determined duration the subject's cognitive state and engagement in a task. Stimuli are presented in alternated sets with different epochs, during which a particular condition is presented. In this experiment an alternation of two conditions, called 'A-B block' design, was employed, where in the task condition (A block) there is an optokinetic stimulation and in the rest condition (B block) a white cross is plotted on a dark screen. All block share the same basic on-off pattern with a period of duration equal to 22 second. Twelve cycles were used, a cycle corresponds to two epochs of each condition. The experiment thus created is shown in the figure 9.
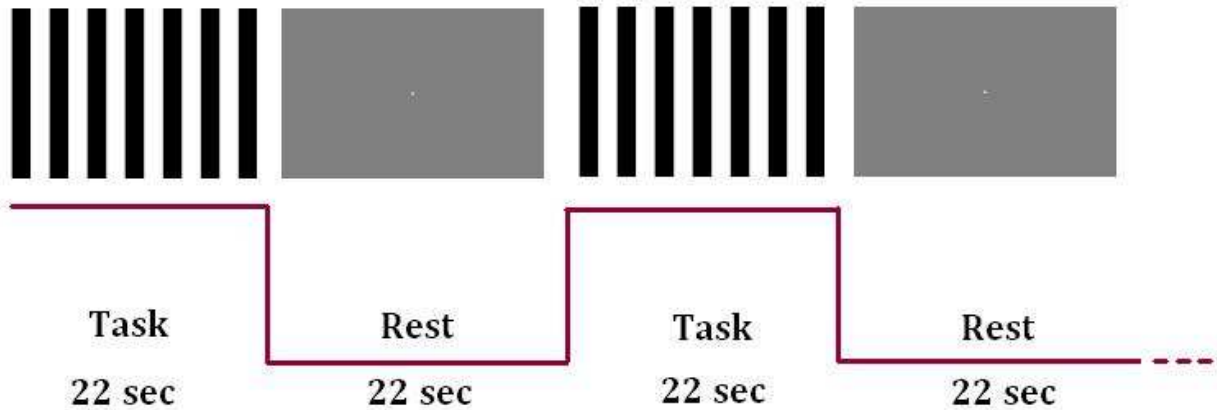
Figure 9 Experimental block design. Time series used to evoke BOLD activation in the visual system in functional experiments. During the task period OKN is performed, as in the rest periods a small with cross is projected on a dark background. Each single cycle (Task-Rest) is repeated 12 times.

The optokinectic stimulation consists in 14 horizontal (or 10 vertical) black and white stripes of identical width. They move with velocity of 8 degree/second in the same direction and orientation during a whole run. The stimulus pattern has been created using *Psychophysics Toolbox*, a free set of *MatLab (The MathWorks, Natick, MA, USA)* and uploaded in a computer connected with the projector, with the Eye-Tracker and with a device that receives the triggers from the scanner.

2.2 Optimization acquisition sequence

The first part of the project was dedicated to the development of an acquisition sequence suitable for functional studies. This aim was achieved step by step evaluated experimentally how a parameter or a certain device (e.g. head coil) influences the quality of the signal measured. A method was sought to optimize these factors. The experimental results and theoretical verification presented in these steps were also used for improving the acquisition strategies in the next experiments.

2.3 TE optimization

In this session four volunteers took part to the measurements. The necessity to measure more than one subject was arose after the data analyses for the first data set, when the results appeared very influenced by the noise. Thus, it was useful acquired more data set to make the average between the subjects and decrease noise. This

choice led to change the post processing of the data and introduced the normalization of each brain volume to be able to merge the data from different subject.

2.3.1 Measurement sequence

To assess how the signal in EPI and GRASE vary due to the echo time used, single shot EPI and GRASE images with different TE were recorded. A proper range of seven TE values was considered for each technique:

- TE (ms) = [16, 24, 32, 36, 40, 50, 58] for GE-EPI;
- TE (ms) = [70, 80, 85, 90, 100, 110, 125] for GRASE;

A total of 50 volumes in condition of resting state were measured for each acquisition sequence and subject. For both the techniques SENSE image reconstruction was used for accelerate the acquisitions. The other parameters were: 18 oblique transverse slices tilted by() and 3 mm isotopic dimensions, gap between slices = 1 mm, FOV = 192x192 mm, TR = 1.5 s, and flip angle = 90°. In beginning of each sequence five dummy scans were added to avoid non-equilibrium effects; thus, after that a steady state signal was assumed. These do not gives images, hence they are not in the data set to analyze.

2.3.2 Data analysis

After conversion in *Analyze* format, volumes acquired at different TE were corrected for the head motion and normalized. To direct comparison of the results from different volunteers the first of them was considered as template. The first step was to estimate the optimal parameter to perform the matching of the anatomical images to the template, using the same smoothing for both volumes (8 mm). Then the EPI magnitude images were registered using the parameter derived from the normalization of the structural scan. In this phase the option *'preserve concentration'* was selected to preserve the intensity of the original images and the voxel size was fixed to 3 x 3 x 3 mm to maintain the original dimensions. Finally, the normalized images were coregistered on an functional volume of the first subject to obtain functional images with the same dimension, same voxel size and orientation, for all data sets. The same post-processing was done for each subjects except for the first, whose images have only been realigned.

The TE maps were calculated to assess whether an optimization of time echo can maximize the BOLD contrast to noise ratio (CNR) in the brainstem area and nearby regions, such as orbitofrontal cortex (OFC) and temporal lode. A binary mask was built for each TE value at a threshold of 10% of the relative voxel intensity. The first volume of each data set was used to calculate the mask, which was applied to the other volumes. For the voxels inside the mask an statistical analyses was carried out using an approach presented in (Poser, Versluis et al. 2006). In the following demonstration the contribution to the effective transverse relaxation time $T_2^* = 1/R_2^*$ which arise from microscopic gradients is considered. The intensity of a signal received from a single voxel depends even of *TE* and can be expressed in a general form as

$$S = S_0 \cdot h(TE) \cdot \exp\left(-TE \cdot R_2^*\right)$$

where the exponential component describes the BOLD spin dephasing caused by the susceptibility difference between oxy- and deoxygenated hemoglobin (Yablonskiy and Haacke 1994). The term h(TE) incorporates T_2 decay and any other time-dependent modulation of the signal decay curve caused by inhomogeneities in the main magnetic field that are unrelated to the BOLD effect. Since BOLD contrast as a function in TE is proportional to the signal change per unit change in $R_{2(BOLD)}^*$; where $R_{2(BOLD)}^*$ is the baseline value, considered in this study the value of R_2^* during the resting state. On the other words, the BOLD effect causes a local change ΔR_2^* of the effective transverse relaxation time which leads to an intensity changes ΔS. Thus, it is necessary to maximize the rate $\Delta S / \Delta R_2^*$ to increase the fMRI signal. To this aim, from the above can be expressed the differential:

$$\frac{dS}{dR_{2(BOLD)}^*} = -TE \cdot S_0 \cdot h(TE) \cdot \exp\left(-TE \cdot R_{2(BOLD)}^*\right) = -S \cdot TE$$

This equation provides a measure of BOLD sensitivity, which if h(TE) represents a purely exponential decay, is well known to be maximal at TE=T_2^*. From the expression above is possible to derive the *differential CNR* (*dCNR*) :

$$dCNR = \frac{S \cdot TE}{\sigma} = SNR \cdot TE$$

where S is the intensity of the signal and σ in this study is the standard deviation (SD) of the time series. This parameter enables to quantify the BOLD sensitivity (BS) in proportion to the noise of a dynamic acquisition; i.e. how sensitive to signal variations caused by field inhomogeneities in a time series of functional images.

SNR was calculated for each voxel as the mean of the time series divided the standard deviation of the time series. Thus, it is possible write the equation above as

$$dCNR_{m,n} = \frac{meanS_{m,n}(t) \cdot TE_n}{sdS_{m,n}(t)} = SNR_{m,n} \cdot TE_n$$

here, m=1,…,M where M is the number of voxels within the mask; n=1,…,N where N=7 is the number of TE values; and t=1,…,T where T=50 is the number of volumes acquired. The differential CNR (called also simply CNR) calculate by this equation has been used in this experiment to assess the sensitivity optimization. Thus, for each data set acquired by different TE a CNR map was obtained. Moreover for all subjects the CNR maps were compared in each voxel to create the optimal TE maps. The voxel in the TE maps contains an integer from 0 to 7, to indicate the TE value index that maximizes the CNR. Finally, the TE maps of different subjects were merged and, for easer interpretation, this map was converted in format analyze and plotted on the structural images (template), using MRIcro.

The further data analysis consisted of investigation of the CNR trend, dependent to the TE values. To localize the analysis in the brainstem 14 ROIs were manually create using MRIcro. One circular area with diameter sufficient for cover the brainstem (3-4 mm) was drawn for each slice, except for the two below and the two above which were out of the volume of interest. Then the merged CNR map were overlaid to the regions of interest and the average over all voxels inside the ROIs was calculated, for each TE. Finally, the results traces were averaged over all ROIs to assess the time echo parameter that maximize the CNR in the whole brainstem.

2.4 Slice tilt optimization

The purpose of this session was to investigate the influence of the slices tilt angle on the signal losses in the brainstem due to the signal dropout near critical areas, such as orbitofrontal cortex and temporal lobes. CNR maps were calculated from functional images with different slice orientation, acquired with a standard single-shot EPI sequence. One volunteer was scanned using seven different angles of the transversal slices. The head was placed in a comfortable position corresponding approximately to a vertical orientation of the posterior to anterior axis. The subject was requested to relax (to simulate a resting state) and keep the head still.

2.4.1 Measurement sequence

A series of 50 single-shot EPI volumes was acquired for each angle to reduce, the random noise during the analysis step. For each volume 18 transversal slices were measured with a localized FOV of 192 x 192 mm, as showed in Figure 10. The voxel size was 3 x 3 x 3 mm and the other parameters: TR = 1500 ms, TE = 36 ms, gap of 0.5 mm and a flip angle of 90°. The orientation angle α were 44°, 30°, 15°, 0°, -15°, -30° and -44°. These limits of slice tilt were considered to avoid that the acquisition plane changes from transversal to coronal The slice orientation correspond to a positive value of α when the field of view in the sagittal plane rotates from transversal to coronal orientation counterclockwise. Further, the following conventions are assumed: for an acquisition with transverse imaging slice orientation, the gradient directions are read (right to left), phase (anterior to posterior), and slice (foot to head).
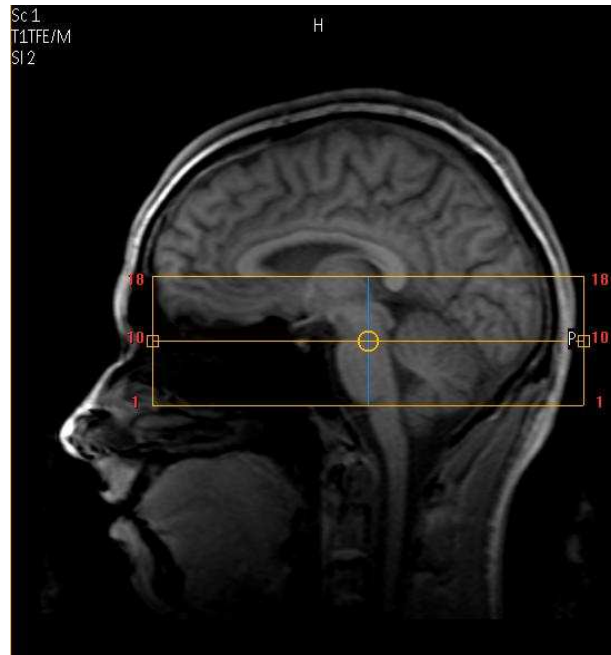
Figure 10. Example of the localized FOV in the sagittal plane, with orientation angle of zero degree. The volume of acquisition is centered on the brainstem and positioned in order to contain the cerebellum and the V1 in the horizontal dimension and the whole brainstem, from the medulla to the SC in the vertical dimension.

2.4.2 Data analysis

Each time series of images acquired from the same angle was realigned to remove movement artifacts, using a least squares approach and a six parameter spatial transformation. The first image was used as a reference to which all other scans were realigned. Moreover, before performing the realignment the images were smoothed with a Gaussian smoothing kernel (FWHM = 5 mm). Second, another rigid transformation was performed to obtain the tilted volumes in the horizontal plane. Six series of functional volumes measured by slices orientation different to zero were thus coregistered on the horizontal images. At the end of this step the images have the same dimensions, voxel sizes and orientation, this enable to compare them in the next analysis.

For all data sets, a mask was created from the first volume using a threshold of 10% of the normalized signal intensity. The mask was applied on each volume acquired by the same slices orientation and CNR maps were calculated for the voxel underneath the threshold, using the same equation as in the previous session:

$$dCNR_m = \frac{meanS_m(t) \cdot TE}{sdS_m(t)},$$

where m is the voxel considered and t represent the time series of 50 volumes. The echo time was constant for each acquisition. The dropout of the signal (the signal to noise ratio) is measured relative to the slices' orientation. Finally, the CNR maps were normalized on the maximum values found. This enable a direct comparison between the values calculated. From the functional images obtained by zero degree, 14 ROI were manually created using MRIcro. The ROIs were drawn of circular shape and with a diameter (3-4 mm) sufficient to cover the brain stem area. Four slices located in the beginning and in the end of the volume of acquisition were excluded because they did not show anatomical areas of interest. The masks were applied in the CNR maps and for 14 slices was calculated the mean using the voxels within the ROI.

2.5 Spatial resolution and different head coil

Before define the protocol for the functional study, two experimental sessions were used to evaluate the influence of the spatial resolution and head coil on the functional data. Three different kinds of head-coil were tested: 8 channels head coils, 16 channels head coils (Volume coils) and Surface coils The comparison between the different coils was carried out to investigate whether the Volume coils provides a uniform distribution of the energy in the brainstem zone and thus ensure a signal intensity major, and also whether the Surface coil provides higher SNR in the investigated area.

Different values of spatial resolution were investigated to verify whether the optimization of this parameter reduces the susceptibility effect *(Deichmann, Josephs et al. 2002)* and therefore leads to greater signal in the functional images. It has been demonstrate that a smaller voxel size can increase the BOLD signal changes, due to the reduction of partial volume effect (Frahm, Merboldt et al. 1993). Nevertheless, to use a high resolution lead to acquired more samples in the same FOV and hence may lead to decrease the SNR.

2.5.1 Measurement sequence

For both investigations, fMRI visual studies were carried out. OKN was used to raise the BOLD signal in the neuronal visual system. The purposes were to use the same parameters and conditions to be able compare the features of the different techniques, but during the experimental preparation a few complications are arisen. For the volume coil a smaller mirror was necessary to use because of the dimensions of the coil, furthermore the experimental with the Surface coil was dismissed because it is not possible to use the SENSE images reconstruction. The acquisitions have been carried on with the 8 channels head coil and the 16 channels head coil. Three subjects took part of this experiment. For each of them, 337 EPI volumes were acquired with both coils and using the SENSE image reconstruction. The other parameters were : 17 transversals slices with 3 isometric voxel dimensions, slice tilt = 20°, gap = 0.05, TR = 1.5 ms, TE= 36 ms, flip angle = 90°, FOV = 192x192 mm. For the anatomical reference, a high resolution IR T1-weighted volume was acquired in the same session, using the parameters: 24 transversal slice with thickness 4 mm and FOV=230 x 184 mm, TR=2000 ms, TE=20 ms and angle=120°.

One subject was scanned for the spatial resolution investigation with a single-shot EPI sequence and the 8 channels head coil. Two sequences of 337 volumes and 18 slices each, were acquired with different spatial resolution: 2 mm isometric voxel and 3 mm isometric voxel. All other EPI parameters were identical to those from the sequence measured with different coil. Furthermore, an anatomical image was acquired as above. Only one subject involved in this phase of the study because the results found in this first session were considered enough for the intended purpose.

2.5.2 Data analysis

The same image pre-processing has been done for the data acquired in this session. The time series of EPI images were realigned to correct for rigid-body motion and distortion, using a spatial transformation. Moreover each image was spatial smoothed by a Gaussian smoothing with a 5 mm kernel. All functional images were registered on the T1-weithed images by coregistration. Then, for the statistical analyses a general linear model (GLM) was applied to time series of each voxel. The block

experimental design was convolved with the Canonical Hemodynamic Response Function (HRF) to simulate the BOLD signal during the experimental. Temporal correlations were modeled by a first order autoregressive model (AR). The parameters of linear model thus created were estimated using the classical (Restricted Maximum Likelihood) algorithm. The activation maps were determined by testing for significant positive correlation of the voxel signal with the model response. Using a statistical method (t-test) a parameter (T) was estimated for each voxel. The threshold for consider the voxel activated was fixed using the uncorrected threshold, p=0.001 (corresponds to t=3.12).

2.6 Functional brainstem study

Ten students with a mean age of 21 years (age range: 19-24) participated in the functional study. Two subjects who were not able to perform the task for several causes were excluded from the study. Realize this problem was possible in real time from the control room due to the projection on a screen of eye image and of eye movements' tracking. Moreover, in the end of the acquisition one of them confirmed the difficulty to perform the stimulus because of the screen was much bright during the task block. In the second case the eye-tracker did not work properly. The device missed the pupil position for most of the experiment duration.

The subjects were requested to follow the stripes during the task (OKN) and look passively at the screen during the rest (a small white cross on a dark screen). The block paradigm alternates first the task periods and then the rest periods for twelve repetition. The duration of each of them was 21 seconds for a total of 5 minutes and 35 seconds. The whole experimental session was composed to four functional acquisition with different stripes movement direction and either one or two anatomical acquisition. The four directions were: from right to left (called *left*), from left to right (called *right*), from down to up (called *up*) and from up to down (called *down*). But, in three sessions was not possible measure using the four direction because of was spent much time during the experimental set up, thus the available time has expired before the end of the measurement.

In each functional acquisition, eye position and pupil diameter were monitored on line via a video screen and recorded at 500 Hz by the eye-tracking system. In additional, cardiac and respiratory functions were monitored during each functional scan run. These data were sampled at a frequency of 500 Hz and logged by the scanner's physiological monitoring unit. To ensure accuracy in the relative timing of physiological data and volumes acquisition, the recorder of the heart beat and respiration rate starts by a trigger from the scanner.

2.6.1 Measurement sequence

During the whole execution of the experimental design 337 volumes were acquired. The functional images were measured using 8 channels head coil and a T2*-weighted EPI single-shot sequence an echo time of 36 ms and a repetition time of 1.5 ms. Eighteen transversal slices tilted by 25° were acquired from a FOV of 192x192 mm with 3 mm isometric voxel. The other EPI sequence parameters were: gap between slice = 0.5 mm and flip angle = 90°. The techniques SENSE image reconstruction was used for accelerate the acquisition. Further, five dummy scan were added in beginning of the sequence to avoid non-equilibrium effect and to can reach the stability state. After this scans the scanner start to recorder the volumes and simultaneously sends a trigger to the stimuli computer which start the experimental design. By the reference image was possible the position and orientation of the FOV was manually adjust for each subject at the start of the first dynamic sequence. In the sagittal plane the FOV was inclined of 23° from the default position and positioned how the whole brainstem (from the medulla to the SC) was within.

For anatomical reference were acquired T1-weithed images using two different techniques: inversion recovery (IR) T1-weighted 2D and high resolution T1-weighted 3D. The first acquisition sequence was used from the beginning of the functional experiment for all subjects; it has a high resolution (0.6 x 0.7 mm) in the slice plane but a low resolution (4 mm) in direction perpendicular to the slices. The second acquisition sequence has a voxel dimension of 1.2 x 1 x 1 mm and it was used to be able to display the whole head volume using an analyze viewer of medical images, such as *MRIcro*. The other IR T1-weighted parameters were: 24 transverse slices with size 230 x 184 mm,

TR=2000 ms, TE=20 ms and angle=120°. Instead, the 3D T1_weighted parameters were: 90 transversal slides with size 176 x 176 mm, TR=8.3 ms, TE=4.6 ms and flip angle=8°.

2.6.2 Data analysis

The first step to analyze the eye-tracker data was to convert the file saved by Eye-Link in a format compatible with MatLab, using the software 'edf2asc'. In this file, in addition to the position end diameter of the pupil, were recorded also the time series, the instants in the time when the experimental blocks starts and the instants in the time when the periods of signal loss, starts and end. From this information regression function were obtained. These regression functions were used either as effects of interest or as effects of no interest in the setting up the design matrix to create a linear model. The times at which the experiment starts was used to model a reference function to describe the experimental design. The information about the periods of signal loss were used to create two regressions functions; one of them to describe the events in which the subject blinks and the other one to describe the events in which the subject closes his eyes. To decide whether a period of signal loss must be considered a blink was fixed a threshold of 200 msec. Furthermore, two-dimensional position data were reconstructed in the periods of signal loss by interpolation and subsequently low-pass filtered. The pupil position in the same direction of the stimulus was used to build a regression function. A script matlab was written to analyze the eye-Tracker data; it allows to decide which parameters using to create the linear model to describe the data with SPM and it create a file 'condition.mat' that enable to upload the several regression functions during the set up the SPM design matrix in one go.

The heart beat and the respiratory signals were used to performed an retrospective physiological motion compensation performing a method presented in (Glover, Li et al. 2000). This approach called RETROICOR assumes that the cardiac and respiratory signal are semi-periodic and the components of these processes are contained in the time series of interest in the voxel. The analysis program was adapted for this study from an existing analysis software, which has been tested in a study of brainstem fMRI at 7T (Kasper 2009). This MatLab script in accordance to (Harvey, Pattinson et al. 2008) creates the regressors from the physiological noise components;

which are given by a low-order Fourier series expanded in terms of cardiac phase (4° order) and respiratory phase (3° order). Each sine, cosine and multiplicative term (four terms) was fitted to the image data by under-sample (on) number of volumes acquired, as well a total of eighteen signals were applied as regressors to removing correlated components present in the fMRI data. Figure 11 shows the eighteen physiological terms included in the GLM basis set. The required input for the explained method include recordings of the peripheral pulse data, the relative time of each slice acquisition and the parameter of the acquisition sequence. This information was logged in the 'physiological' file and in the 'parameter' file by scanner.
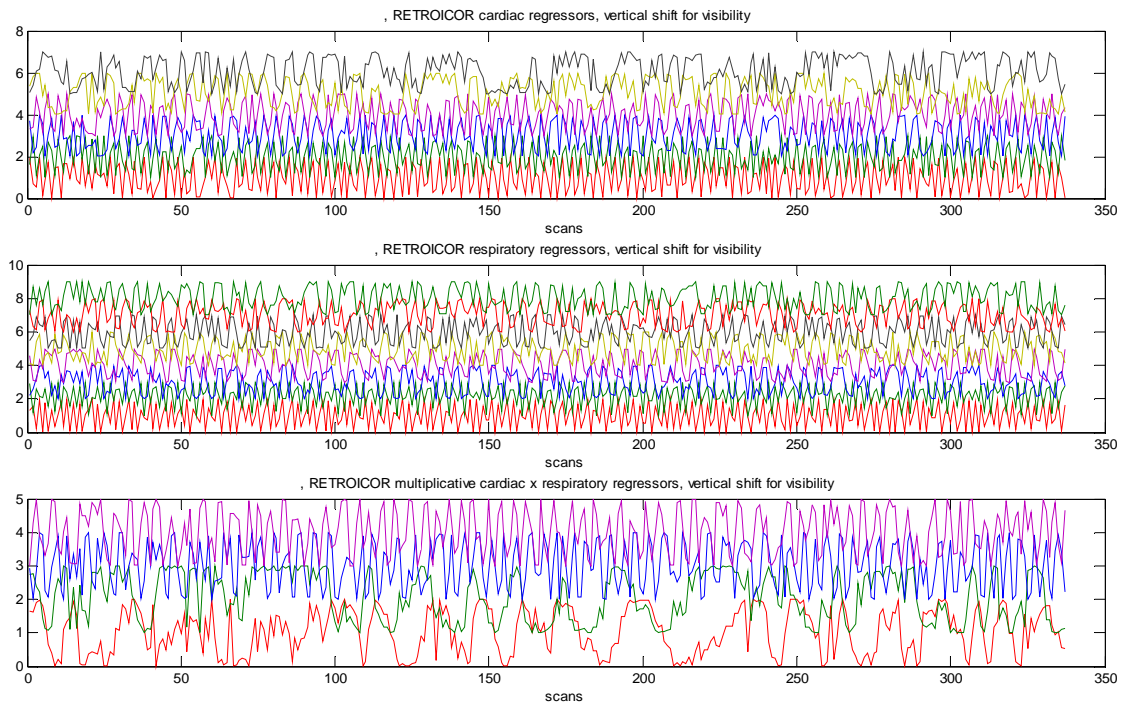
Figure 11. Physiological regressors included in the GLM basis set as effects of no interest. These terms are calculated by Fourier series expanded of cardiac phase (3° order) and of respiratory (4° order), plus the multiplicative term.

Initially, the data sets measured were converted in 'Analyze' format to permit to carry on the preprocessing using SPM8. Afterwards, the time series of functional images acquired in each experimental run were realigned to correct for the rigid body motion, using the first image as a reference. Moreover, the functional images were smoothed by

a Gaussian smoothing using a 5 mm kernel. The parameters estimated by this transformation were checked and saved for each session, to realize when a subject showed a significant head movement. All subject showed translations in the three principal directions lower than 4mm and rotations around the three axes lower than 4°. Subsequently the functional images were registered on the anatomical volume, by a rigid-body transformation. Finally, the coregistration was checked for each run using the function 'check' of SPM8. The data thus preprocessed were used to the single subject analysis.

The purpose of the first fMRI data analysis was to canvass whether the additional regressors built with signal loss information can compensate the noise components of the signal, related with blink or phase of eyes closed. For the statistical analyses a general linear model was applied to the time series of each voxel. Two different model design matrix were specified for each data set. First step to build the model was to define the conditions, which are convolved with the canonical HRF to account for the delayed and dispersed blood flow response. Eighteen covariates per scanned volume, derived from each condition, were included in the matrix design. The conditions defined during the GLM set up contained different information; in the first model the experimental design (block information), was used. On the other hand, in the second model in addition to the block information the blink and eyes closed information was added, for a total of three conditions. The second step to build the model was to define the regressors. This setting is the same for both the models and consists on a matrix contained the eighteen physiological terms. The error correlation assumed in each models was modeled by a first order autoregressive model. The design matrixes of the models thus achieved are shown in Figure 12. Finally, each linear model was estimated using Restricted Maximum Likelihood.
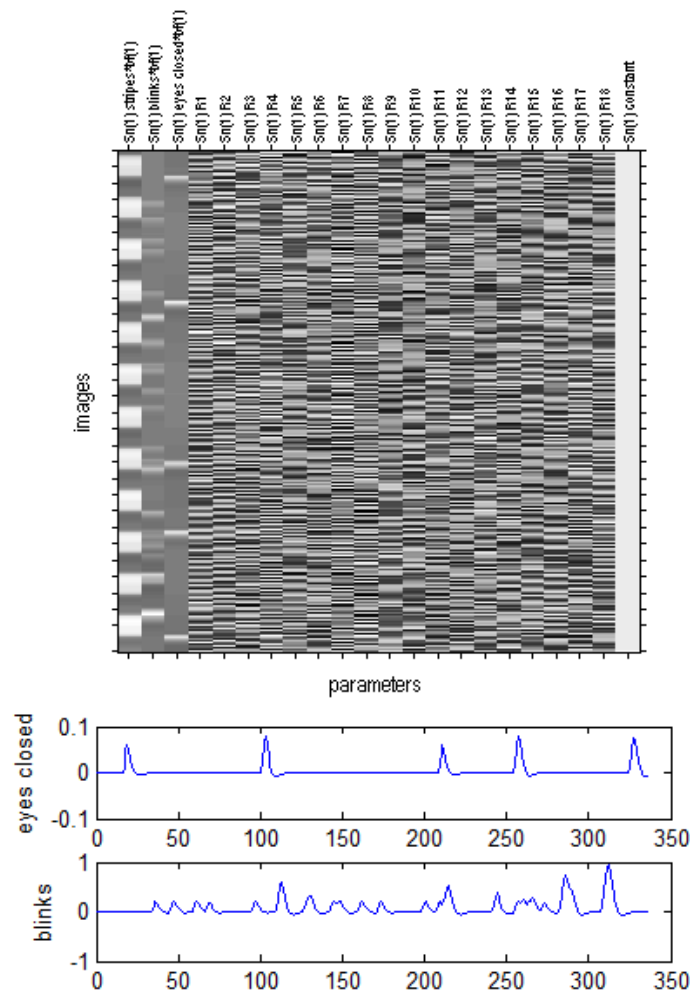
Figure 12. The image above shows a design matrix for the general linear model, how it appear after its creation with SPM. The matrix is achieved by including blink and eye closed regressors (cloumns 2, 3), and 18 RETROICOR terms (columns 4 : 21) in the GLM basis set. Here, the basis model is considered the blocked effect (column 1) and the constant function (column 22). The signals in evidence are the blink and eyes closed regressors resampled and convolved with HRF.

Activated voxels were determined by testing when the time series in a voxel increase due to first condition (block design). A statistical test (t-test) was used for this analysis. *T* values were estimate for each voxel and the significant threshold to activation passing was fixed to *P* = 0.001 (uncorrected threshold), that corresponds to *t* = 3.11. Different models were compared between each other to see which method achieves major activation in the zones of interest. This investigation was carried out using the resulting statistics maps (T maps) calculated for each GLM. Using the software of imaging MRIcro, the T maps were overly on the T1-wieghted images and for each region of interest a mask was manually created. Six were the area of interest, which overlap with: left and

right superior culliculus (SC), left and right oculomotor nuclei (OMN) and left and right lateral geniculate nuclei (LGN). Thus for each subject were created six mask; except for two of them who did not show activation in the OMN. Using these masks were localized the same ROIs in the T maps of the first model and in the T map of the second model; for this voxel was calculated mean and standard deviation to compare the T values assessed for each model.

In addition to the method described above, a comparison between different models was done using F-test. This statistics test quantitatively describes how well a specific regressors added to the basic model improves the fit of the GLM on the data; in particular, in this investigation allows to quantitatively assess whether the signal loss information enables to compensate the noise terms related with blinks and phases of eyes closed. The estimated model built including the blink and eyes closed regressors was used for the test; it was compared with the base model. F-test was applied using an uncorrected threshold, P = 0.001. The same test was utilized for the whole brain and for each ROI created in the previous step. The number of voxels exceeding the threshold for the statistic test was than countered for each region considered and for each subject.

The purpose of the second fMRI data analyses was to investigate whether including the movement velocity in the design matrix can improve the GLM in a within-subject analysis. Use this information could help to compensate the delay between the start of the experimental block and the instant at which the subject start to perform the task. Velocity of motion was generated by derivative from the position of the eyes in the direction of the stimulus, which was previously reconstructed for the signal loss by interpolation. The achieved signal was then low-pass filtered to remove the peaks do not related with the movement caused by the task. To utilize the velocity as a condition (stimulus function) in the GLM the time series was then resampled at the acquisition time of each slice. This can be specify when building the design matrix specifying the design in seconds and set the microtime resolution to 18. SPM will build the regressor resampling the signal in input at the time series with unit $TR/18$. During the set up was tried also to use microtime resolution higher (e.g. 144 sample per scan) to minimize loss of information, but computation time request to generate the design matrix was too long. Finally, the resultant trace was convolved with the basis hemodynamic function by

first order convolution. This regressor was added to the design matrix, in addition to the experimental information, blink and eyes closed regressors and physiological regressors. Even though the signal loss information and the physiological noise are effect of no interest, by including these artifact in the design matrix reduces the residual errors, and hence improve the statistical analysis for the effects of interest. The whole model was estimate using the classical method (ReML).

To assess the effect of visual stimulus, as characterized by both block design and movement velocity, the F-contrasts was employed. Two contrasts were defined to asking which benefits entail the addition of a condition to the basic model built with the other condition. In the first test basic model is composed by the block information plus the regressors, instead in the second basic model is composed by velocity plus regressors. The results of the tests were compare visually and the voxels exceeding the fixed threshold (P = 0.001) were counted for each subject.

In the last phase of functional images analysis the goal was assess the activation maps for each subjects. For this activation study were investigated the time series of images used in the previous analysis plus other volumes measured with different stimulus directions. The images were pre-processed as described above. A general linear model was applied of each voxel with a design matrix selected on the strength of the finding achieved in the previous steps. T contract was utilized to the statistic t-maps and voxel exceeding the threshold of t>3.11 (corresponds to P<0.001) were considered significant.

Chapter 3: Results

3.1 TE optimization

In this stage, the purpose was to assess a optimal TE value for two different techniques of acquisition: GE-EPI and GRASE. Here was assessed how a different time echo used in the acquisition sequence can influence the quality of the functional signal. This analysis was in particular carried on for brainstem area. Besides another aim of the experiment was to investigate the dependence of the signal loss on the time echo TE, for the EPI sequence. CNR maps produced using time series of EPI images acquired with different TE are compared in the figure 13.
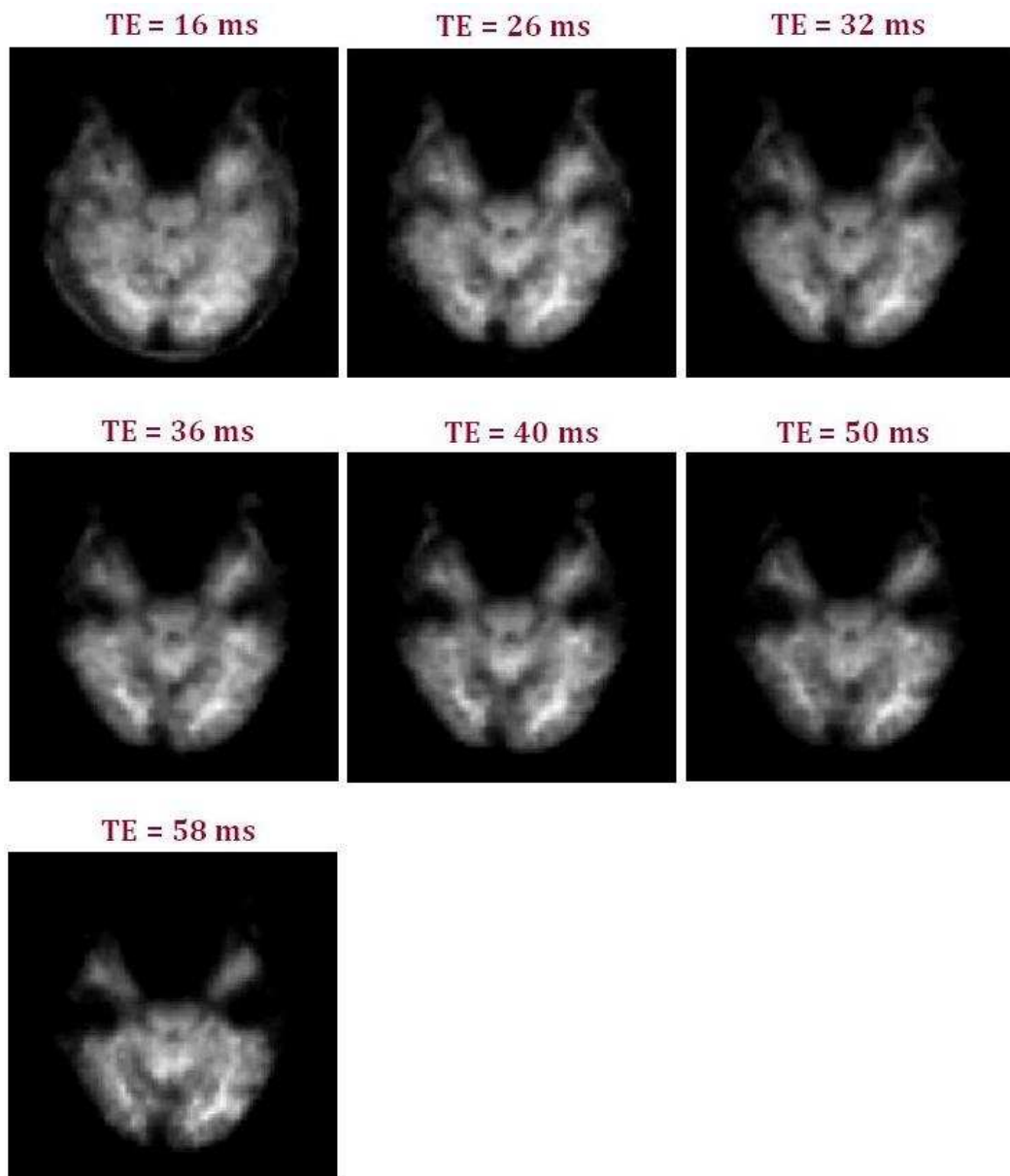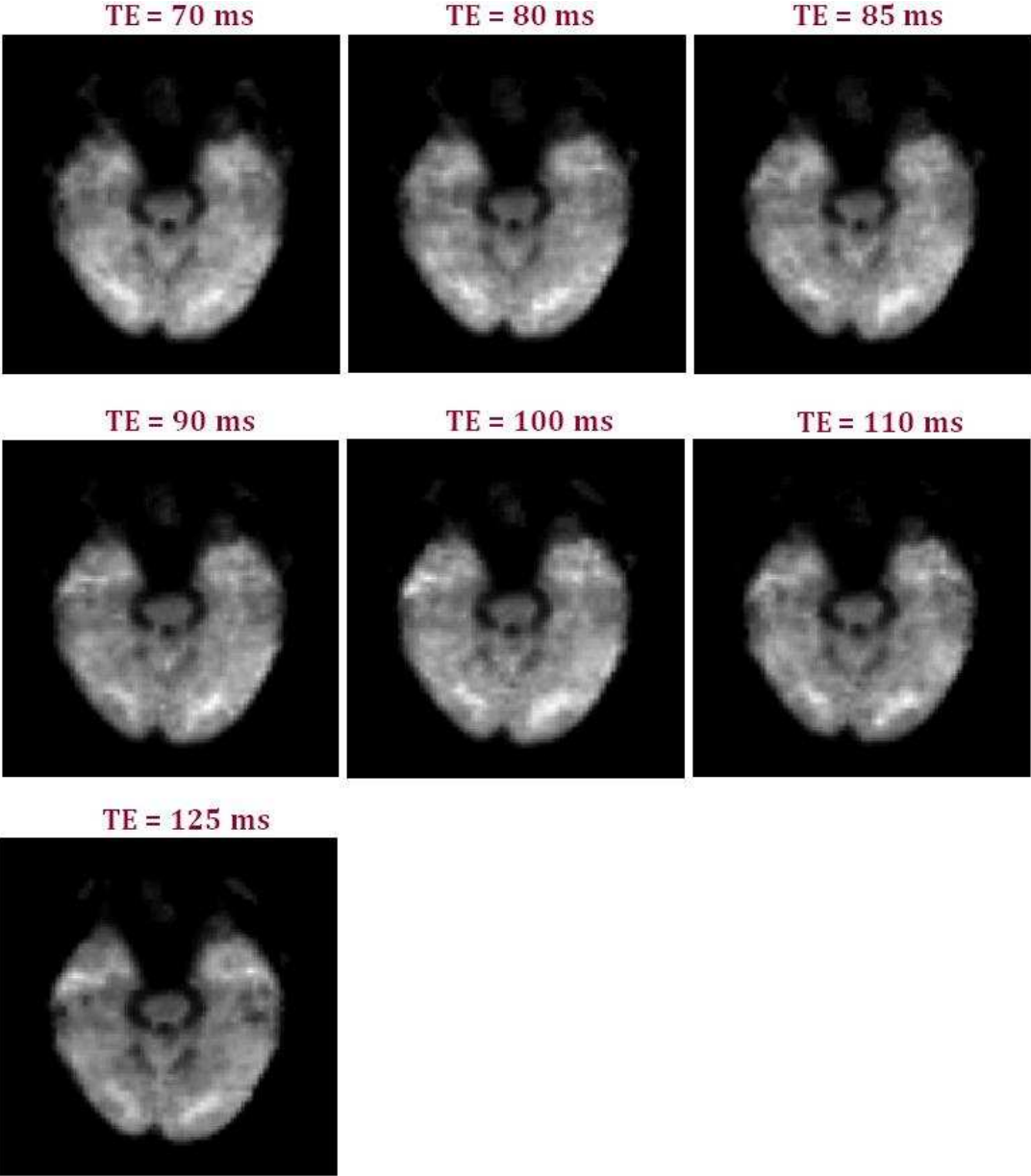
Figure 13. Averaged of CNR maps for time series of EPI images acquired with TE = 16, 26, 32, 36, 40, 50, 58 ms. The slice z = 30.8 mm(slice 9) plotted shows the region where the signal drops out.

CNR-maps represented are averaged over the subject for each different TE. The slice plotted was chosen to show the significant signal losses in the ventral frontal lobes and inferior medial temporal lobes, due to magnetic susceptibility artifacts resulting from the B0 field inhomogeneities present at the boundaries between brain tissues and the air-filled cavities. The comparison of the maps for each TE show the increased signal dropout in the critical zones as the time echo rises. In addition, for higher values of TE,

an increased CNR in the cerebellum and in the gray matter is shown. One of the possible methods that can be found in the literature (Scott, Allen et al. 2009) to compensate field inhomogeneities and to reduce this artifacts is to introduce a excitation pulse to provide a good recovery of signal. The GRASE technique is based on this methods and as is possible to see in the Figure 14, this techniques achieves to contain the signal dropout in the critical areas.

Figure 14. Averaged of CNR maps for time series of GRASE images acquired with TE = 70, 80, 85, 90, 100, 110, 125 ms. The slice z = 30.8 mm(slice 9) plotted was shows the region where the signal drops out.

The figure is arranged as the above (Figure 13), it shows the averaged CNR maps calculated from time series of GRASE images acquired with different TE. To investigate the artifacts induced by the air and the bones in the sinuses and auditory canals was considered the same transversal slice used for the previous representation. But, as can be seen in these images there is much less signal loss due to inhomogeneities, that leads to major CNR in the critical areas and more brain region are clearly visible.

The images shown (Fig 13 and 14) enable to verify the disadvantage of the EPI sequence and show a qualitative information about the signal measured with both techniques and the influence of time echo on artifacts. Furthermore, to optimize the time echo parameter the TE maps were calculated for both the technique. In Figure 15 is shows the TE map averaged over all subjects achieved from functional images acquired by EPI sequence.
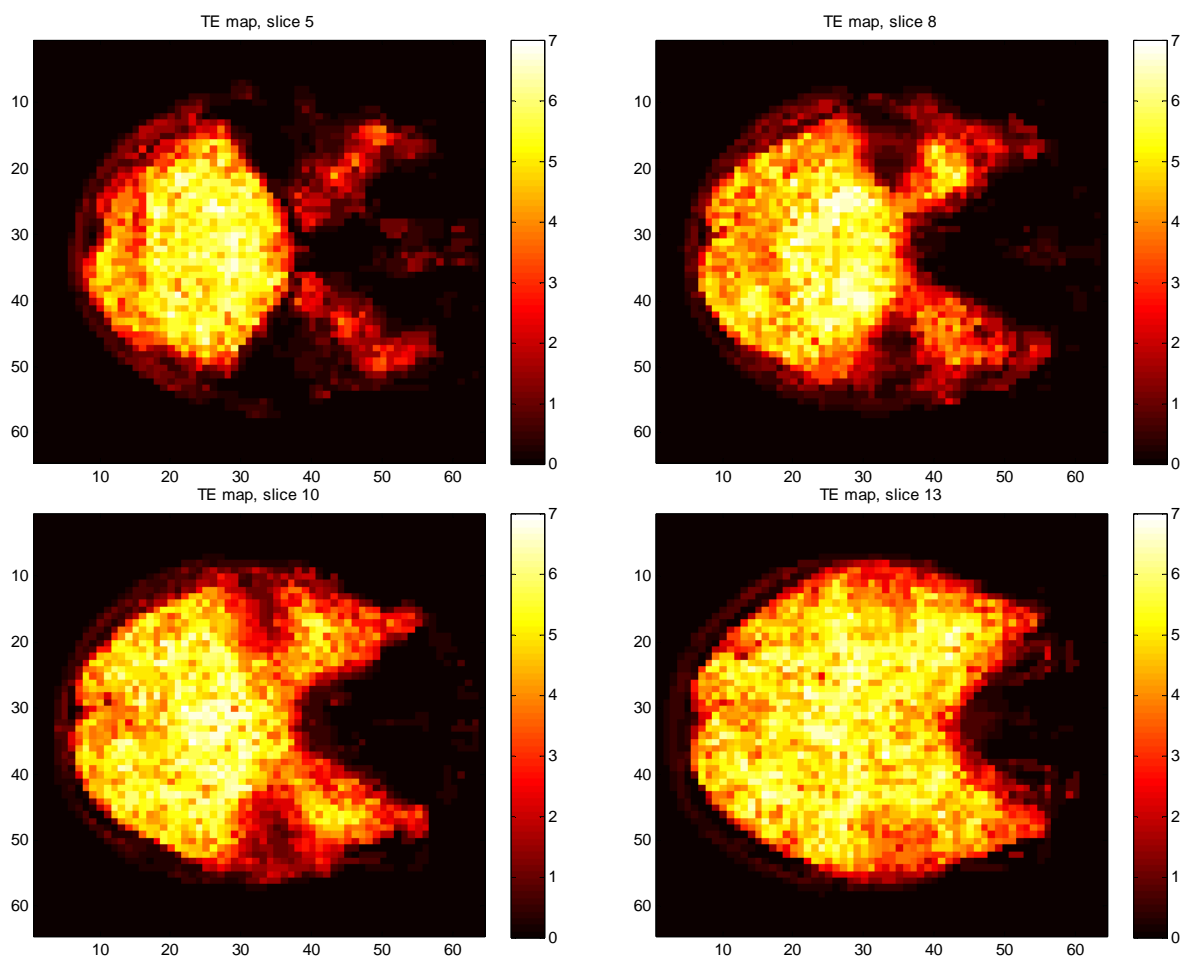
Figure 15. Slices 5, 8, 10,13 of TE map overlaid on the T1-whieted images. The TE map is averaged over all subjects. The scale displays the tones of color which matches to the 7 TE values used for EPI acquisition.

In this matrix the value of each voxel represent a number in a range from 0 and 7 by step of 0.25; where the 0 shows the background, besides units from 1 to 7 matches to the series of seven time echo used in each technique. The TE indicated in a voxel in the TE maps correspond to the time echo that maximize the CNR calculated for this voxel. In EPI sequence the time echo values used are 16, 26, 32, 36, 40, 50, 58 ms. The images were chosen to have information of the optimal TE in whole brain. All images shows that the maximum CNR in the areas subject to magnetic field inhomogeneities is ensure by lower TE values. Further, in the slices 5, 8, and 10 TE map indicates a TE = 36 ms to get the higher CNR around the brainstem in the sides near the temporal and frontal areas.
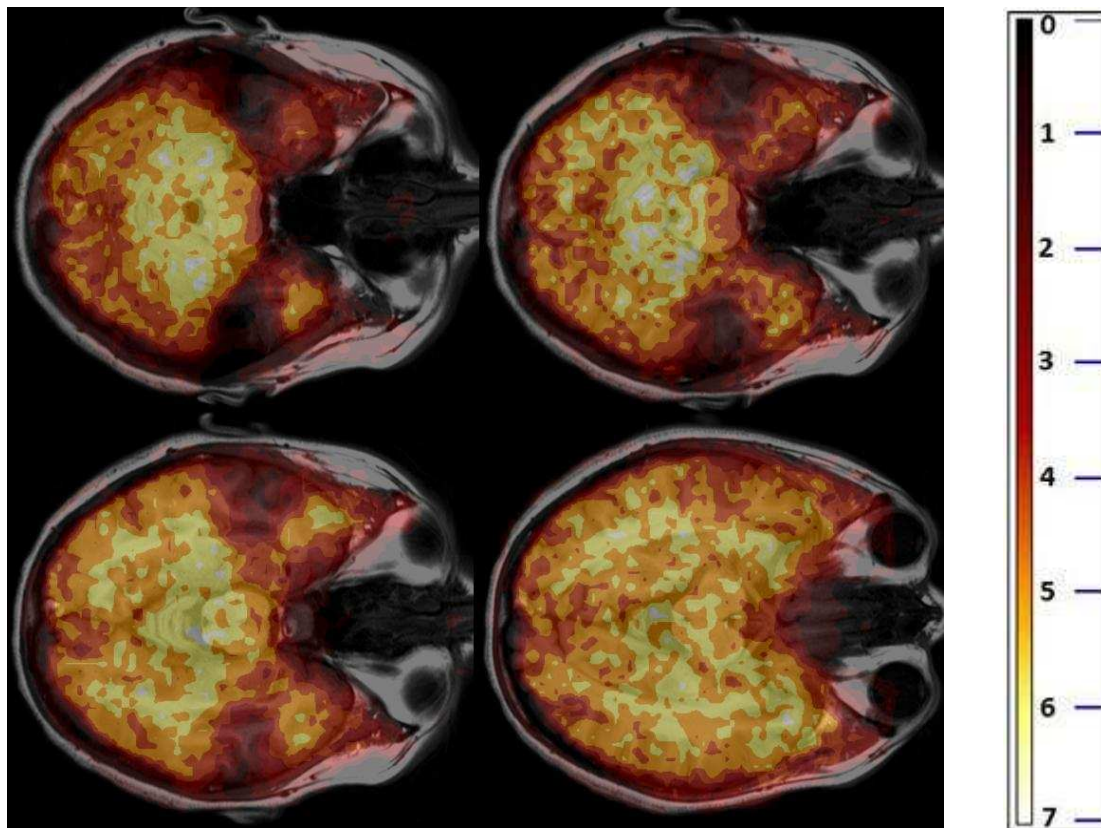
Figure 16. Merged TE map, calculated from the TE maps obtained for each subject. The possible voxels values range on a scale from 0 to 7 in steps of 0.25. Units 1 to 7 matches to the time echo used in the EPI sequence. Each voxel assumes value corresponding to the TE that maximize the CNR in that voxel.

Figure 16 allows to improve the anatomical information, here is displayed the TE map overlay atop the T1-whethed image. Thereby, from the lower slices (slice 5 and 8) it can be seen that in the anterior side of the brainstem the CNR is optimal for lower

values of TE (around 26 and 32 ms), where the contribution of inhomogeneities field by air-filled cavities gains influence. Besides, in the internal side and in the whole brainstem, when the contribution of critical zone is past (slice 13), the CNR is optimal for values of time echo around 40 and 50 ms. It is possible also to refer to the theory to verify the result, thus by this map is achievable the dependence of signal amplitude, and therefore, BOLD sensitivity on the physical characteristics of the tissue, such as relaxation time. In tissues with more water, such as cerebellum and white mater, where the time of relaxation (T2) is longer, a higher time echo value ensures a major CNR; instead in the tissues with less water, such as gray matter, where the time of relaxation is shorter, a lower time echo ensures a major CNR.

To localize the investigation, a ROI for each of fourteen slice was manually created around the brainstem. The ROIs were applied on the averaged CNR maps (over all subjects) calculated for each TE. The Figure 17 shows the values of the mean CNR in different ROIs, for each echo time.
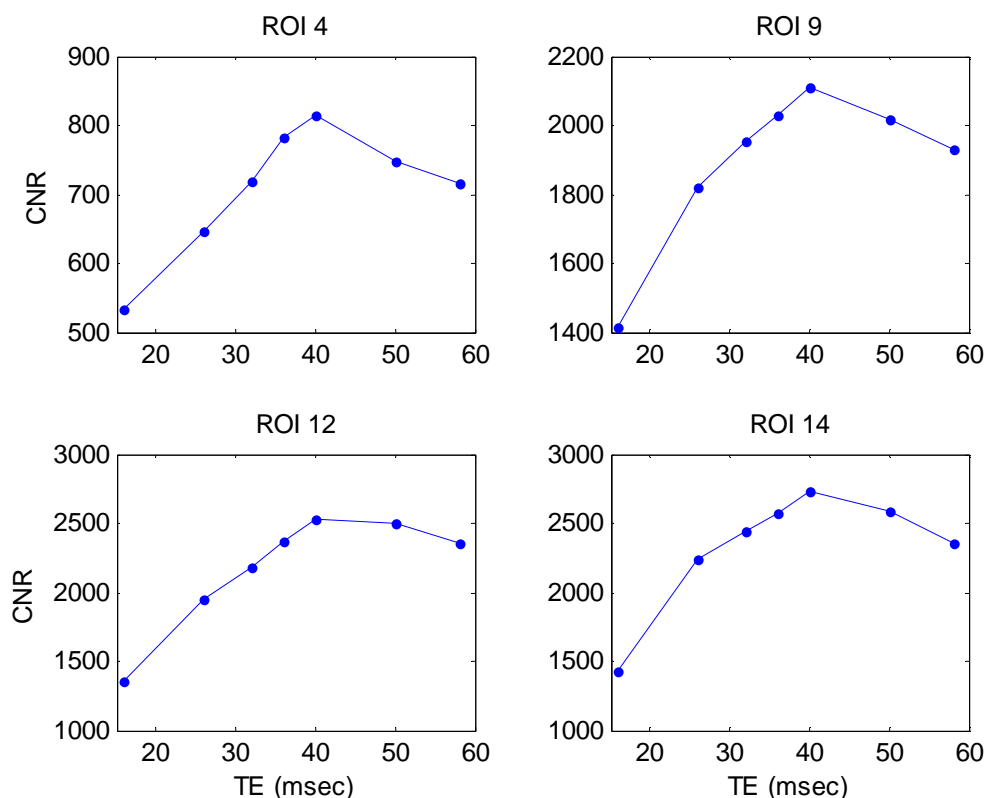
Figure 17. Plot of mean CNR in different ROIs, for each echo time. CNR maps were calculated from time series of EPI images acquired by TE = 16, 26, 32, 36, 40, 50, 58 ms. The considered ROIs matches to the slices 4, 9, 12, 14.

As can be seen from the charts, the trend of the CNR calculated for different TE is quite similar in the ROIs chosen, which are representative of the down part, the mid part and the top part of the brainstem. The CNR is maximal for TE around 40 ms; on the other hand the TE should be at least 32 ms because for lower values CNR decrease rapidly. Besides this, the decrease of CNR for values of TE higher than 50 ms suggests to consider values of echo times lower than this threshold. Figure 18 shows the mean CNR averaged over all subjects and regions of interest as a function of TE and compares these values with the fit of a non-linear model provided to the relation used to calculate the BOLD sensitivity.
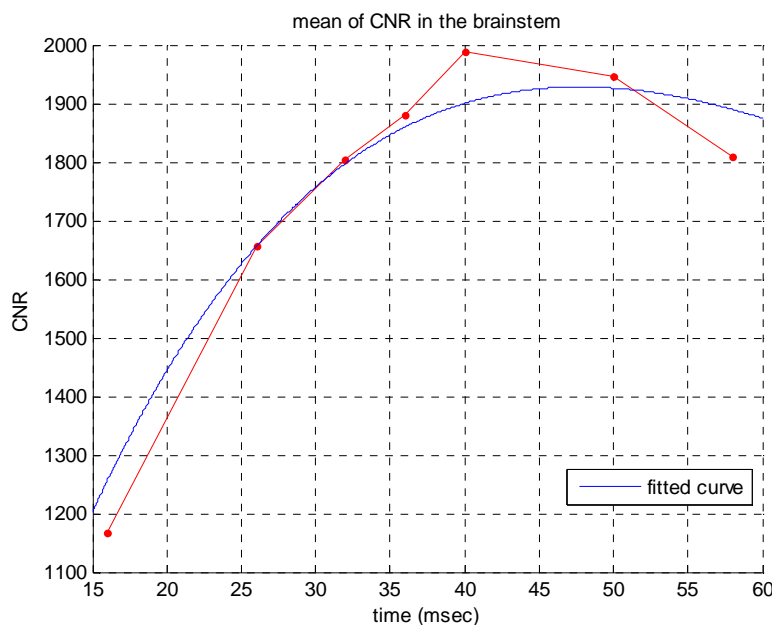
Figure 18. Contrast to noise ratio (CNR) dependence on TE for the whole brainstem, plus the fit of the model used to calculate the BOLD sensitivity. The CNR is derived from time series of single-shot EPI images with TE = 16, 26, 32, 36, 40, 50, 58. The predicted curve was achieved fitting the model $TE \cdot \rho \cdot \exp\left(-TE/T_2^*\right)$, on the CNR values; where ρ is a term that does not depend of T_2^*. The results of estimation gave a value of T_2^* of 48 ms.

From the CNR trend plotted in this chart is important to note that the maximums is rather flat, indeed for TE included between 36 ms and 53 ms the CNR amount to 90% of its maximum value. However, using high TE leads to acquisition sequences with longer duration (TR longer) and the dephasing effect of through plane gradients becomes significant, which has been demonstrated experimentally (Ojemann, Akbudak et al.

1997). Hence, on the one hand it is opportune to use acquisition sequence with a lower echo time; on the other hand TE should be at least 32-36 ms because for the lower values the CNR decreases rapidly.

The CNR maps have shown that the GRASE technique can recover the contrast to noise ratio in the OFC and temporal lobe, dropout areas. Figure 10 shows maps of the time echo that ensure the highest achievable CNR, when for each voxel the best value of TE was chosen.
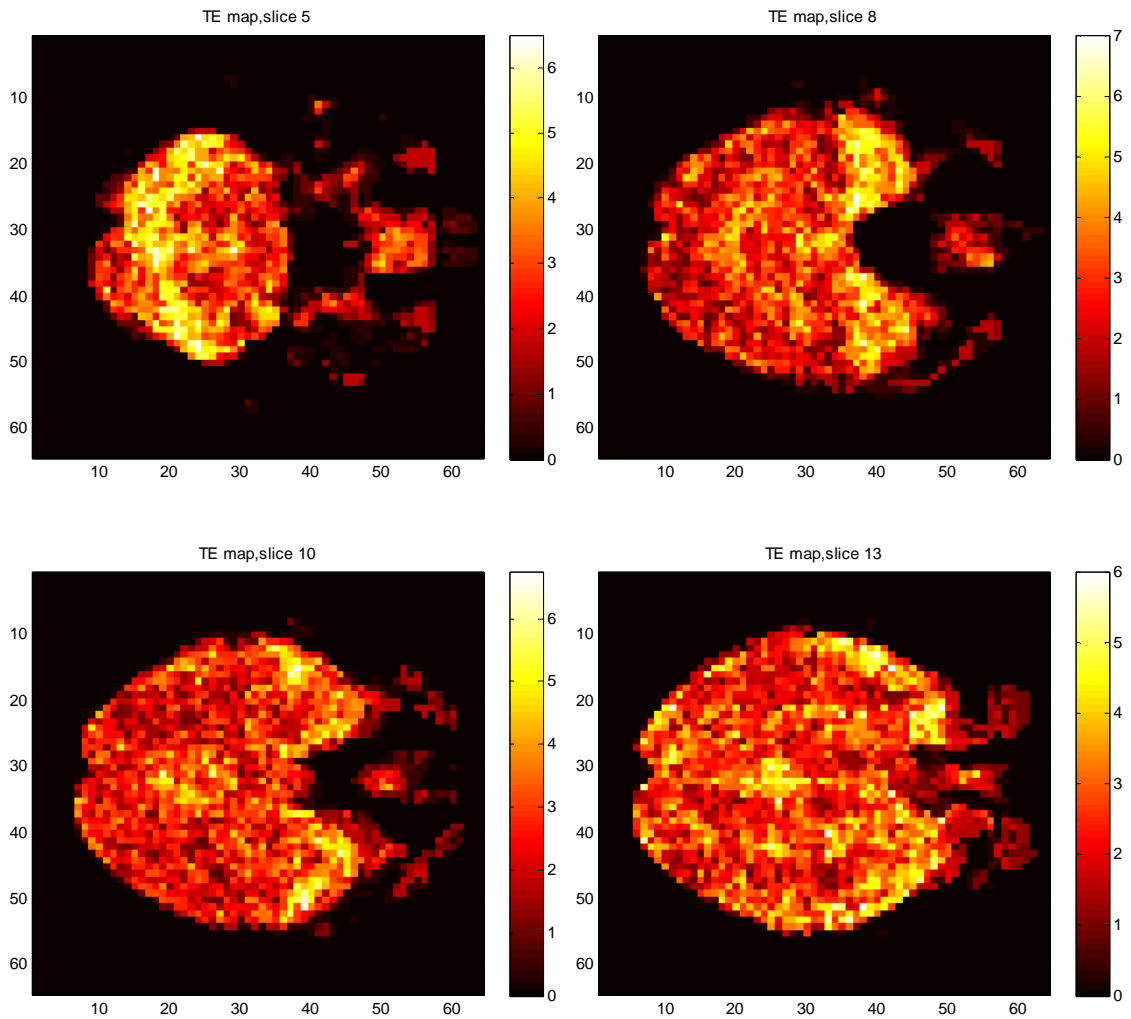

Figure 19. Merged TE map, calculated from the TE maps obtained for each subject. The possible voxels values range on a scale from 0 to 7 in steps of 0.25. Units 1 to 7 matches to the time echo used in the GRASE sequence. Each voxel assumes value corresponding to the TE that maximize the CNR in that voxel.

The brain structure is well defined, this indicates a smaller influence of artifacts using this technique. Moreover, it can be seen that in the most brain the voxels assumes

values matching with low TE; from these results is to be expected to gain a low time echo value also to optimize the CNR in the brainstem. Also for the GRASE the TE maps were overlaid on the anatomical reference image to investigate whether the optimal TE is correlated with the different brain structures. As it can be seen from the Figure 20 the optimal TE appears homogeneous in almost all brain; where it assumes low values. This results might suggests to use a time echo around 70, 80 ms to optimize the CNR of functional signal acquired with GRASE sequences.
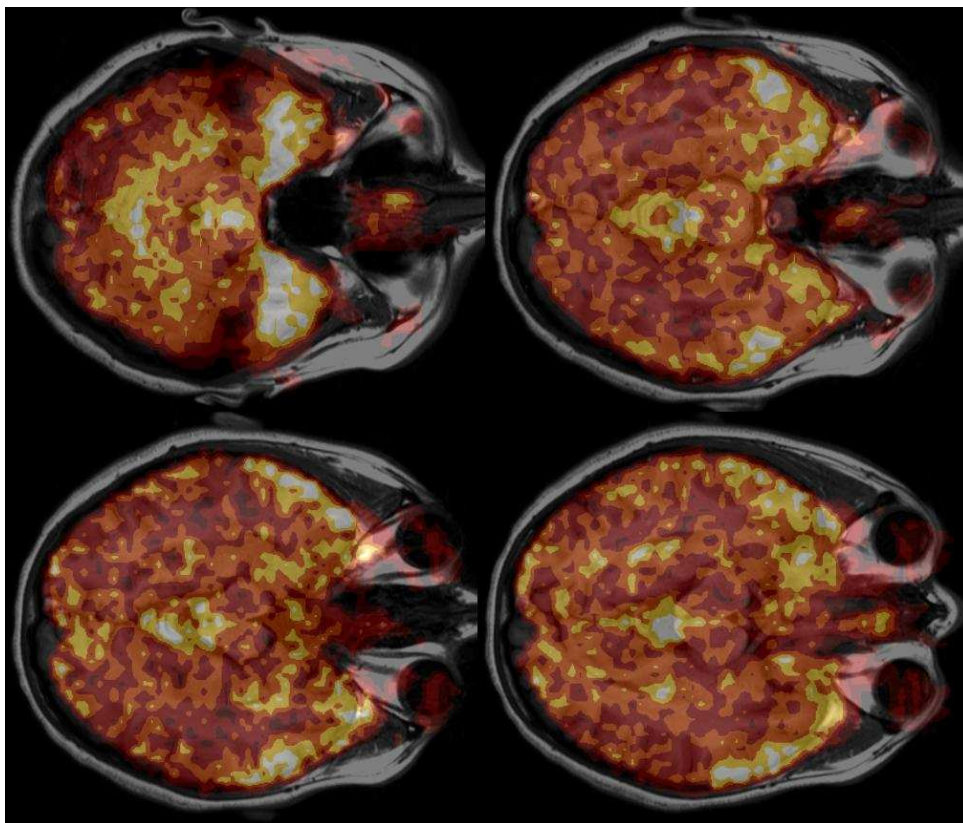
Figure 20. Selected slices of TE map overlaid on the T1-whieted images. The TE map is averaged over all subject and the images chosen corresponds to the slices 5, 8, 10, 13. The scale displays the tones of color which matches to the 7 TE values used for GRASE acquisition. Seve different echo time were used to acquire the images: 70, 80, 85, 90, 100, 110, 125 ms.

To localize the investigation in the brainstem area the same analysis used for EPI was done. Fourteen slices were manually created around the brainstem and overlaid on the CNR maps calculated with different TE. Afterward the CNR on the voxels within each ROI was averaged to get an information of CNR in that specific area. Figure 21 shows the CNR trend dependent on TE in four meaningful ROIs, averaged over all subject. Unlike

the findings found for the sequence EPI, these results do not clearly demonstrates superior CNR when its value is plotted for the TE used. Also the mean over all ROI, displayed in Figure 22 is little informative. In this experiment the range of TE values chosen does not allows to catch the possible peak and thus assessing the optimal time echo value to use in GRASE. On the other hand it can be seen that for TE = 70 ms the average CNR values over all ROIs is maximized, while for value of TE higher its values decreases; this finding might suggest that the chosen range of investigation is shifted on the right to the peak.
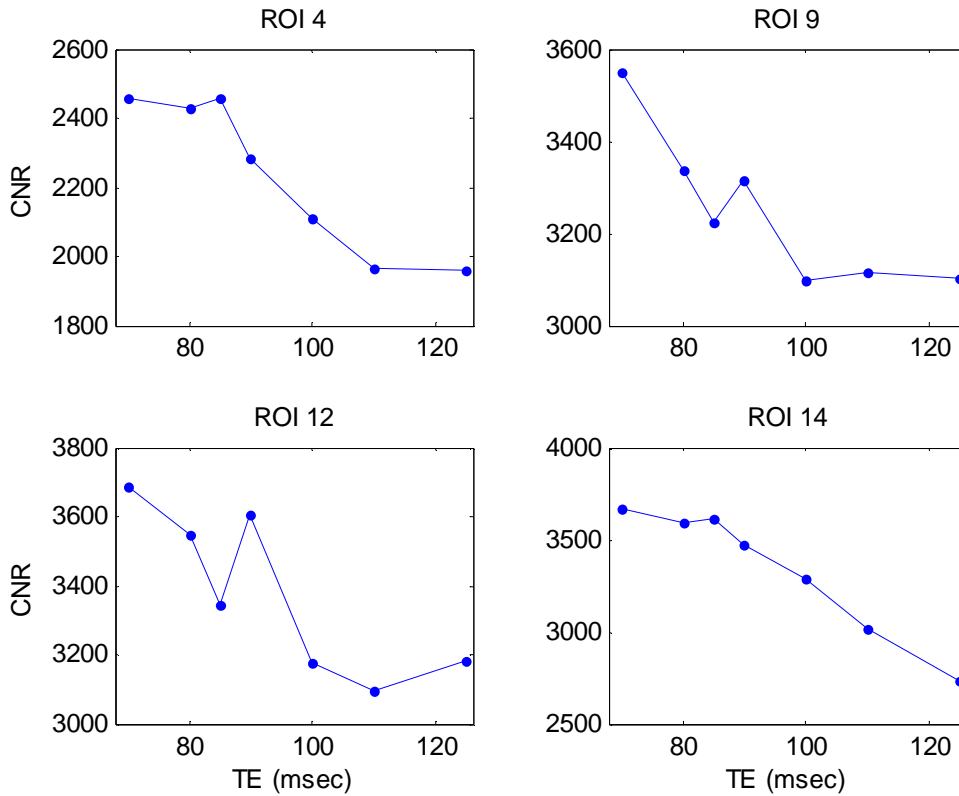
Figure 21. Plot of CNR mean calculated from the voxel of CNR maps within ROIs and averaged over all subject. CNR maps were calculated from time series of GRASE images acquired by TE = 70, 80, 85, 90, 100, 110, 125 ms. The considered ROIs matches to the slices 4, 9, 12, 14.
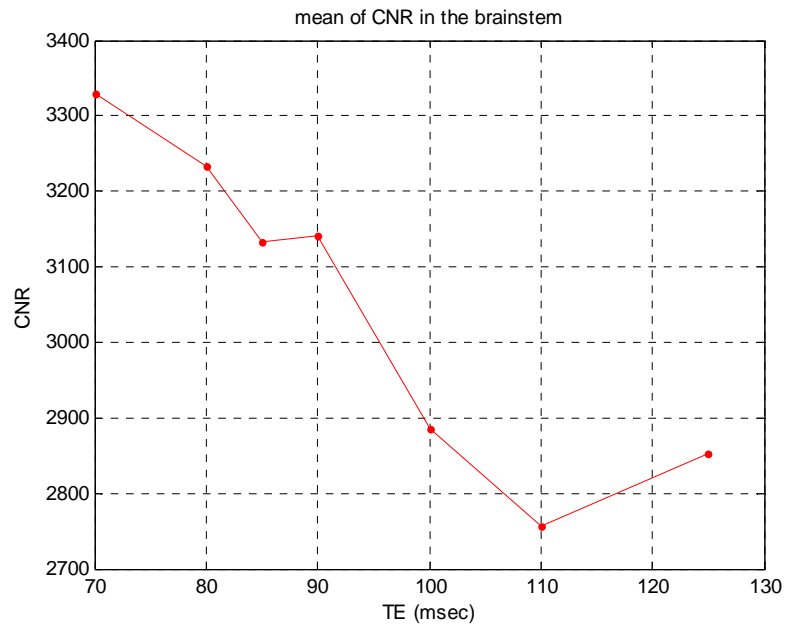
Figure 22. Contrast to noise ratio (CNR) dependence on TE for the whole brainstem, plus the fit of the model used to calculate the BOLD sensitivity. The CNR is derived from time series of single-shot GRASE images with TE = 70, 80, 85, 90, 100, 110, 125.

3.2 Slices tilt optimization

In this experiment, the dependence of the signal quality on the slices orientation was investigated to assess a optimal value for brainstem functional studies. It has been demonstrated that the dropout effects may be reduced in certain areas by changing the orientation of the imaging slice (Deichmann, Gottfried et al. 2003).To detect how the BOLD sensitivity changes with different orientations, form the time series of functional EPI images the CNR maps for seven different slices tilts were calculated. The parameter
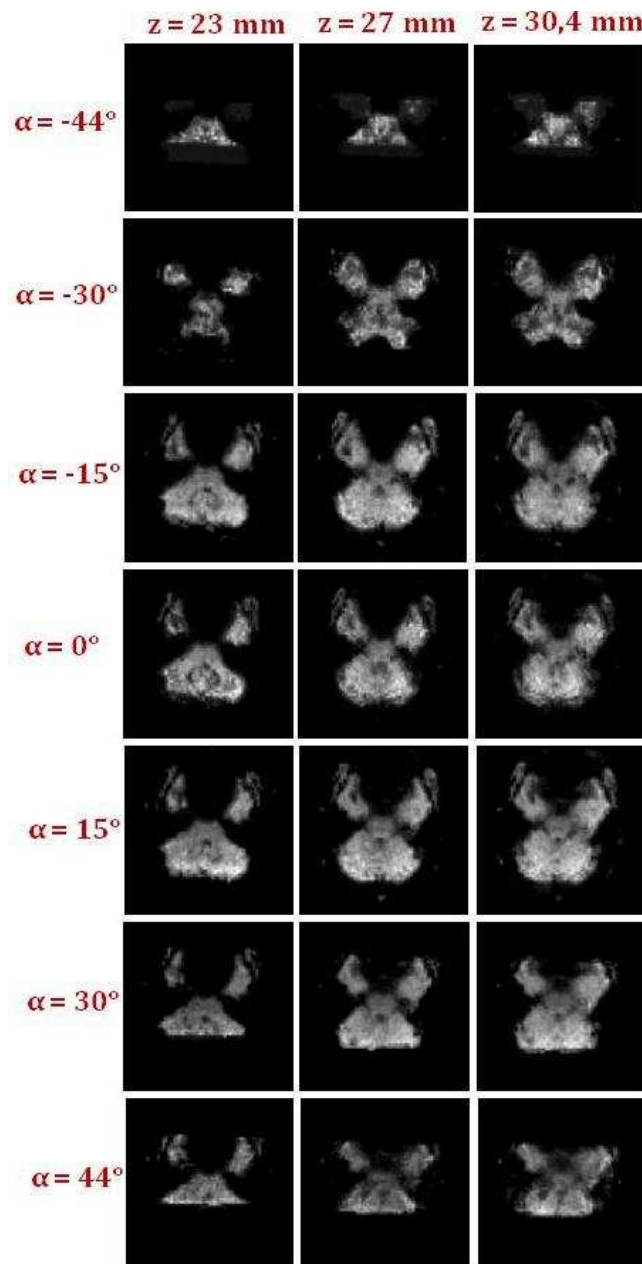
Figure 23. Images of CNR maps calculated from EPI functional data, which were previous registered on the volume with angle 0° using a rigid-body model. For each angle of acquisition are presented the sixth, eighth and ninth slice. In the FOV space, these slices are equivalent to z=20.8 mm z=27.2 mm and z=30.4 mm.

CNR allows to quantify the BOLD sensitivity (BS), i.e. how easily is possible to see difference caused by field inhomogeneity. The CNR maps obtained from the voxels within the masks are shown in Figure 23.

The slices orientation is transversal and the angle of acquisition changes from -44° to 44° in seven steps of about 15°. For each angle three images with different positions in the FOV are displayed. The positions considered are the same for each tilt and assumes the values z = 23 mm; z = 27 mm and z = 30,4 mm that correspond to the slices 5, 7 and 9. The dimension z is considered in relation to the FOV and shows the distance from the first slice to the considered slices. Under this disposition is possible to compare the CNR maps to investigate whether for the different slices tilt the CNR assumes low values in the brainstem area caused to the signal loss. For the angles at -44°, -30° and 44° the brainstem structure is not defined clearly and the CNR around seems very low, instead, for the other angles there was sufficient signal intensity to detect a response through nearly all of the brainstem. Further, from Figure 14 it can be seen also that the CNR map achieved with α = 15° is more brightest in voxels within visual cortex compared the same voxels of the CNR map achieved with α = -15°. On the other hand, for a quantitative analysis, mean values of the CNR in the interest area were compared. Regions of interest were drawn manually from the anatomical images using MRIcro. To cover the whole brainstem 14 slices were considered; for each of them a circular ROI with different diameter (3-4 mm) were traced. The number of voxels within each region considered for the analysis is around 80±20. The areas exceeds the structure of interest to investigate also the effects of the signal dropout due to the susceptibility field, in the brainstem.

In the figure 24 are plotted the mean values of the CNR within the regions of interest, calculated from images with different slices tilt. The ROIs considered are equivalent to the slice 7, 11, 14, and 16; this allows to have an information from bottom part, the meddle part and the top part of the brainstem.
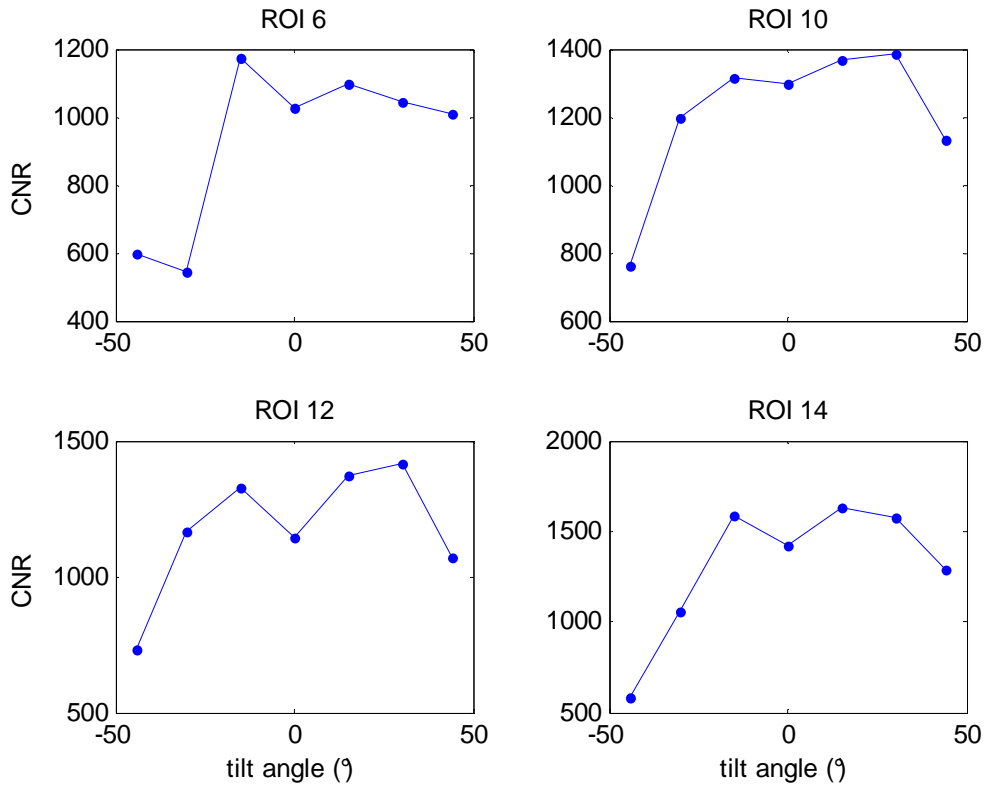
Figure 24. Variability of mean CNR in different ROIs, for different tilt angles. CNR maps were calculated from time series of EPI images acquired by α = -44°, -30°, -15°, 0°, 15°, 30°, 44°. The considered ROIs matches to the slices 7, 11, 13, 15.

As can be seen from the charts the maximum is rather flat in each ROI: for tilt angle included between -15° and 30° the mean CNR keeps amount 90% of its maximum value. Unlike, for the other values of tilt angles the mean CNR decrease rapidly in each ROI. This results could indicate that the effects of susceptibility gradient are heavier in the images acquired using slice orientations of -44°, -30° and 44°. Moreover, Figure 25 shows the mean CNR averaged over all regions of interest as a function of tilt angles to display the CNR trend throughout the brainstem. The CNR trend in this chart underline that there is not a clear superior CNR, hence there is not a slice tilt angle which maximize the contrast to noise ration. Furthermore, from this finding might be inferred that the same BOLD sensitivity acquired with tilt angle of -15°, 0°, 15° and 30° are similar because of these orientations are not affected by strong susceptibility gradient. Thus, it is advisable to work with angle tilt values between -15° and 30°. In the functional study carried out in this project it was be chosen to use a tilt angle between 15° and 25° to ensure of do not use orientation affected by susceptibility effect. Further during the manual orientation of the FOV it was sought not to include the eye orbit in the field of

view; it may cause ghost artifacts in the functional images (Chen and Zhu 1997). An example of the FOV orientation in the sagittal plane used for the functional measures is shows in Figure 26.
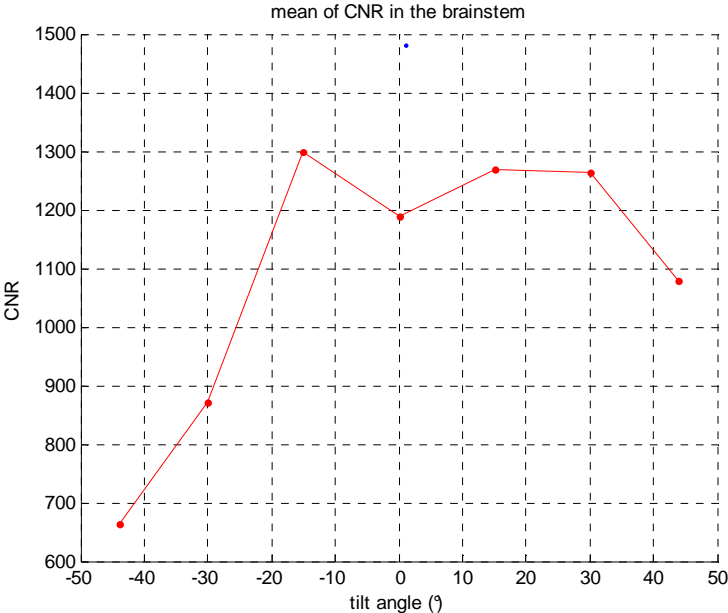

Figure 25. Contrast to noise ratio (CNR) dependence on slice tilt angle, for the whole brainstem. The CNR is derived from time series of single-shot GRASE images with tilt angle = -44°, -30°, -15°, 0°, 15°, 30°, 44°.

Figure 26. Example of the localized FOV in the sagittal plane, with orientation angle of 17°. The volume of acquisition is centered on the brainstem and positioned in order to contain the cerebellum and the V1 in the horizontal dimension and the whole brainstem, from the medulla to the SC in the vertical dimension.

3.3 Spatial resolution and different head coil

In this section it was investigated whether either improve spatial resolution or use different head coil carries advantages for fMRI studies. For both the analysis to assess the possible benefits, the activation maps obtained by measurement with different features were qualitatively (visually) compared. Figure 27 shows fMRI results from the healthy volunteers performing the OKN stimulus. Time series of EPI functional images were acquired both low spatial resolution (3 mm iso-volumetric voxel) and high spatial resolution (2 mm iso-volumetric voxel). Voxels exceeding the corrected threshold $P < 0,05$ were overlaid on the anatomical T1-whited images by MRIcro. These images (Fig. 27) demonstrate how spatial morphology of functional activation obscured by low resolution data acquisition. For example, the activation in the visual cortex (V1) detected at low resolution (Fig. 27A) appears grossly extended over throughout the surface, covering the brain sulcuses. While, with an increase of spatial resolution of 2 x 2 x 2 mm (Fig. 27B), the activation follows the brain morphology and show a localizer activation.
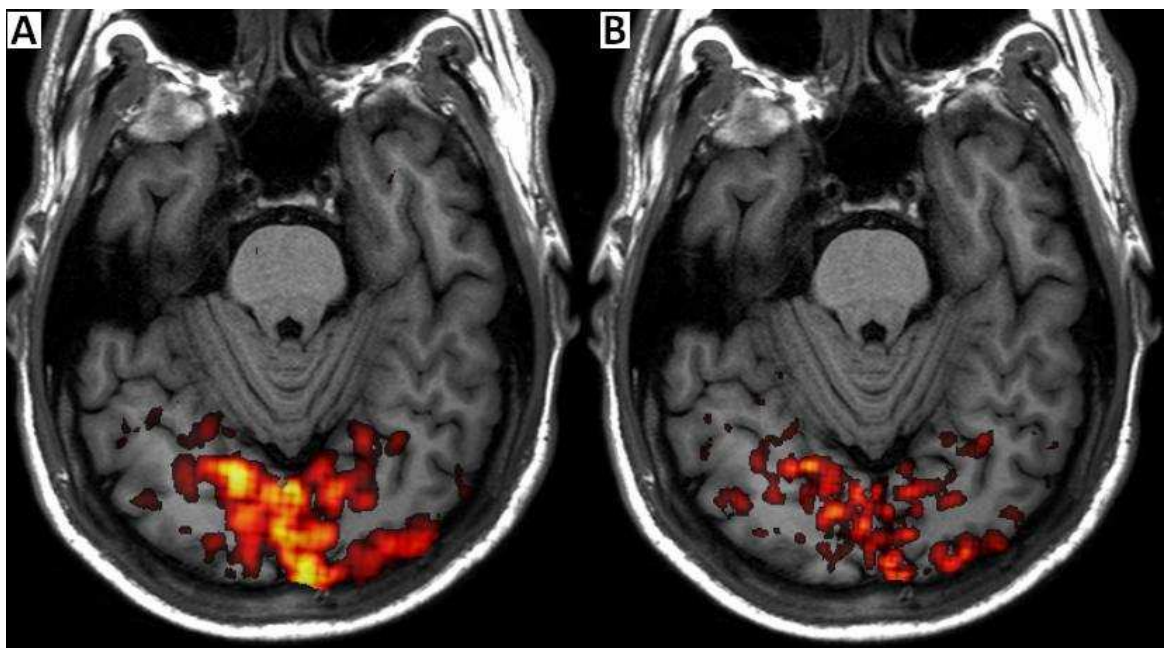

Figure 27. Activation in the visual cortex (V1) from healthy subjects performing OKN stimulus. The activation maps were achieved from time series of functional EPI images acquired with 3 mm iso-volumetric voxel dimension (Image A), and 2 mm iso-volumetric voxel dimension (Image B). Voxels considered of activation exceeds the correct threshold of $P < 0.05$.

Figure 28 shows an enlargement of the region of interest to analyze the result yielded with both spatial resolution in the brainstem. The voxels considered of activation were achieved using an uncorrected threshold of P < 0.001 and overlaid in the anatomical images by MRIcro using the tonality '5redyell'. In the figure is reported also two drawing of brainstem nuclei to check the meaning of the obtained activation; this to strengthen
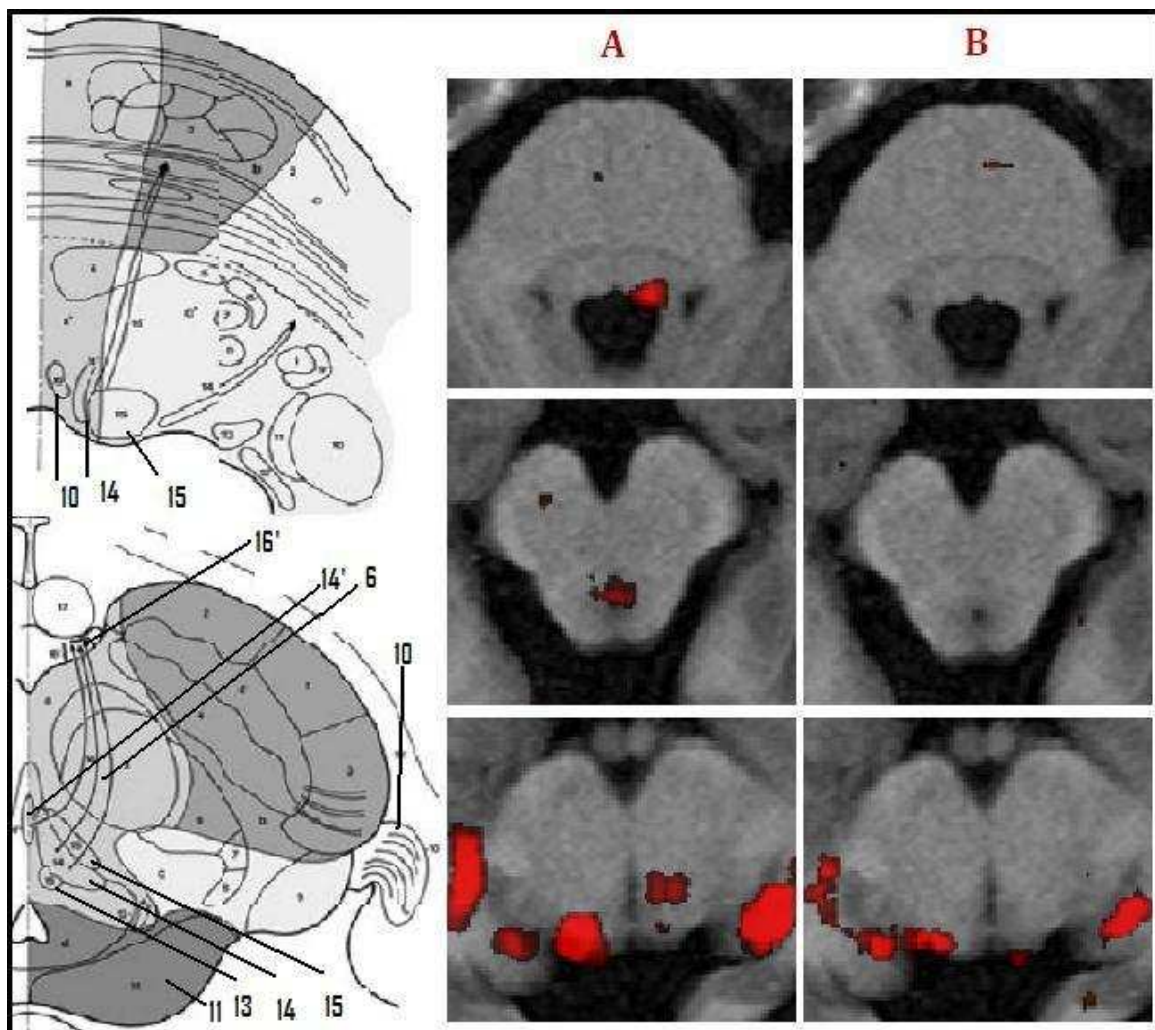

Figure 28. Enlargement of activation map (whole brain) showing activated areas in the brainstem as a result of functional study with OKN stimulus. The time series of functional EPI image were acquired using both spatial resolution of 3 x 3 x 3 mm (images column A), and spatial resolution of 2 x 2 x 2 mm (images column B). Significant regions are displayed with an uncorrected threshold of P < 0.001. Showed images matches to the slice 11, 15 and 16. References drawing above: 10 Inferior cerebellar peduncle, 14 Fibers of the facial nerve, 15 Abducens nucleus. Reference drawing bellow: 6 Fibers of the oculomotor nerve, 10 Lateral geniculate body, 11 Superior culliculus, 13 Accessory oculomotor nucleus, 14 Principal oculomotor nucleus, 14' Nucleus of Perlia, 15 Medial longitudinal fasciculus, 16' Oculomotor nerve. Line drawing adapted from Duvernoy's atlas of human brainstem (Thomas 2009).

the inference that the voxels exceeding the threshold matches to the brainstem nuclei encompassed in the visual system. The activation appearing in the images of column A (low spatial resolution) is likely to be analogous to activation in the abducens nucleus, the nucleus of Perlia, the oculomotor nucleus, the superior culliculus and the lateral geniculate body. For the activation in the middle of the second and thirds images, may refer to the nucleus connected with the fibers of optical nerve drawn in the second pictures. These nuclei are close to each other and therefore are difficult to distinguish with functional images. An higher resolution should be better to investigate in this small structures, but as can be seen by the images of column B (high spatial resolution) the activation is significantly reduced. Note that the slight disparities in activation pattern between the results achieved with different spatial resolution are expected considering that the data were acquired in two separated runs; it is well known that activation patterns can vary considerably from scan to scan.

In the Figure 29 are shows the fMRI results (one subject of three) achieved using either a 16-channel head coils (Fig.29 A) or a 8-channel head coils (Fig. 29 B). Activation maps were yielded adopting an uncorrected threshold of P < 0.001 and then overlaid on the anatomical images T1-whegthed. The purpose of this experiment was to evaluate whether use a 16-channel coils provides an enhancement of the BOLD signal recorded. By visual comparison of the images displayed it can be seen that the four upper slices of the map found with 16 head channel (Fig.29 A) shows an activation following the brain morphology. Instead, the same slices of the map found with 8 channel head coil (Fig.29 B) shows an blot activation. Moreover, it can be observed that the four slices representing the below part of the brain the activation obtained with the functional images acquired with 16 channel head coils shows an stronger activation. This result probably is due to the better field homogeneity in the underneath by this head coils. The subject analyzed with the same technique provided the same findings.
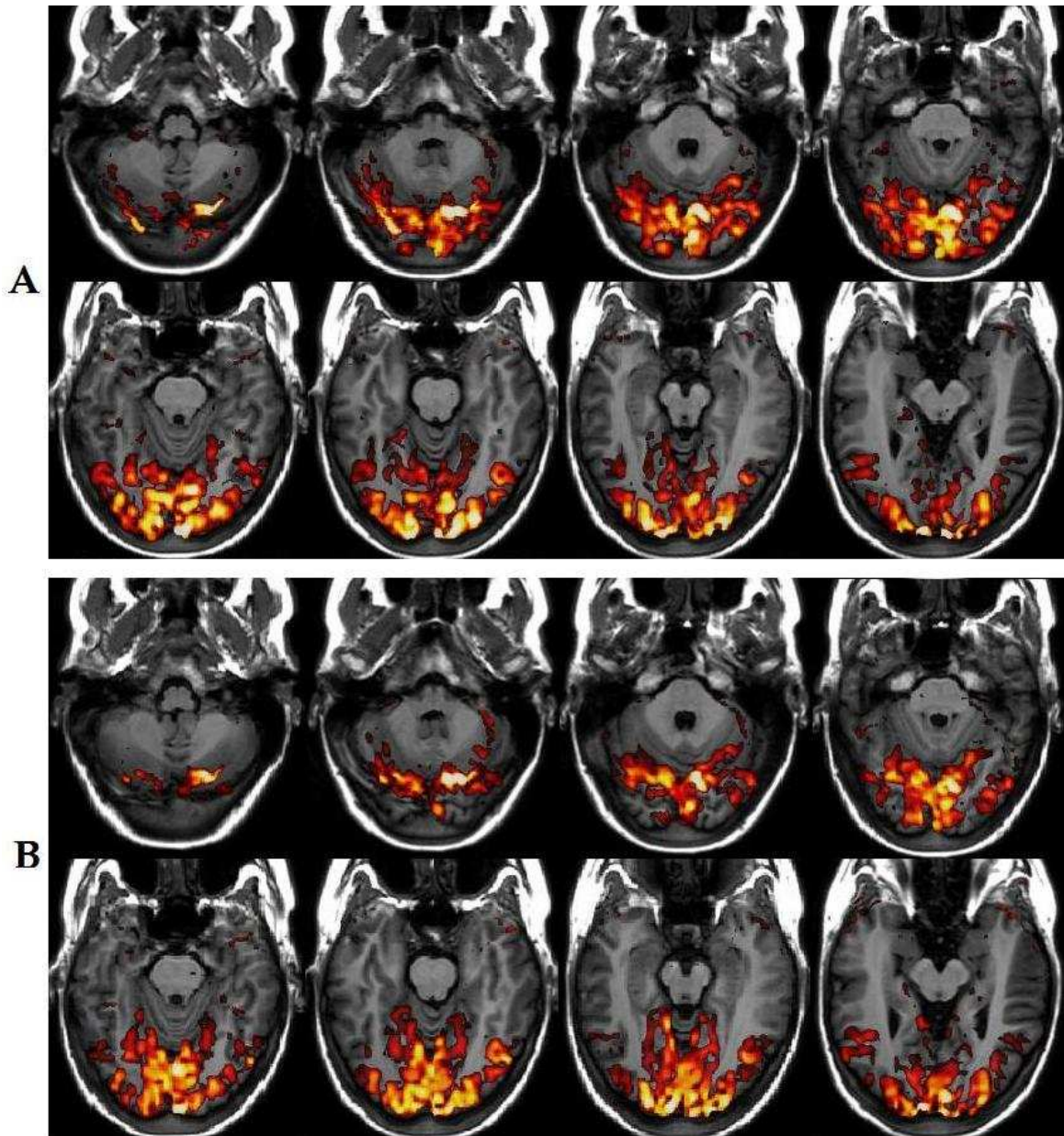
Figure 29. fMRI t statistic maps of a representative subject. Time series of functional EPI images were acquired both with 16-channel head coils (A) and with 8-channel head coil (B), during a visual stimulus (OKN). The activation maps calculated using an uncorrected threshold of P<0.001, have been superimposed on T1-weighted images. The images displayed corresponds with the slices from 8 to 14.

3.4 Functional brainstem study

The first purpose of the statistical analysis of the functional data was to assess the importance of the considered regressors in the general linear model. First, were tested the nuisance regressors built from blink events and periods of eyes closed. The first idea was to investigate the two T-maps achieved with the basic linear model (block information and physiological regressors), and with the model including also the regressors blink events and periods of eyes closed. The T values in the voxels within specific region of interest, such as lateral geniculate nuclei (LGN), superior culliculuc (SC), and oculomotore nuclei (OMN), were compared to evaluate which model ensures an higher T value. The results are proposed in six charts each representing a specific region of interest. The difference of the mean T-values calculated with the two models were plotted in function of the correlation between block regressors, and blink and eyes closed regressors, for each subject. The six chars are shows in Figure 30. The results should show a positive value of the difference whether in the considered voxel the first model (basic model) fits better functional time series; on the other and the results should shows a negative value of the difference whether the second model compensate the noise terms assumed to compose the time series in the considered voxels. The analyzed difference was plotted on the correlation between the block regressors, and the blink and eyes closed regressors, to investigate whether blink and eyes closed periods are related with the experimental design, and whether this relation influence the found results. In two chars there are the results for less than 8 subjects because no activation was found in the investigate nuclei for these subjects and consequently the analysis was not necessary.
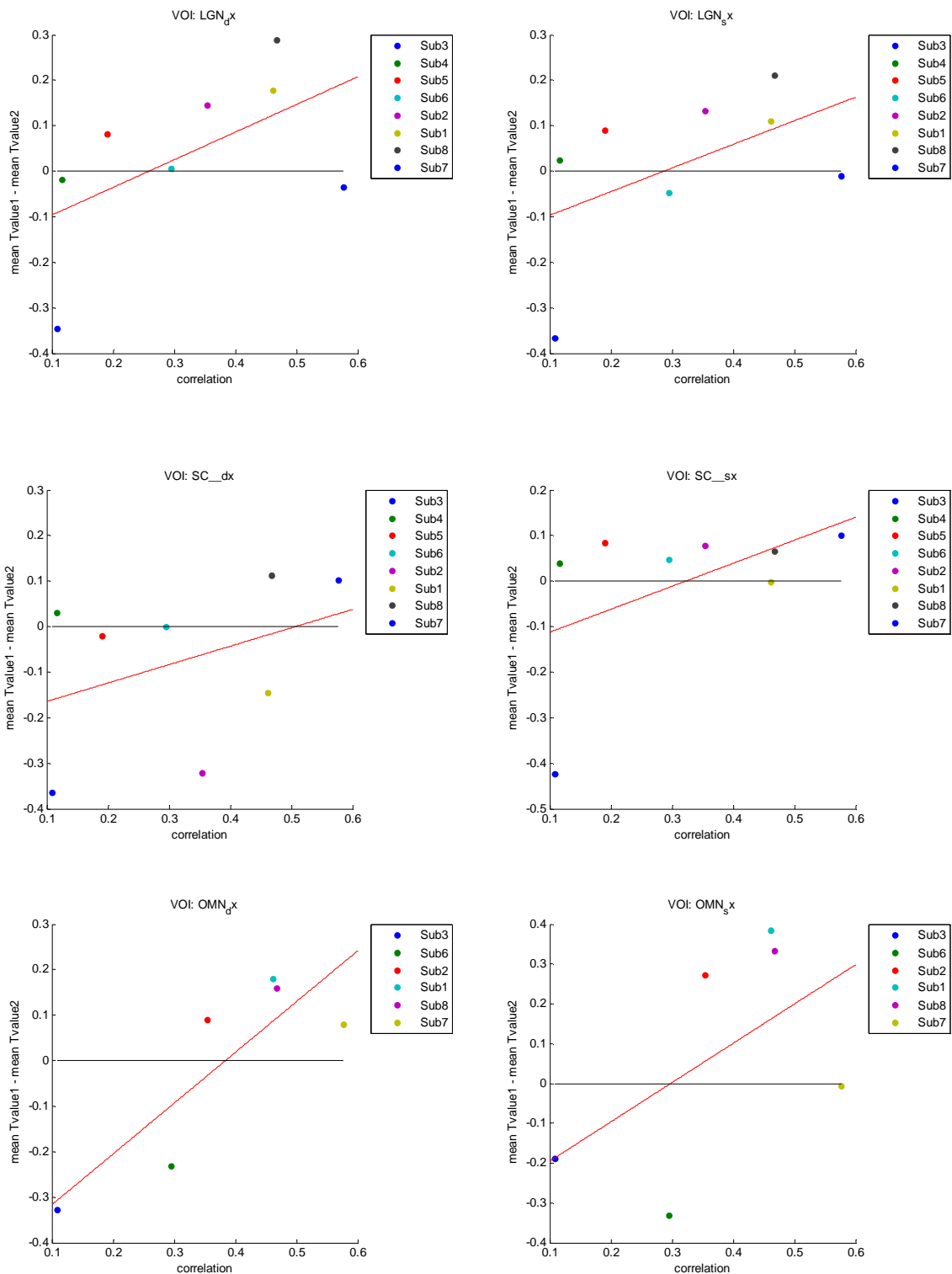
Figure 30. These chars shows the diffrence of two mean T-values in the several region of interest in function of the correlation bettween the block regressors and the blink and eyes closed regressors, for each sobject. The matrixs of T-value were caluculated with two different linear models. The first composed by block regressors and physiological regressors and the second built including in the first the blink and eyes closed regressors. The region of interest are: left and right lateral geniculate nuclei (LGN), left and right superior culliculus (SC), and left and right oculomotor niclei (OMN).

In the second step of the analysis for investigate the model built including the blink and eyes closed regressors to the base model (block information and physiological regressors) the comparison was done using F-test. This statistic test allows to quantitatively describe how well specifics regressors extracts the investigate terms. The idea is to work by tacking some model and comparing it to a base model, which then determines whether the additional regressors (that are not in the base model) act to explain significant amounts of signal, that is, more than could be expected from a random correlation with the residual noise. For each subject the model built including blink and eyes closed regressors was compared with the base model. The voxels exceeding the uncorrected threshold P < 0.001 are overlaid on the T1-weithed image and showed in Figure 31. The voxels exceeding the threshold shows in which voxels the general linear model including blink and eyes closed regressors enable to achieve lower residual error, in the other words, shows in which voxel the added terms are expressed. Hence, the displayed voxels can be considered the neuronal activation yielded by blink event and eyes closed phases. Indeed, several subjects shows activation in the visual cortex and in the cerebellum; the latter is known to be involved in the eliciting on blink response. In the end to verify the results achieved with the previous non-statistical methods of analysis, the voxels within the ROIs exceeding the fixed threshold were counted. The results showed no voxels of activation for almost all region of interest and for almost all subject, except the right SC of the subject 2 (18 voxels), the left LGN of the subject 3 (31 voxels), and the right LGN of the subject 4 (9 voxels).
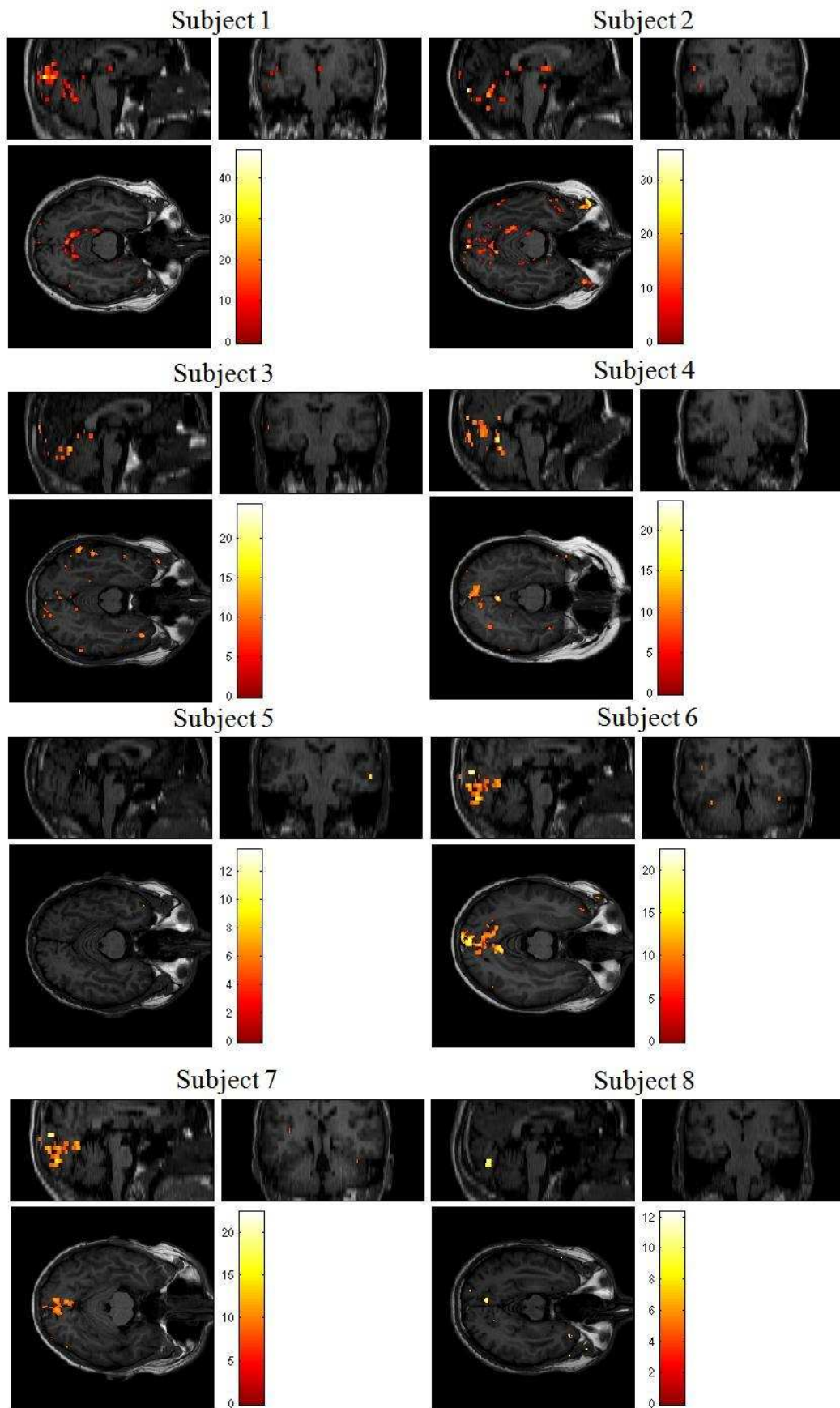
Figure 31. Results of F-test using uncorrected threshold of P < 0.001. The maps show the voxels where the model inclusing the blink and eyes closed regressors allow to get lower residual, i.e. shows the voxel where these terms are expressed.

Next step was to investigate the how the block design regressor and the velocity of eyes movement regressor, contribute to fit the functional time series in each voxel. For this purpose two statistical test (F-test) were carried out using the same linear model that includes the block design information, the velocity regressor, the blink and eyes closed regressors, and the physiological noise regressors. In the first test was investigate whether adding the velocity regressors improves the GLM, as the velocity information expresses the right instant when the subject start to perform the task. The results are shows in Figure 32. Images in the sagittal, transversal, and coronal plane are displayed to show the voxels exceeding the uncorrected threshold of $P > 0.001$. For these voxels the GLM including the velocity regressor ensure lower residual error. The activation maps show voxels exceeding the threshold in the visual cortex, and in some cases in the lateral and anterior part of the head, the later are probably involved noise terms caused by eyes movement. No voxels exceeding the threshold were found in the brainstem. Besides the second test was done adding the block design information to the base model including velocity movement regressor, blink end eyes closed regressors, and physiological noise regressors, to assess whether using the velocity has regressor of interest was enough to describe the information related to the experimental design. The results are shows in Figure 33. Also in this analysis the results are displayed by a sagittal, a transversal and a coronal slices showing the voxels exceeding the uncorrected threshold of $P < 0.001$. From these results can be seen that there are many voxels where the GLM has yielded lower residual error including the block design information as a regressor of interest. These areas encompasses the visual cortex, the cerebellum and in some subjects nuclei in the brainstem, such as SC.
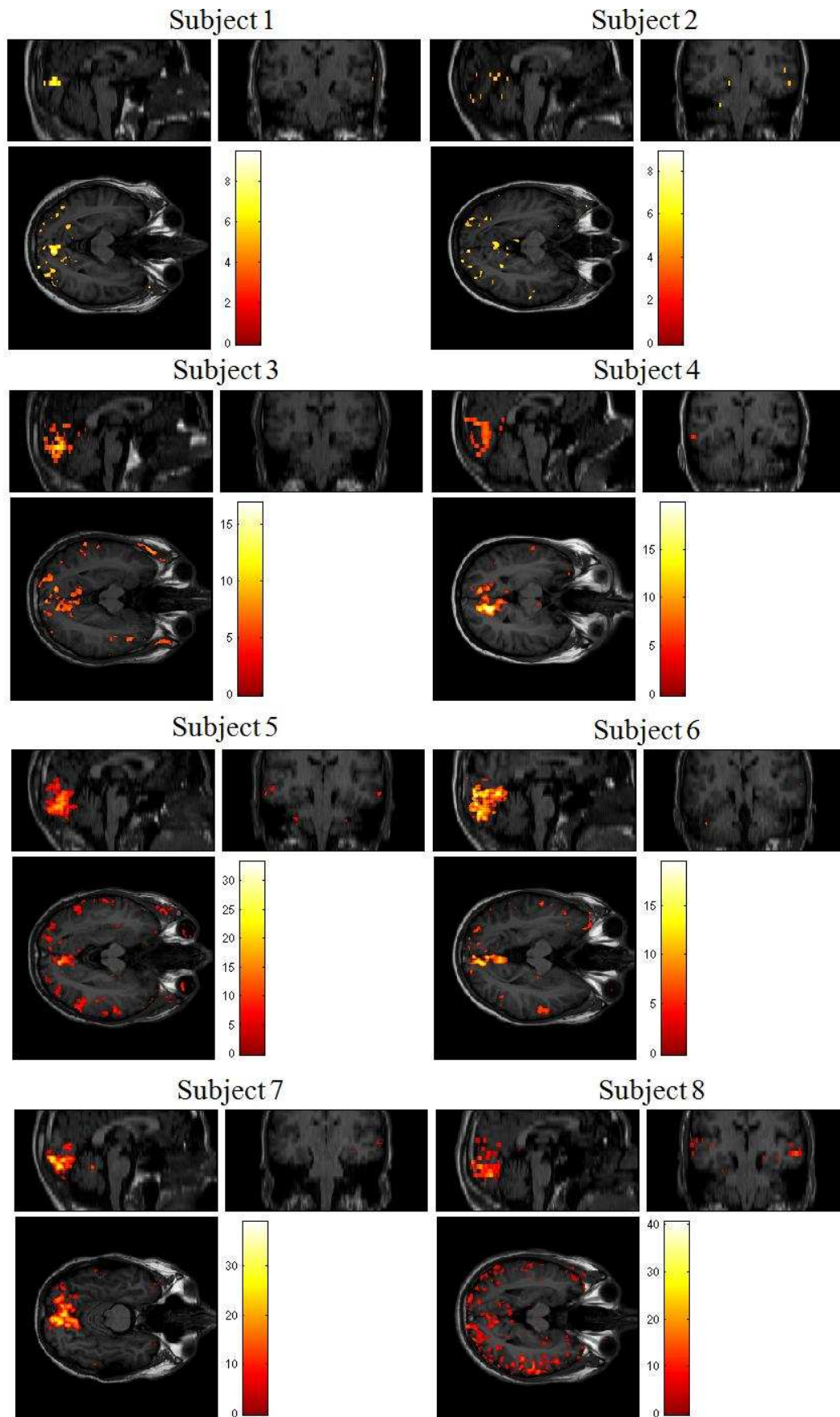
Figure 32. Results of F-test using uncorrected threshold of P < 0.001. The maps show the voxels where the model built inclusing the eyes movement velocity regressors to the base model (block, blink, eyes closed and physiological regressors), allow to get lower residual, i.e. shows the voxel where these terms are expressed.
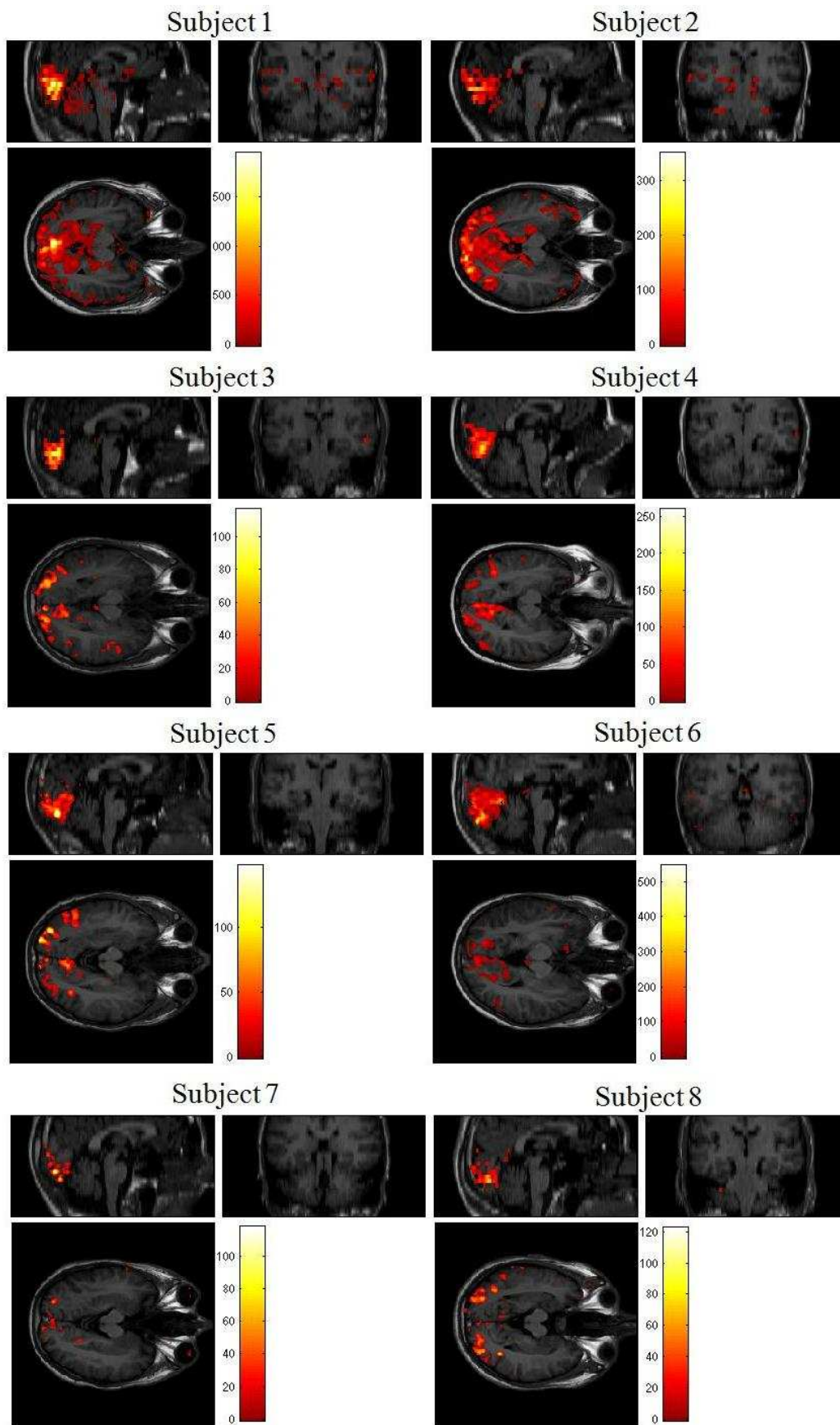
Figure 33. Results of F-test using uncorrected threshold of P < 0.001. The maps show the voxels where the model built inclusing the block design regressors to the base model (velocity, blink, eyes closed and physiological regressors), allow to get lower residual, i.e. shows the voxel where these terms are expressed.

To investigate neuronal activation elicited by OKN stimulus a GLM built considering the findings achieved in the previous steps was applied to the functional time series. The linear model includes blinks and eyes closed regressors, and physiological noise regressors to reduce the noise caused by breathing, heart beating and events of blink and eyes closed; furthermore the model includes the block design information as regressor of interest. Activated voxels were determined by statistical analysis (t-test) assuming an uncorrected threshold of $t > 3.12$ that corresponds to $P < 0.001$. The functional analysis single-subject has led to display the results of each subject separately. First image, Figure 34, shows an example of whole brain image where was extracted and zoomed a particular brain region as it will be show in the following images. This transversal slice in particular was achieved from an activation map calculated with a threshold corrected with FEW of $P < 0.05$. This to show also that for some subjects (four of eight subjects) is possible to see activation in the brainstem nuclei (SC) using the corrected threshold.
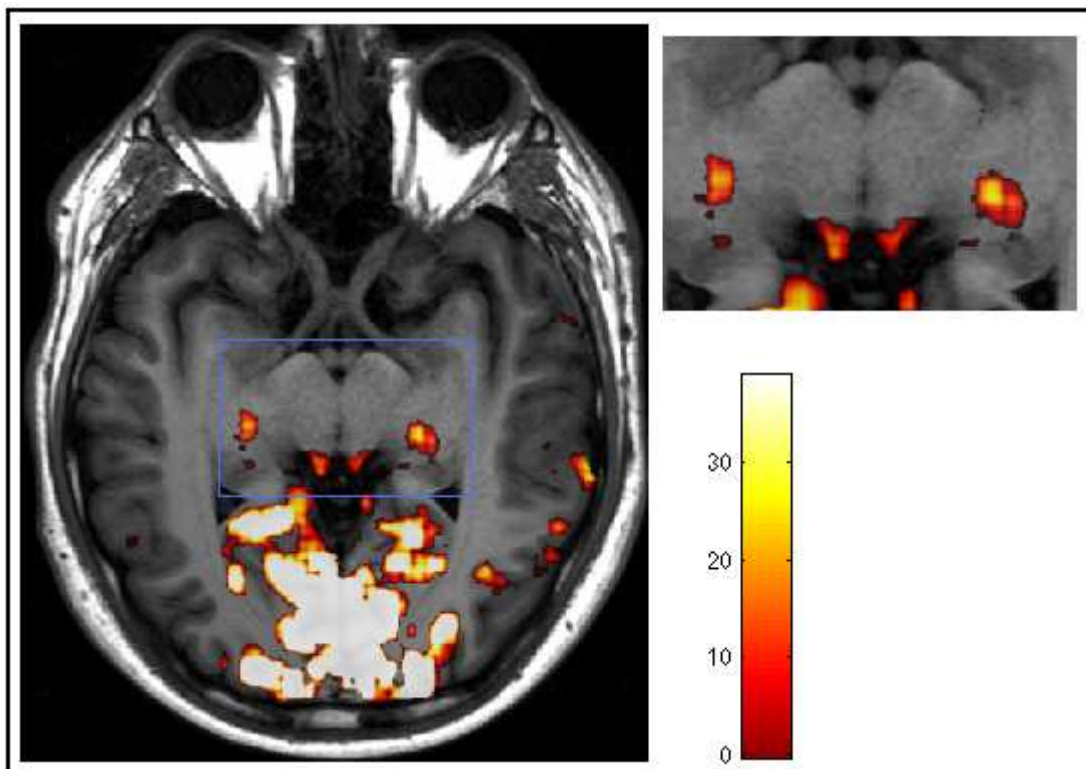

Figure 34. Activation map overlaied on a transversal slice of the anatomical volume (z = 15). Moreover the enlargement shows a transversal image of the brainstem structur. The avtivation maps was calculated from the functional image of the Subject 1, using a corrected threshold (FWE) of P < 0.05.

Under all stimulation conditions, direction and orientation, neuronal activation were found in the visual cortex (V1) as well as in the cerebellum and in the brainstem structures. In more detail, the neuronal activation in the brainstem nuclei was investigated for each subject, by comparing the activation maps with the anatomical structures depicted from the Duvernoy's atlas of human brainstem (Thomas 2009). The results submitted in the following images concerns activation maps achieved under horizontal OKN stimulus. The results of the analysis conducted for the first subject is showed in Figure 35; activations maps in the slice 9 reveals vexels exceeding the fixed threshold located at the abducens nuclei (structure number 35, drawing A), and others located in the anterior part of the pons where end up the fibers of the facial nerve (which controls the muscles of facial expression). Moreover, activation clusters in the anterior part of the pons, showed in the slice 10 and 11, could involved other fibers connected with the facial nerve, such as corticospinal tract. Furthers, small activation clusters in the slice 11 are located in the tectospinal tract (structure number 19, drawing B), which is a nerve pathway that coordinates head and eyes movements. The activation in the slice 12 shows activation clusters which could match with the trochlear nucleus (structure number 13 and black arrow, drawing C) and the mesencephalic trigeminal nucleus (structure number 18, drawing C). In the same slice the activation in the anterior part of the midbrain may be analogous to activity in the interpeduncular nucleus (structure number 7, drawing C). Finally, the activation clusters in the slice 13 and 14 are likely to be analogous to activity in the oculomotor nuclei (structures number 12 and 13, drawing D) and the fibers of oculomotor nerve (structure number 13', drawing D), as well as the superior culliculus (structure number 18, drawing D) and the lateral geniculate nuclei (structure number 35, drawing D).

The statistical analysis of the functional data acquired with
 the second subject (Figure 36), reveled hypothetical activation matching with medial longitudinal fasciculus (structure number 22, drawing A) in the slice 10, and a small activation cluster matching with the abducens nucleus (structure number 24, drawing A) in the slice 12. Moreover, in the midbrain (slice 14 and 15) activation is likely to be analogous to activity in the oculomotor nuclei (structures number 12 and, 13 drawing B),

as well as the superior culliculus (structure number 26, drawing C) and the lateral geniculate body (structure number 37, drawing C).

Activation maps achieved from the functional images acquired with the subject 3 (Figure 37) shows hypothetical activation (slice 9) in the area of the pons where there are fiber which serve to control of motor activity. In the other slices (13 and 14) the activation clusters do not clearly corresponds with the investigated structures but they can be associated with the superior culliculus (structure number 28, drawing C), and the medial and lateral geniculate body (structure number 40 and 41, drawing C).

From the activation map of the subject 4 (Figure 38), voxels exceeding the fixed threshold in the slice 9, are arranged on the abduncens nuclei (structure number 24, drawing A), on the medial longitudinal fasciculus(structure number 22, drawing A), and on the corticospinal tract(structure number 1, drawing A). Furthermore, as can be seen from slice 13, 14, and 15 the activation clusters matches to the trochlear nuclei (structure number 13, drawing B), the oculomotor nerve (structure number 9, drawing C), the oculomotor nuclei (structure number 20, 21 and 22, drawing C), the superior culliculus (structure number 28, drawing C), and the medial and lateral geniculate body (structure number 40 and 41, drawing C).

The results from the functional images of the subject 5 (Figure 39) shows in the slice 14 and 15 activation clusters which matches with the superior culliculus (structure number 18, drawing A) and the lateral geniculate body(structure number 35, drawing A and number 37 drawing B).

The activation map for the remaining subjects were calculated using both 2D anatomical images and 3D anatomical images; following results are proposed overlaying the activation map on the 3D T1-weithed images. Figure 40 shows an activation cluster in the slice 35 which could match with an abducens nucleus (structure number 24, drawing A). Moreover, can be seen from the slice 45 hypothetical activation on the oculomotor nuclei (structure number 12 and 13, drawing A), the superior culliculus (structure number 18, drawing B), and lateral geniculate body (structure number 35, drawing B).

Figure 41 shows the results achieved from the functional images of the subject 7; in this case the analysis revealed activation just in the superior culliculus (structure number 18) and in the lateral geniculate body (structure number 35).

Finally, in the Figure 42 are displayed the activation maps achieved for the subject 8. The activation clusters shows in the slices 44 and 45 are likely to be analogues to activity in the oculomotor nuclei (structures number 12 and 13), the superior culliculus (structure number 18), and lateral geniculate body (structure number 35).
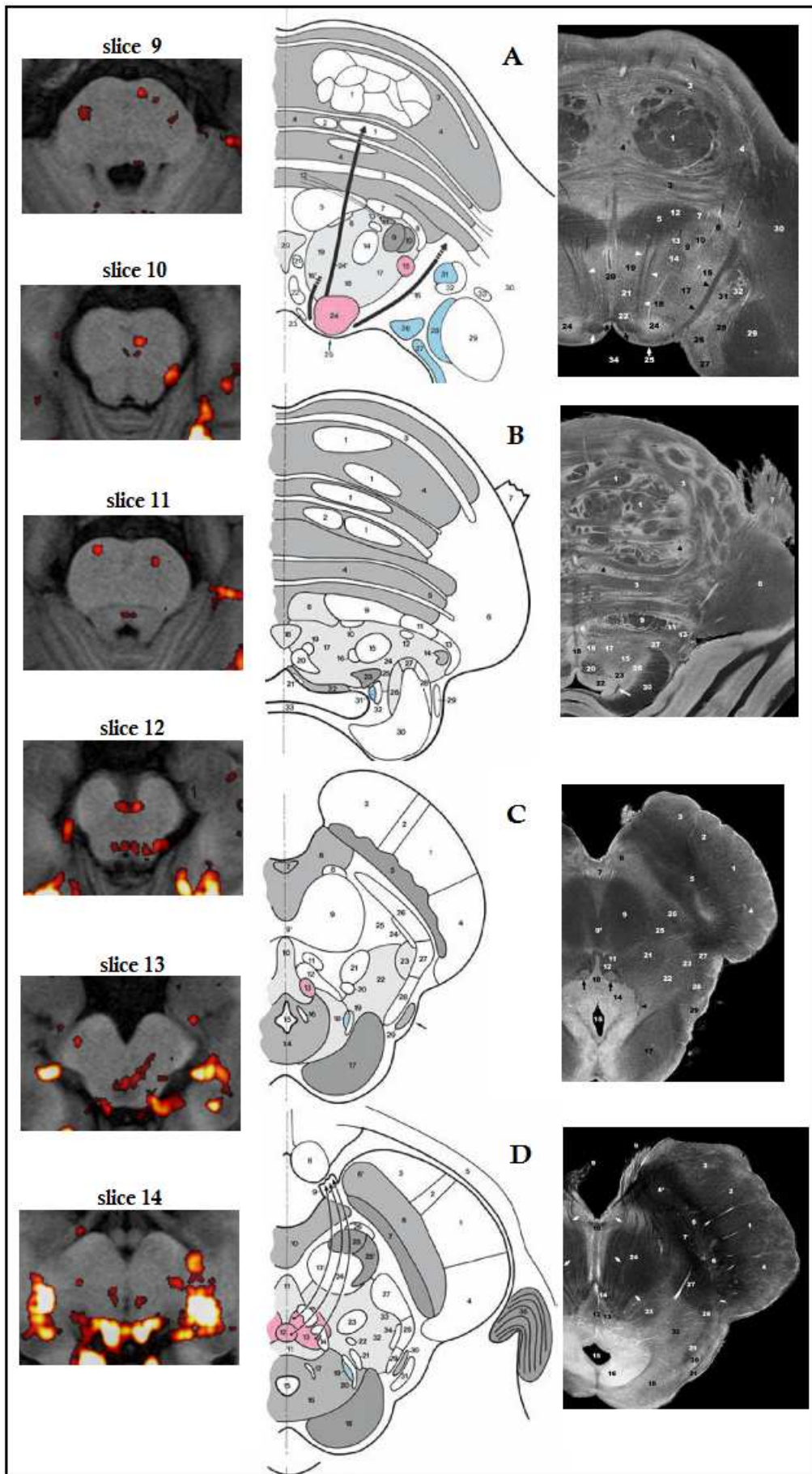
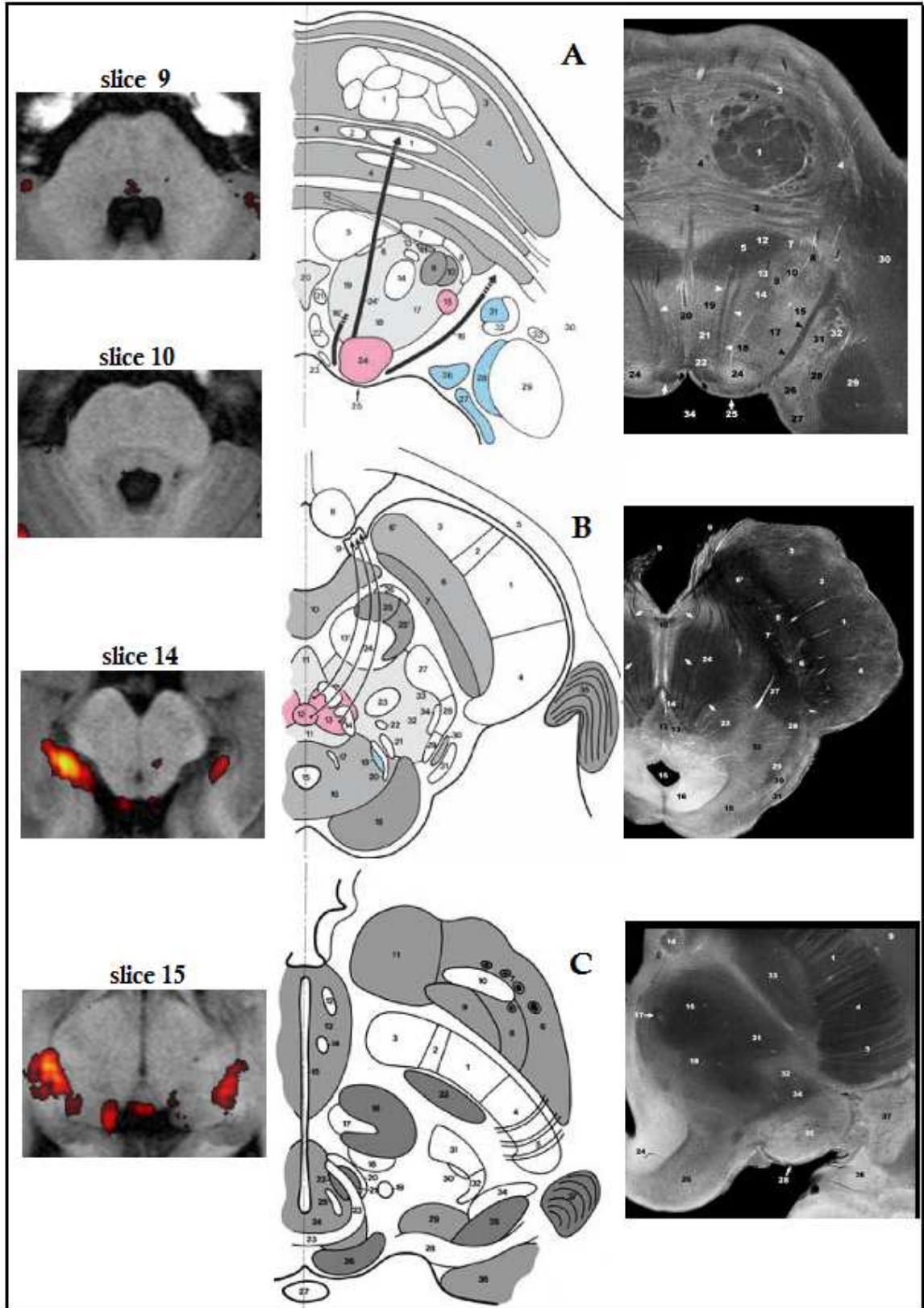**Figure35.** Activation map calculate with uncorected treshold P<0.001. Source: Thomas 2009.

Figure 36. Results functional study, subject 2. Group map showing areas in the brainstem with neuronal activity elicited by horizontal OKN. Specific regions are displayed with an uncorrected threshold of P < 0.001. Drawing and matching MR microscopy at 9.4 T adapted from the Duvernoy's atlas of human brainstem (Thomas 2009).

Figure 37. Results functional study, subject 3. Group map showing areas in the brainstem with neuronal activity elicited by horizontal OKN. Specific regions are displayed with an uncorrected threshold of P < 0.001. Drawing and matching MR microscopy at 9.4 T adapted from the Duvernoy's atlas of human brainstem (Thomas 2009).
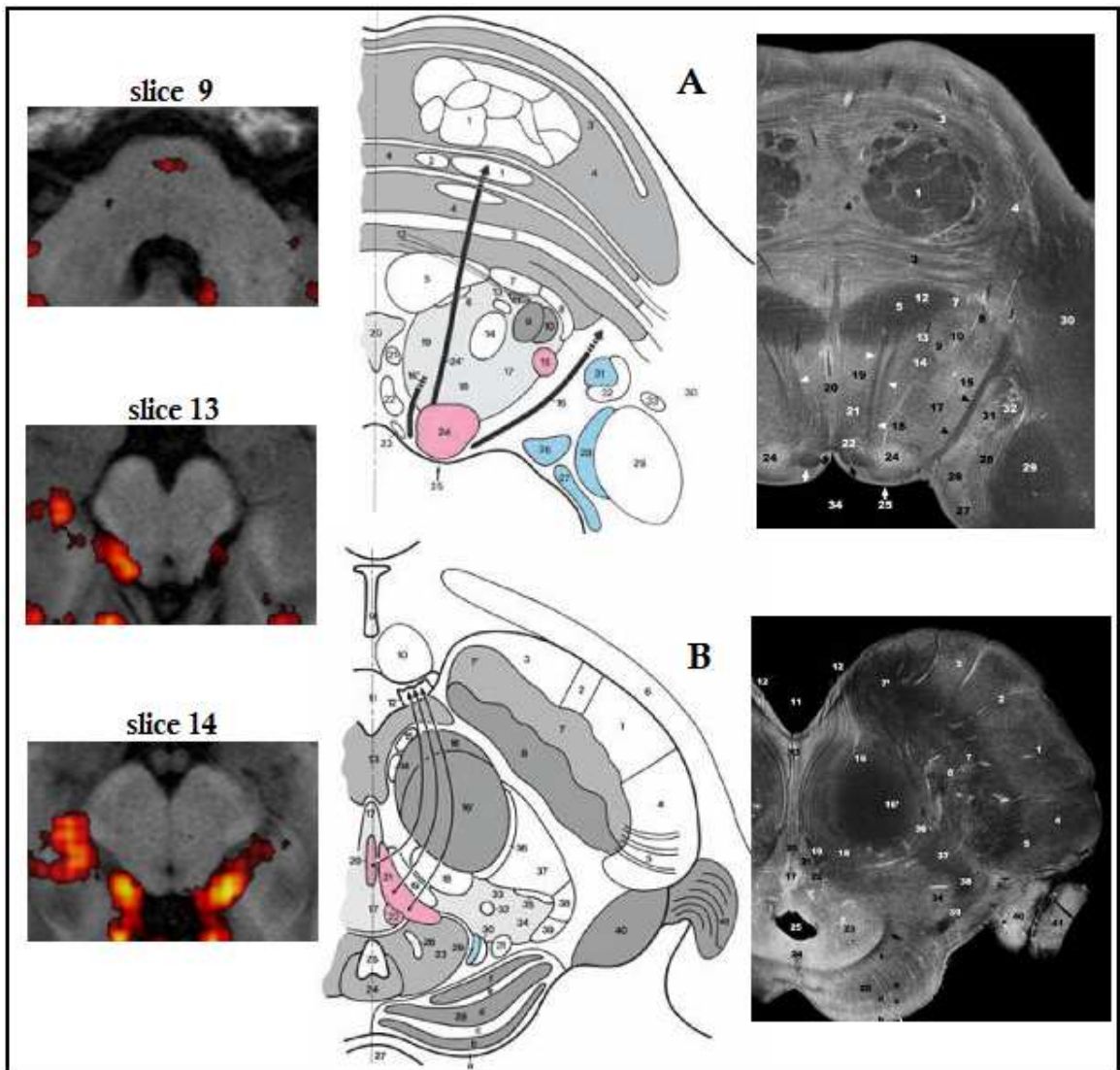
Figure 38. Results functional study, subject 4. Group map showing areas in the brainstem with neuronal activity elicited by horizontal OKN. Specific regions are displayed with an uncorrected threshold of P < 0.001. Drawing and matching MR microscopy at 9.4 T adapted from the Duvernoy's atlas of human brainstem (Thomas 2009).
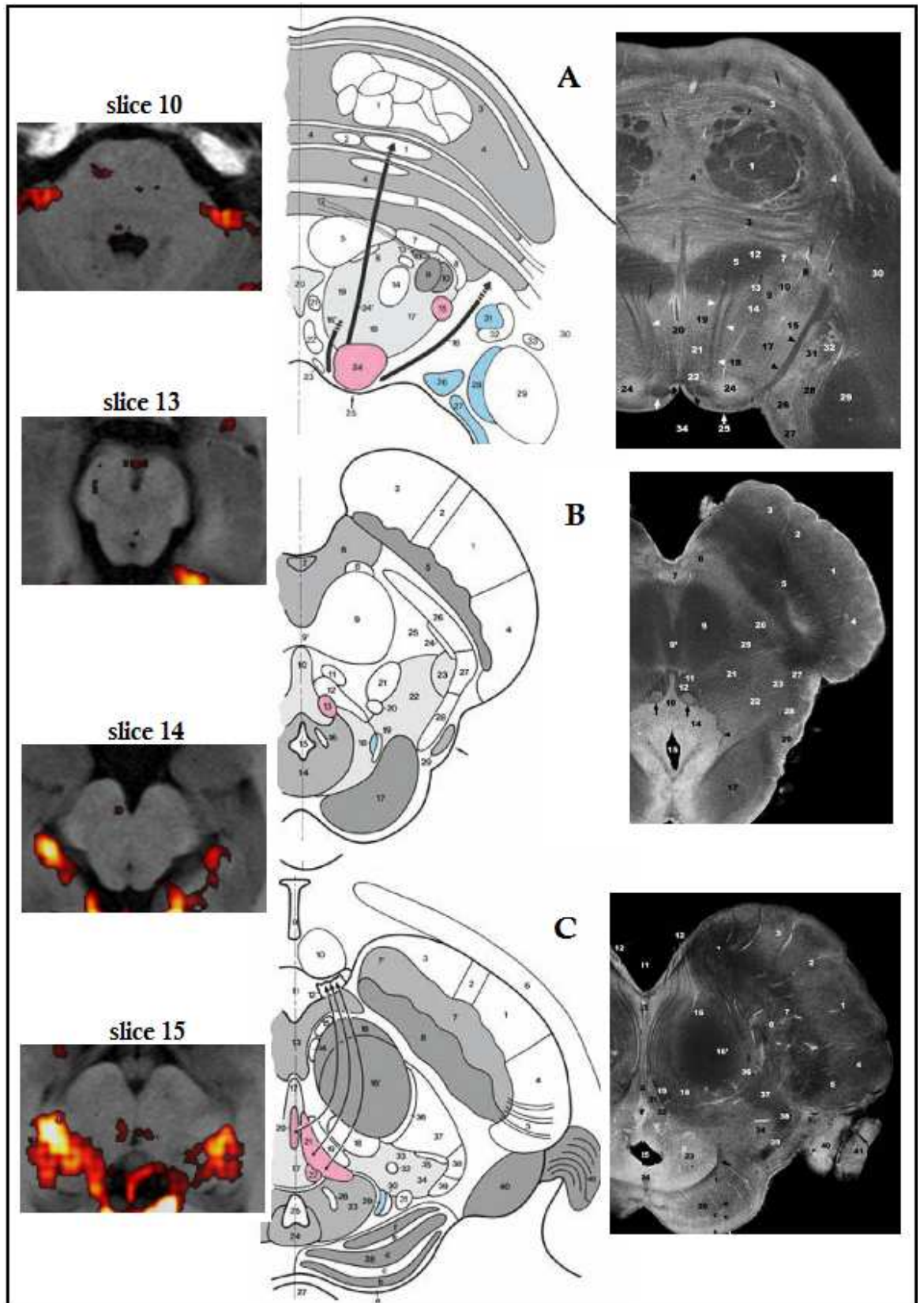
Figure 39. Results functional study, subject 5. Group map showing areas in the brainstem with neuronal activity elicited by horizontal OKN. Specific regions are displayed with an uncorrected threshold of P < 0.001. Drawing and matching MR microscopy at 9.4 T adapted from the Duvernoy's atlas of human brainstem (Thomas 2009).

Figure 40. Results functional study, subject 6. Group map showing areas in the brainstem with neuronal activity elicited by horizontal OKN. Specific regions are displayed with an uncorrected threshold of P < 0.001. Drawing and matching MR microscopy at 9.4 T adapted from the Duvernoy's atlas of human brainstem (Thomas 2009).
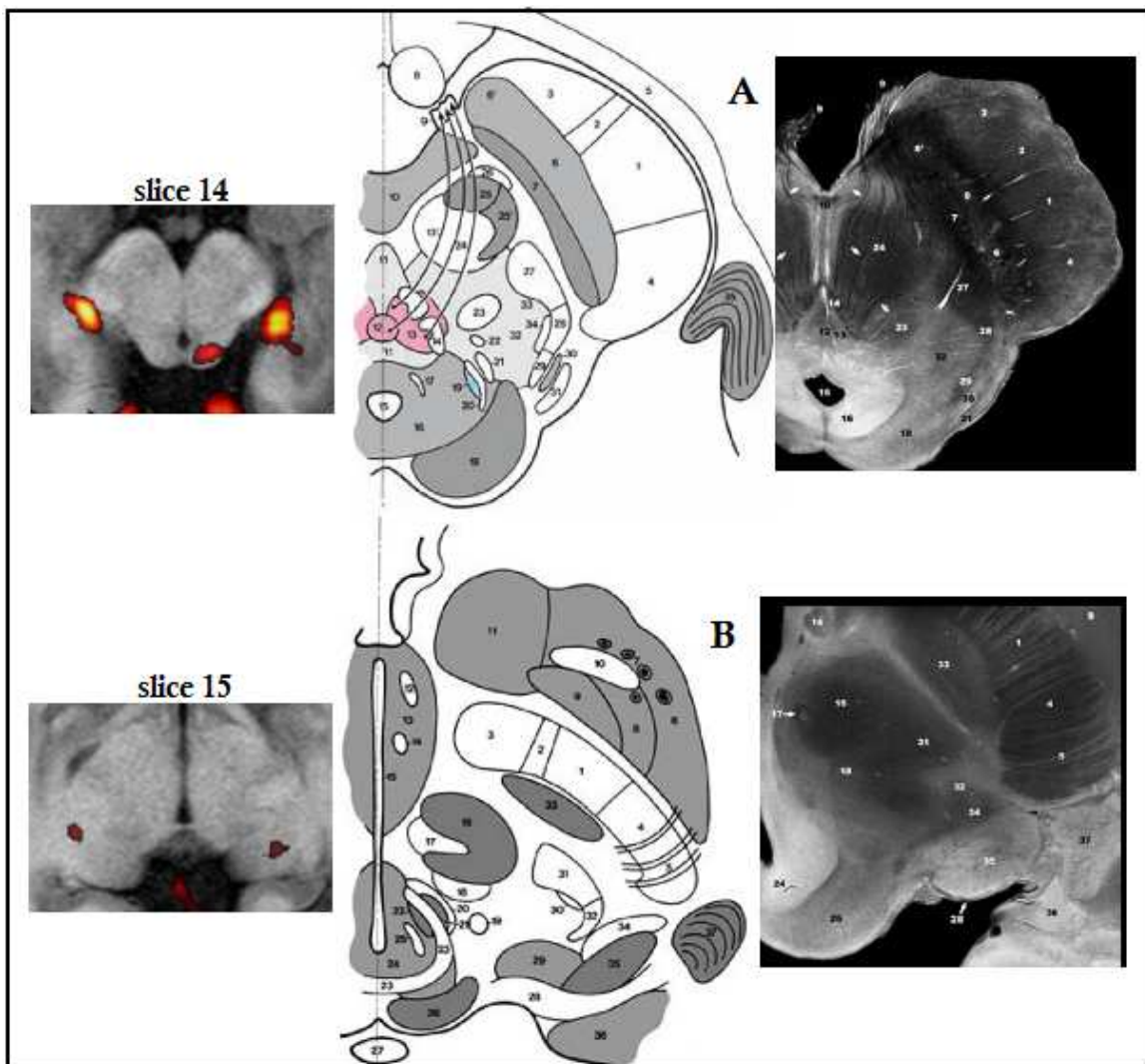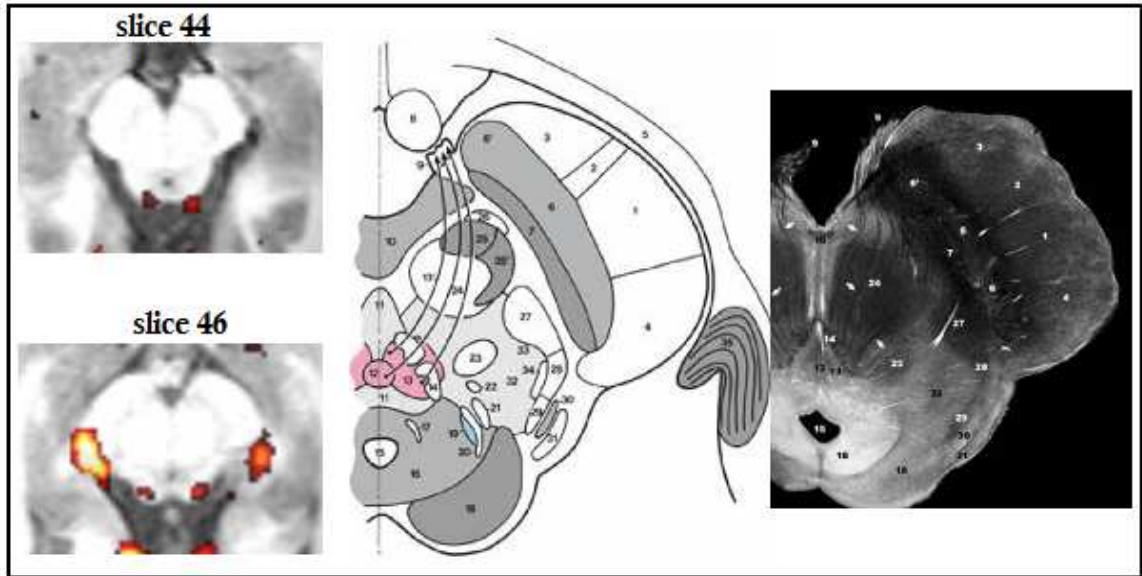
Figure 41. Results functional study, subject 7. Group map showing areas in the brainstem with neuronal activity elicited by horizontal OKN. Specific regions are displayed with an uncorrected threshold of P < 0.001. Drawing and matching MR microscopy at 9.4 T adapted from the Duvernoy's atlas of human brainstem (Thomas 2009).
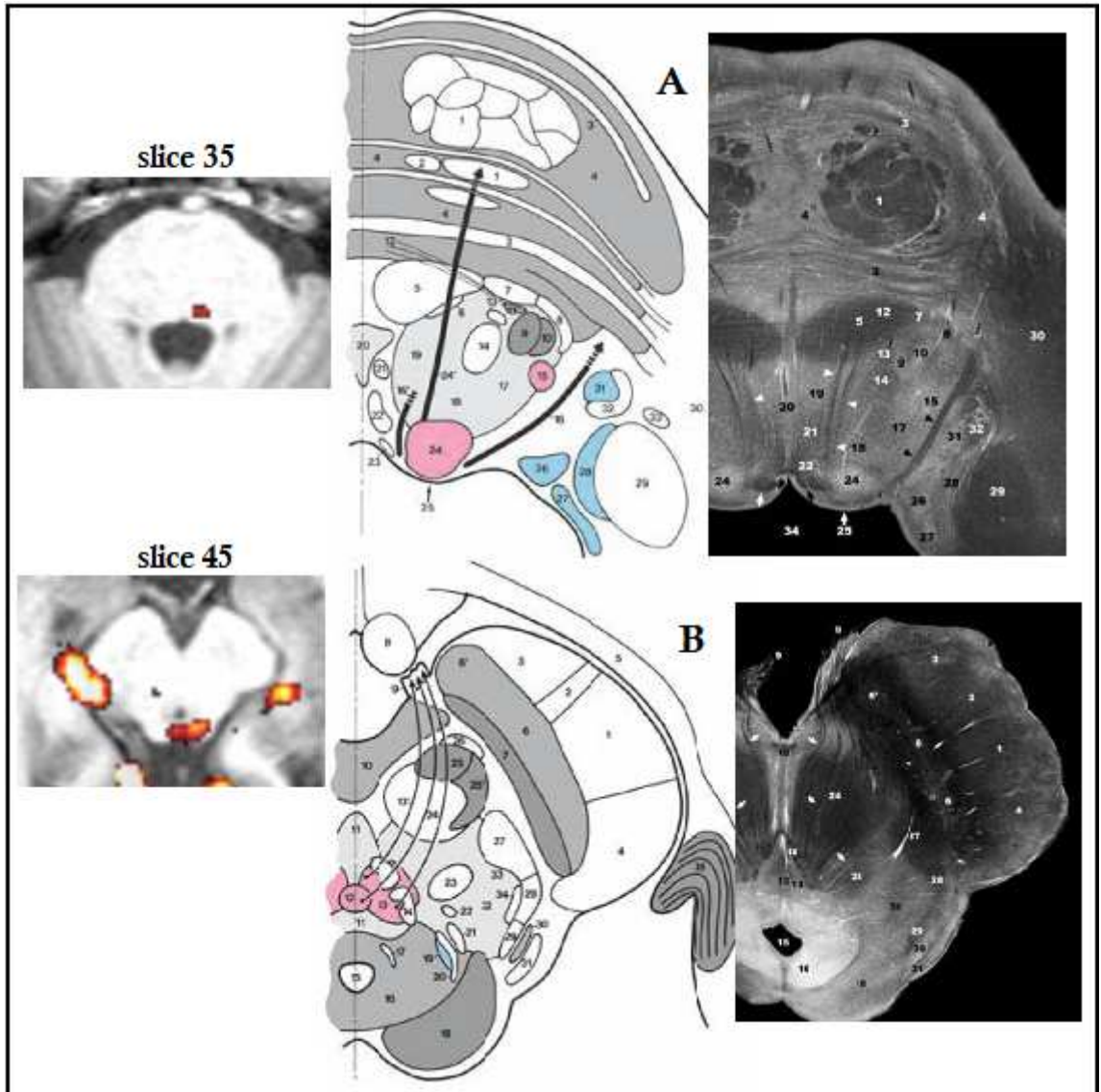

Figure 42. Results functional study, subject 8. Group map showing areas in the brainstem with neuronal activity elicited by horizontal OKN. Specific regions are displayed with an uncorrected threshold of P < 0.001. Drawing and matching MR microscopy at 9.4 T adapted from the Duvernoy's atlas of human brainstem (Thomas 2009).
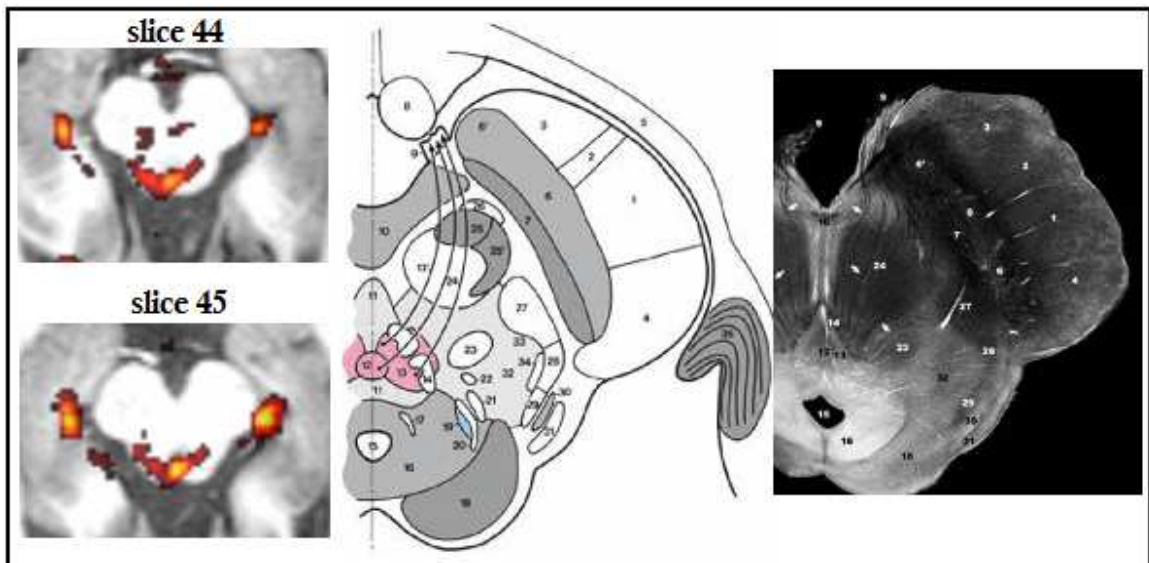
Chapter 4:

Discussion and conclusion

This project provides guidelines to improve functional MRI study of the brainstem at 3T. It first focused on the optimal choice of the echo time, slice tilt, and spatial resolution as well as the most suited head coil. The appropriate choice of slice tilt and echo time primarily reduces BOLD sensitivity loss due to susceptibility induced gradients in the phase-encoding (PE) direction. Since the direction and magnitude of the susceptibility-induced gradient varies across the brain, the optimal EPI parameters are location dependent (Weiskopf, Hutton et al. 2006). Herein the optimal values of the parameters were assessed for the brainstem region. The results in the TE optimization showed (Figure 16) the BS assume the 95% of its maximum value for TE values between 36 and 53 ms. For the acquisition of the functional images a echo time of 36 ms second was chosen for two reasons. As it can be seen from the TE map (Figure 18) a lower TE ensure

higher BS and reduce the signal loss in the areas near the brainstem affected by magnetic susceptibility. Furthermore, a lower echo time enable to use a shorter time repetition, yielding sequence of acquisition with shorter duration. However for recovery of the BS caused magnetic susceptibility, the GRASE technique was investigated. The optimization of TE for this technique did not yield good results, probably because of the wrong choice to the TE values investigate; thus, the visualized trend (Figure 22) of the BS appear shifted on the right of the hypothetical peak showed for the EPI technique. Furthers, GRASE has been used in preliminary studies where no strong activation was found in the involved brain structures, such as visual cortex and LGN. For these reasons, although it showed to compensate the artifacts caused by magnetic susceptibility (Figure 19), GRASE was considered out of line with the purposes of this study. Moreover, titling the imaging slice causes a redistribution of in-plane and through-plane susceptibility gradient. The results in this study showed for the brainstem that a tilt angle between -15° and 30° ensure that the BS assume the 90% of its maximum. Slice tilt optimization was carried out for single subject, this has been a important limit to verify the achieved results. Also the spatial resolution was investigate to assess whether decrease the effect of partial volumes leads a benefit in the activation maps. On the contrary, the results showed that use high spatial resolution yields a too low SNR to reveal neuronal activation in the nuclei of the brainstem. Additionally different head coil were investigate to evaluate their features. The reactivation maps calculated from the functional images measured with different did not show clearly difference, but no quantitatively analysis was carried out to compare the data. One of the more significant benefits to neuroscientist using this MRI coil design (16 head coil) is to achieve a higher spatial resolution (Bellgowan, Bandettini et al. 2006), but it was demonstrate that in this functional study is advised use a low resolution; for this reason and why the 16 head coil has been proved less workable during the procedure of preparation of the experiment, the functional study was carried on using the 8 channel coil.

The purpose of the second part of the project was to build the GLM including several information detected during the functional study. It has been supposed that events as blink and periods of eyes closed could contribute (as terms of noise) to compose the MR signal; hence, resressors of no interest were built to compensate these noise sources.

The models built with and without blink and eyes closed regressors were compared using two methods. The statistical analysis by F-test revealed no voxels exceeding the fixed threshold (uncorrected threshold of P < 0.001) in the brainstem structures showing the inefficiency of the first method; indeed, the difference between the two models found with the first method can not be quantitatively defined and it has not a statistical meaningful. However, in the almost all subject the maps shows voxels exceeding the threshold in the visual cortex and in the cerebellum; this suggest that is recommended use these information in the GLM to compensate the noise. The velocity of the eyes movement was investigated as regressor of interest. Two F-test were carried out to evaluate first the benefit of add this information on the base model (including block and noise regressors) and second, whether is possible build the linear model just with the velocity information as regressor of interest. The results of the second F-test revealed voxels exceeding the fixed threshold in the visual cortex as well as in the cerebellum and in the brainstem; this suggests that including the block information in the linear model is necessary to achieve activation in the detected areas. The first statistical test revealed narrow clusters of voxels exceeding the threshold in the visual cortex, and in some volunteers in the temporal lobe in the boundaries between brain and non-brain and in the eyes; these activations may be due to the correlation between the eyes movement and noise components cause by rigid movements.

In the functional study, the sequence implementation and the data analysis were carried out considering the finding found in the previous steps to find a suited approach of investigation. The purpose was to determine nuclei and pathway in the brainstem that are involved in the OKN stimulus. Statistical analysis revealed robust neuronal activation throughout the visual cortex as well as in the lateral geniculate nuclei (LGN); but the main findings revealed in the brainstem were neuronal activation in the superior culliculus (SC) for all participants, and in the other nuclei and pathway involved in the investigated task, such as the oculomotor nuclei (OMN), the oculomotor nerve, and the abducens nucleus. The comparison between the activation clusters and the structures in the anatomical drawing is limited because of the different tilt of the matched axial section. Further, to understand the roles of these brainstem nuclei in the perform of

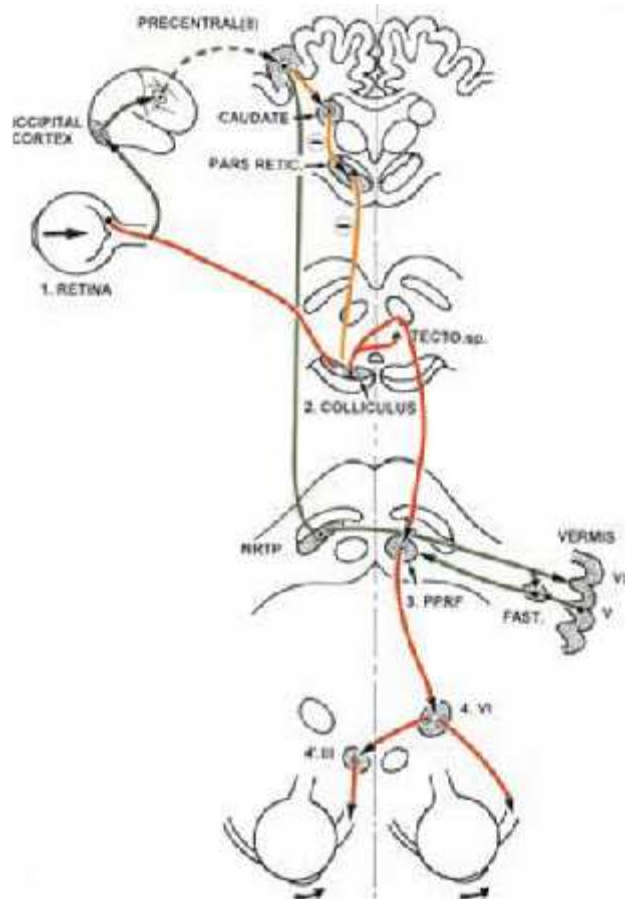OKN, a drawing of the pathway of neuronal signal during the horizontal saccades is displayed in the Figure 29.

Figure 29. Nuclei and pathway involved in the horizontal saccades. Abbreviations: III Cranial nerve III (oculomotor nucleus), VI Cranial nerve VI (abducens nucleus), FAST Factigial nucleus, NRTP Nucleus reticularis tegmenti pontis, PARS RETIC Pars reticularis of the substantia nigra, PPRF Paramedian pontine reticular formation, TECTO tectospinal tract, VERMIS V Lobule V (of Larsell) (posterior culmen), VERMIS VI Lobule VI (of Larsell) (declive). Drawing adapted from the Duvernoy's atlas of human brainstem (Thomas 2009).

The saccades consist of rapid eye movements that bring the image of an object situated in the visual field onto the fovea (central portion of the retina) and allow fixation to passrapidly from one object of interest to another. The principal pathway of the horizontal saccades originating from the retina successively involve the deep layer of the superior colliculus, the paramedian pontine reticular formation (nuclei reticularis pontis caudalis and oralis), and the abducens nucleus, which projects to the oculomotor nucleus (Thomas 2009). Other nuclei and pathway which appears active during the analysis are involved either in the eyes movement control, such as trigeminal nucleus

and tectrospinal tract, or in the control of facial expression such as facial nerve. These action and reaction can be related with the task used to evoke the BOLD signal.

There are relatively few human functional neuroimaging studies which investigate brainstem nuclei and in particular of visual control. The SC have been shown in other fMRI studies using stimuli to elicit horizontal (Wall, Walker et al. 2009) and vertical (Bense, Janusch et al. 2006) optokinetic reflexes; both of which do not find robust activation in the SC in all subjects and no other brainstem nucleus is clearly showed.

Different research problems have different propriety end trade-offs must be made when deciding upon a strategy to use. To investigate other nuclei and pathway of the brainstem the same acquisition sequence can be used, while employing other stimulus, others information can be used to build regressors. In conclusion it can be said that the developed approach provides the best detection in the brainstem activity during visual stimuli.

References

Amaro, J. E. and G. J. Barker (2006). "Study design in fMRI: Basic principles." <u>Brain and Cognition</u> **60**(3): 220-232.

Backes, W. H. and P. van Dijk (2002). "Simultaneous sampling of event-related BOLD responses in auditory cortex and brainstem." <u>Magnetic Resonance in Medicine</u> **47**(1): 90-96.

Bellgowan, P. S. F., P. A. Bandettini, et al. (2006). "Improved BOLD detection in the medial temporal region using parallel imaging and voxel volume reduction." <u>NeuroImage</u> **29**(4): 1244-1251.

Bense, S., B. Janusch, et al. (2006). "Brainstem and cerebellar fMRI-activation during horizontal and vertical optokinetic stimulation." <u>Experimental Brain Research</u> **174**(2): 312-323.

Chen, W. and X.-H. Zhu (1997). "Suppression of physiological eye movement artifacts in functional MRI using slab presaturation." <u>Magnetic Resonance in Medicine</u> **38**(4): 546-550.

Cho, Z. H. and Y. M. Ro (1992). "Reduction of susceptibility artifact in gradient-echo imaging." <u>Magnetic Resonance in Medicine</u> **23**(1): 193-200.

Deichmann, R., J. A. Gottfried, et al. (2003). "Optimized EPI for fMRI studies of the orbitofrontal cortex." <u>NeuroImage</u> **19**(2): 430-441.

Deichmann, R., O. Josephs, et al. (2002). "Compensation of Susceptibility-Induced BOLD Sensitivity Losses in Echo-Planar fMRI Imaging." <u>NeuroImage</u> **15**(1): 120-135.

Figley, C. R., J. K. Leitch, et al. "In contrast to BOLD: signal enhancement by extravascular water protons as an alternative mechanism of endogenous fMRI signal change." <u>Magnetic Resonance Imaging</u> **28**(8): 1234-1243.

Frahm, J., K.-D. Merboldt, et al. (1993). "Functional MRI of human brain activation at high spatial resolution." <u>Magnetic Resonance in Medicine</u> **29**(1): 139-144.

Glover, G. H., T.-Q. Li, et al. (2000). "Image-based method for retrospective correction of physiological motion effects in fMRI: RETROICOR." <u>Magnetic Resonance in Medicine</u> **44**(1): 162-167.

Harvey, A. K., K. T. S. Pattinson, et al. (2008). "Brainstem functional magnetic resonance imaging: Disentangling signal from physiological noise." <u>Journal of Magnetic Resonance Imaging</u> **28**(6): 1337-1344.

Jovicich, J. and D. G. Norris (1999). Functional MRI of the human brain with GRASE-based BOLD contrast, John Wiley & Sons, Inc. **41:** 871-876.

Kasper, L. e. a. (2009). "Cardiac artefact correction for human brainstem fMRI at 7T." Proceedings of the 15th Annual Meeting of the Organization for Human Brain Mapping: 395.

Krauzlis, R. J. (2004). "Recasting the Smooth Pursuit Eye Movement System." Journal of Neurophysiology **91**(2): 591-603.
.

Ogawa, S., T. M. Lee, et al. (1990). "Brain magnetic resonance imaging with contrast dependent on blood oxygenation." Journal Name: Proceedings of the National Academy of Sciences of the United States of America; (United States); Journal Volume: 87:24: Medium: X; Size: Pages: 9868-9872.

Ojemann, J. G., E. Akbudak, et al. (1997). "Anatomic Localization and Quantitative Analysis of Gradient Refocused Echo-Planar fMRI Susceptibility Artifacts." NeuroImage **6**(3): 156-167.

Poser, B. A., M. J. Versluis, et al. (2006). "BOLD contrast sensitivity enhancement and artifact reduction with multiecho EPI: Parallel-acquired inhomogeneity-desensitized fMRI." Magnetic Resonance in Medicine **55**(6): 1227-1235.

Raphan, T. and B. Cohen (1978). "Brainstem Mechanisms for Rapid and Slow Eye Movements." Annual Review of Physiology **40**(1): 527-552.

Scott, A. H., W. S. Allen, et al. (2009). Functional magnetic resonance imaging, Sunderland, MA : Sinauer.

Thomas, P. N. (2009). Duvernoy?s Atlas of the Human Brain Stem and Cerebellum : High-Field MRI: Surface Anatomy, Internal Structure, Vascularization and 3D Sectional Anatomy, Wien : Springer.

Turner, R. and R. J. Ordidge (2000). "Technical challenges of functional magnetic resonance imaging." IEEE engineering in medicine and biology magazine : the quarterly magazine of the Engineering in Medicine & Biology Society **19**(5): 42-54.

Wall, M. B., R. Walker, et al. (2009). "Functional imaging of the human superior colliculus: An optimised approach." NeuroImage **47**(4): 1620-1627.

Weiskopf, N., C. Hutton, et al. (2006). "Optimal EPI parameters for reduction of susceptibility-induced BOLD sensitivity losses: A whole-brain analysis at 3 T and 1.5 T." NeuroImage **33**(2): 493-504.

Weiskopf, N., C. Hutton, et al. (2007). "Optimized EPI for fMRI studies of the orbitofrontal cortex: compensation of susceptibility-induced gradients in the readout direction." Magnetic Resonance Materials in Physics, Biology and Medicine **20**(1): 39-49.

Yablonskiy, D. A. and E. M. Haacke (1994). "Theory of NMR signal behavior in magnetically inhomogeneous tissues: The static dephasing regime." <u>Magnetic Resonance in Medicine</u> **32**(6): 749-763.

Abbreviations

BOLD   Blood Oxygen Level-Dependent

CNS   Central Nervous System

EEG   Electroencephalogram

FOV   Field of View

FEW   Family Wise Error

GLM   General Linear Model

Hb   Oxygenated hemoglobin

HDR   Hemodynamic response

LGN   Lateral Geniculate Nuclei

MLF   Medial Longitudinal Fasciculus

OFC   Orbitofrontal Cortex

PE   Phase encoding

RF   Radiofrequency

ROI   Region of Interest

SC   Superior colliculus

SNR   Signal to Noise Ratio

TE   Time echo

TR   Time repetition

uzh | eth | zürich
Institute for Biomedical Engineering

Roger Luechinger, PhD
Universityhospital Zürich
MR Center VMR30
Rämistrasse 100
CH-8091 Zürich
Tel: ++41 44 255 30 64
Fax: ++41 44 255 45 06
email: luechinger@biomed.ee.ethz.ch

Certificate of Attendance

Moro Marco

has successfully attend on the

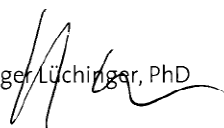### 2nd November 2010 (17:15-19:00 ETZ F71)

the

MRI safety course

organized by the MR Group of the
Institute for Biomedical Engineering, University and ETH Zurich

Course content:

- Potential risks of the three electromagnetic fields of MRI
- Additional risks with implants
- Screening of volunteers
- Safety rules at the MR Center of the USZ

Roger Lüchinger, PhD

Article relating the project

Sequence Optimization for Brainstem BOLD fMRI

Authors:

Marco Piccirelli[1,2], Marco Moro[2,1], Saskia Klein[1], Lars Kasper[1,2], Klaas Enno Stephan[1,3]

Institutions:

[1]Laboratory for Social and Neuronal Systems Research, Department of Economics, University of Zurich, Switzerland, [2]Institute for Biomedical Engineering, University and ETH Zurich, Switzerland, [3]Wellcome Trust Centre for Neuroimaging, University College London, UK

Introduction:

The brainstem is critically involved in almost any aspect of human brain function. Nevertheless, relatively few fMRI studies have focused on the brainstem so far. This discrepancy is due to the technical difficulties in brainstem imaging, including the relative small size of the neuronal nuclei, strong signal dropouts due to magnetic susceptibility artifacts, the higher physiological noise relative to the cortex, and the lower sensitivity of the head coil arrays at the brainstem location relative to the cortex. In addition to reduction of physiological noise (e.g., pulsation, breathing), these problems require careful optimization of parameters for standard EPI sequences. To our knowledge, however, no such systematic optimization of parameters has been reported. Here we present preliminary findings from tests concerning standard EPI parameters.
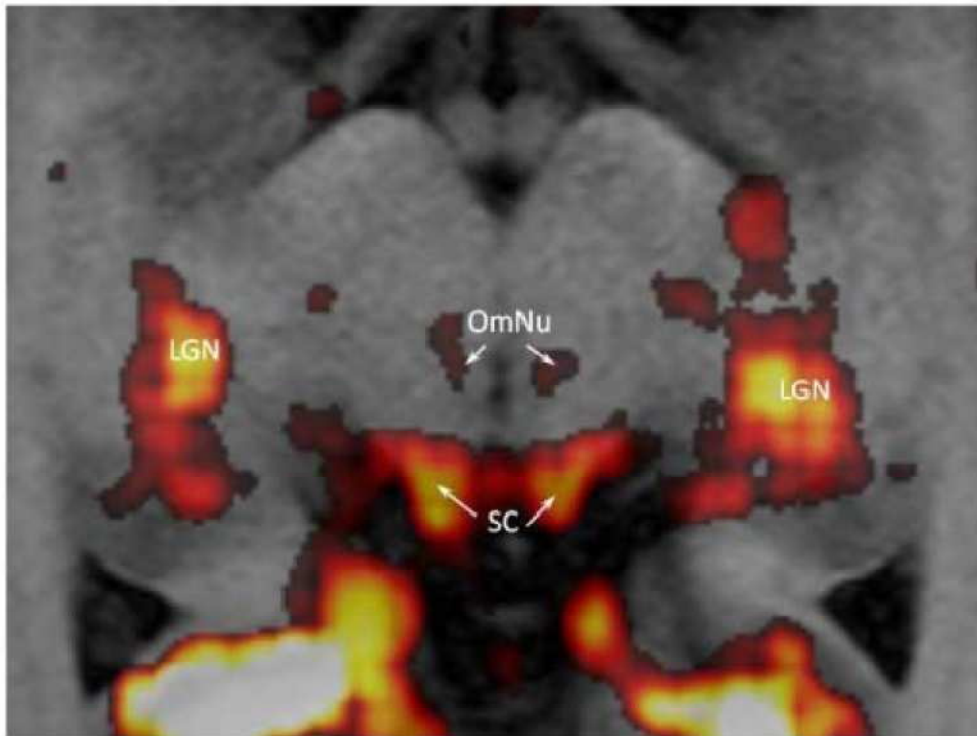
Methods:

To optimize the BOLD contrast of brainstem fMRI data, several acquisition procedures were compared, using a 3T Philips Achieva scanner and a visual paradigm inducing optokinetic nystagmus (OKN) in several directions. This task was chosen to elicit activation in small, but anatomically identifiable brainstem nuclei, like the superior colliculus. We used sequences with a constant TR (no cardiac gating), correcting pulsation artefacts post-hoc, using RETROICOR [1,2]. We compared (i) gradient echo (GE) sequences vs. spin echo (SE) and GRASE [3] sequences, (ii) head coils with 8 vs. 16 receive channels, (iii) different resolutions (ranging from 1.5^3 to 3^3 mm^3) and (iv) slab orientation angles (rotating around the left-right axis in 15 degree steps). Using the method proposed by Poser, et al. [4] maps of the optimal echo time (TE) were obtained for GE and GRASE sequences. SPM8 was used for data analysis, with statistical thresholds of $p<0.05$ (corrected) and $p<0.001$ (uncorrected), respectively. Below, we report results from a single volunteer.

Results:

With SE and GRASE almost no activation could be detected within the brainstem. For GE, maps of the optimal TE could be obtained for the whole brainstem. Although situated in an area prone to intra-voxel dephasing, the optimal TE for high SNR in the brainstem was found to be around 48 ± 8 ms. The head coil array with 8 channels gave higher activations than the 16-channel head coil (although this could have been influenced by the different mirror setup of the two coils). Despite the small dimensions of the brainstem nuclei, the lower resolution scans yielded higher activations (possibly due to insufficient SNR at high resolution). Finally, slab orientation had a major impact on the deformation geometry of the EPI data relative to the anatomical scans.

Conclusions:

Reliable activation maps could be obtained with an optimized GE sequence (see Figures 1 and 2). Activation patterns induced by different OKN directions could be differentiated. Optimization of standard fMRI acquisition parameters considerably improve brainstem activation maps obtained by fMRI.

(SC) Superior Culliculus, (LGN) Lateral Geniculate Nuclei, (OmNu) Oculomotor Nuclei
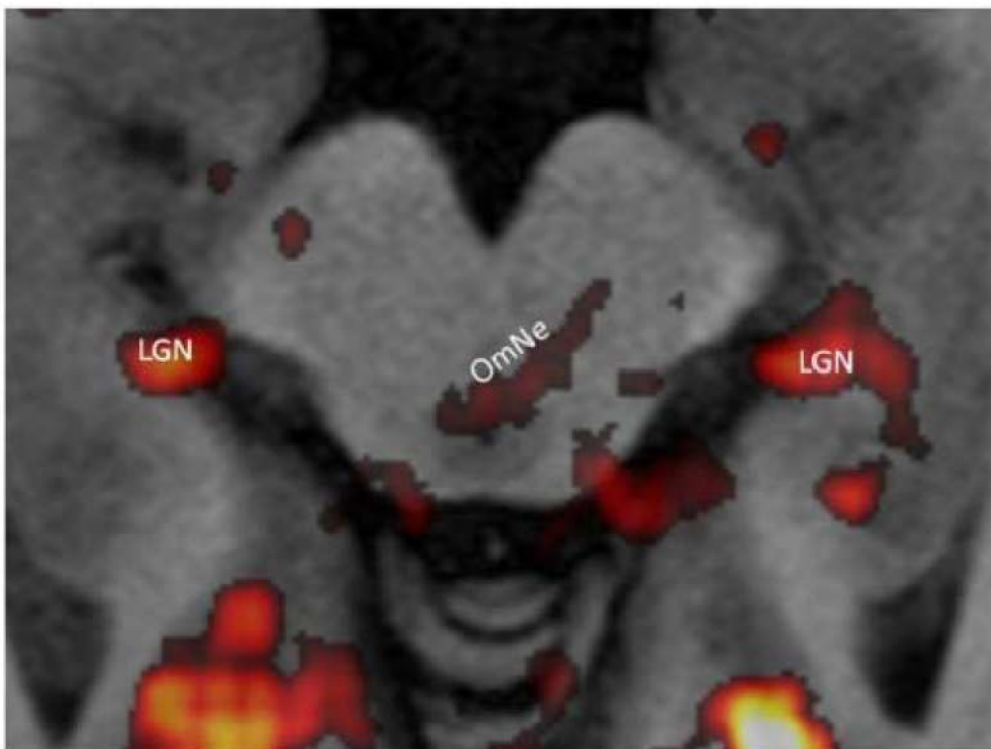
(LGN) Lateral Geniculate Nuclei, (OmNe) Oculomotor Nerve

Imaging Methods

BOLD fMRI

Abstract Information

References

1. Glover, G.H. (2000), 'Image-based method for retrospective correction of physiological motion effects in fMRI: RETROICOR', Magnetic Resonance in Medicine, vol. 44, no. 1, pp. 162-167.

2. Kasper, L. (2009), 'Cardiac artefact correction for human brainstem fMRI at 7T', Human Brain Mapping, no. 395

3. Oshio, K. (1991), 'GRASE (Gradient- and spin-echo) imaging: a novel fast MRI technique', Magnetic Resonance in Medicine, vol. 20, no. 2, pp. 344-349.

4. Poser, B.A. (2006) 'BOLD contrast sensitivity enhancement and artifact reduction with multiecho EPI: parallel-acquired inhomogeneity-desensitized fMRI', Magnetic Resonance in Medicine, vol. 55, no. 6, pp. 1227-1235.